Actin Remodeling in Motile Cells

By Eric A. Osborn

B.S.E. Biomedical Engineering
Duke University, 1998

S.M. Mechanical Engineering
Massachusetts Institute of Technology, 2001

Submitted to the Harvard–MIT Division of Health Sciences and Technology in Partial Fulfillment of the Requirements for the Degree of

Doctor of Philosophy in Medical Engineering
at the
Massachusetts Institute of Technology

June 2004

Signature of Author _____
Harvard–MIT Division of Health Sciences and Technology
May 21, 2004

Certified by _____
C. Forbes Dewey, Jr., Ph.D.
Professor of Mechanical Engineering
Massachusetts Institute of Technology
Thesis Supervisor

Certified by _____
John H. Hartwig, Ph.D.
Professor of Cell Biology
Harvard Medical School
Thesis Supervisor

Accepted by _____
Martha L. Gray, Ph.D.
Edward Hood Taplin Professor of Medical and Electrical Engineering
Co-Director, Harvard–MIT Division of Health Sciences and Technology

Actin Remodeling in Motile Cells

by

Eric A. Osborn

Submitted to the Harvard–MIT Division of Health Sciences and Technology on May 21, 2004 in Partial Fulfillment of the Requirements for the Degree of Doctor of Philosophy in Medical Engineering

Abstract

Non-muscle cell shape change and motility depend primarily on the dynamics and distributions of cytoplasmic actin. In cells, actin cycles between monomeric and polymeric phases tightly regulated by actin binding proteins that control cellular architecture and movement. Here, we characterize actin remodeling in shear stress stimulated endothelial cells and in actin networks reconstituted with purified proteins.

Fluid shear stress stimulation induces endothelial cells to elongate and align in the direction of applied flow. Alignment requires 24 h of exposure to flow, but the cells respond within minutes to flow by diminishing their movements by 50%. Although movement slows, actin filament turnover times and the amount of polymerized actin in cells decreases, increasing actin filament remodeling in individual cells composing a confluent endothelial monolayer to levels used by disperse, non-confluent cells for rapid movement. Hours later, motility returns to pre-shear stress levels, but actin remodeling remains highly dynamic in many cells. We conclude that shear stress initiates a cytoplasmic actin remodeling response that is used to modify endothelial cell shape instead of bulk cell translocation.

We determine the steady state dynamics of purified actin filament networks in the entangled state and after orthogonal cross-linking with filamins using a novel, non-perturbing fluorescence system. Human filamin A or *Dictyostelium discoidium* filamin slow actin filament turnover by ~50% and recruit much of a significant population of actin oligomers that we measure are present in polymerized purified actin solutions into the immobile filament fraction. Surprisingly, these observations occur at very low stoichiometry to actin, approximately requiring only one filamin molecule bound per actin filament, similar to the amount required for actin filament gelation *in vitro*. Networks formed with filamin truncates localize this activity to the actin binding domain and reveal that dimerization and orthogonal cross-linking are not required for dynamic

stabilization. Re-expression of filamin A with or without the actin binding domain in human melanoma cells that naturally lack this protein support the findings in purified actin networks. These results indicate that filamin cross-linking stabilizes filament dynamics by slowing filament subunit cycling rates and by either decreasing spontaneous filament fragmentation or promoting filament annealing.

Thesis Supervisor: C. Forbes Dewey, Jr., Ph.D.
Title: Professor of Mechanical Engineering, MIT

Thesis Supervisor: John H. Hartwig, Ph.D.
Title: Professor of Cell Biology, Harvard Medical School

Acknowledgements

I would like to express my deep gratitude to my advisors, John H. Hartwig and C. Forbes Dewey, Jr. for their wonderful ideas, advice, and support throughout the process of shaping this research. I would also like to sincerely thank the members of my Ph.D. Thesis Committee, Frank Gertler and Doug Lauffenburger, for their guidance and insight. I am grateful for the continued mentorship and collaboration of James L. McGrath, who has immeasurably helped me focus and guide my thoughts about actin dynamics and cell movement. Special thanks to everyone in the Hematology Division at Brigham and Women's Hospital and the Microfluids Laboratory at MIT who contributed their time and expertise to teach me and help me achieve this goal. Finally, I would like to thank the students and faculty of the Harvard–MIT Division of Health Sciences and Technology, a group with which I am grateful to be associated.

This is dedicated to my parents, Margie and Larry, for all of their faith, support, and love, and to Teresia, without whom this would not have been possible.

Biography

Eric Alan Osborn was born on October 2, 1975 in Battle Creek, MI to Larry and Margie Osborn. In 1994, Eric graduated from Port Huron Northern High School in Port Huron, MI and proceeded to attend college at Duke University in Durham, NC where he graduated in 1998 with a B.S.E. in Biomedical Engineering. In 1999, Eric was awarded a Whitaker Foundation Graduate Fellowship and began graduate studies in the Department of Mechanical Engineering at MIT and the Medical Engineering/Medical Physics program at the Harvard–MIT Division of Health Sciences and Technology. His doctoral research was performed at the Hematology Division of Brigham and Women's Hospital located in Boston, MA.

Table of Contents

List of Figures

Description *Page*

List of Tables

Description *Page*

Goals of this Thesis

The fundamental goals of this Thesis are to explore the dynamics and regulatory controls of actin-based processes in an effort to further understand the molecular events governing non-muscle cell shape change and movement. Within this context, the work presented here focuses on two specific entities: the shear stress-induced shape change response of endothelial cells (Chapter II) and the effect of the filamin family of actin filament cross-linking proteins on the actin cycle (Chapter III). The individual goals of each investigation are as outlined below.

Endothelial cells in confluent monolayers subjected to steady, laminar fluid shear stress change shape by elongating and aligning in the direction of applied flow, a process driven by dynamic changes in the actin cytoskeleton. Despite this striking morphological change and its well-described relationship to the cytoskeleton, the dynamics of actin during this process are unknown. **How is the endothelial actin remodeling response modulated in single cells before, during, and after endothelial cells accommodate their shapes to the imposed fluid shear stress?**

Filamins are known for their ability to create stiff actin networks by cross-linking neighboring actin filaments. However, even in cross-linked networks, actin filaments exchange subunits at their ends over time with the unpolymerized actin pool. Filamin binding interactions with actin filaments, in addition to its cross-linking effect, may alter the dynamic properties of actin filaments by unknown mechanisms. **How does the filamin family of actin filament cross-linking proteins affect actin filament diffusion, turnover, length, and the extent of polymerization?**

Chapter I

Background and Literature Review

Non-muscle cells move and change shape by activating cascades of signals and molecular events that require the integrated function of a large number of independent proteins [2-7]. Despite this complexity, these events all converge to influence the cytoplasmic protein actin, which is the final substrate in this pathway. Inside the cell, actin coexists in a dynamic exchange between monomeric and polymeric states [8-11]. Actin polymers are bound together by accessory proteins to construct a dense three-dimensional network [12]. This actin polymer network, commonly referred to as the actin cytoskeleton, dictates the underlying mechanical structure of the cell and determines both coarse and fine aspects of cellular shape [13, 14]. Actin polymers incorporated into the cytoskeleton are not simply mechanical struts, but exhibit a highly dynamic component in which monomeric subunits 'turnover' by adding and subtracting from the different polymer ends [15, 16]. External biological, chemical, and mechanical stimuli can significantly modulate a cell's baseline cytoskeleton organization and dynamics [12]. Understanding these changes underpins the efforts to decipher the vast array of physiologic and pathophysiologic events that rely on cell shape and movement [17].

Actin monomer

Actin is a highly conserved, globular 42 kDa protein [18, 19] that is one of the most abundant proteins contained within the cytoplasm of eukaryotic cells [20]. Actin is of considerable biological significance due to its involvement in many integral cellular functions involving cell shape, mechanics, vesicle transport, and motility. Six isoforms of actin exist in cells: α-cardiac, α-skeletal, α-vascular smooth muscle, β-non-muscle, γ-non-muscle, and γ-smooth muscle [21], all of which are ~ 375 amino acids in length and are highly homologous except near their amino terminus, which may confer isoform-specific properties. While α- isoforms are found predominately in muscle cells and the β- and γ- in non-muscle cells, each isoform may be expressed to varying degrees in spatially and temporally regulated patterns in many different cells [22].

From x-ray crystallography, an actin monomer is approximately 6.7 nm × 4.0 nm × 3.7 nm in size [23, 24], split into a large and small domain separated by a binding pocket that accepts a divalent cation and nucleotide. Actin monomer has one high-affinity divalent cation (e.g. Ca^{2+} or Mg^{2+}) binding site and four low-affinity binding sites [25]. The conformation and properties of the actin monomer are different depending on whether Mg^{2+} or Ca^{2+} occupies this site [26, 27]. *In vivo*, the high-affinity site is believed to be predominately Mg^{2+}-bound, since the polymerization kinetics of actin are enhanced for Mg^{2+}-actin over Ca^{2+}-actin [27]. Actin monomers are also bound to one of three nucleotide species, ATP, ADP•Pi, or ADP, which greatly influence its dynamics, protein binding affinities, structure, and regulation.

Polymerization of purified actin

At physiologic ionic strength, purified actin monomers (globular or G-actin) will slowly self-associate into trimeric nuclei, an unstable intermediate, which serve as nucleation sites for further assembly of monomers [28, 29]. Trimer formation is the rate-limiting step in polymerization, since the addition of actin filament seeds (pre-formed nucleation sites) eliminates the time lag prior to elongation. Once a trimer develops, it rapidly elongates by sequential monomer addition onto its ends forming a helical polymer (filamentous or F-actin). The kinetics of filament elongation are strongly influenced by the nucleotide species bound to actin monomers [30-32]. If unperturbed, polymerization proceeds until only a small concentration of actin monomer, the critical concentration, remains unpolymerized, which for ATP-bound monomers is ~0.1 μM [31, 33]. Eventually, purified actin solutions reach a steady state in which there is no net change in the unpolymerized and polymerized actin monomer concentrations and therefore, assembly and disassembly events perfectly balance.

Actin filaments

Actin filaments are helical polymers stabilized by multiple, noncovalent contacts between adjacent monomeric subunits [34]. The actin filament structure can be described by either a one-start left-handed genetic helix of 5.9 nm pitch or a two-start right-handed helix of 72 nm pitch with a filament diameter of ~7 nm [35, 36]. Actin filaments are polarized structures, where the two ends of the polymer can be differentiated both by conformation

and biochemistry. By electron microscopy, filaments labeled with myosin subfragment-1, a proteolytic fragment of heavy meromyosin, take on an arrowhead appearance leading to the classic definitions of filament ends as 'barbed' and 'pointed'. Biochemically, the kinetics that govern monomer addition at opposite ends of the actin filament are distinct: addition of monomers to the barbed filament end occurs approximately ten times faster than at the pointed end [15, 30].

Actin filament turnover

At steady state, the actin filament lengths are stable since monomer addition at one filament end counters loss at the opposite end [16]. If ATP is in excess, actin filaments slowly elongate from their barbed ends and shrink from their pointed ends due to differences in the affinities for monomers at the barbed and pointed filament ends [15]. This directed growth results in a net flux or 'turnover' of F-actin monomers from the barbed to the pointed end. Actin filament turnover is a cyclic process that relies on ATP hydrolysis to provide sufficient chemical energy to maintain the different filament end kinetics [31].

Turnover in its simplest form functions as a molecular treadmill (Fig. I-1) [15]. In this scheme, unpolymerized actin monomers bound to ATP assemble onto the barbed filament ends, hydrolyze ATP into an unstable ADP•Pi intermediate internally on the filament, and, following inorganic phosphate dissociation, remain bound to ADP in the core of the filament until they eventually disassemble from the pointed end [31]. Once

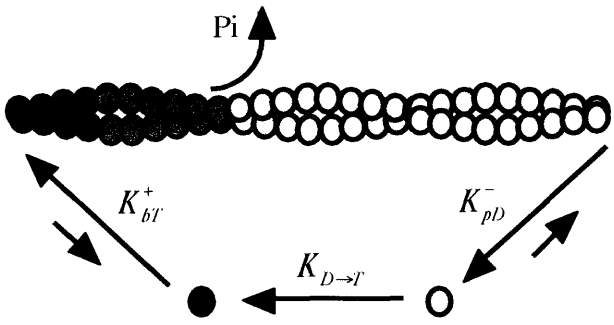

Fig. I-1. *Actin filament treadmilling.* After assembly at the barbed end, ATP-actin monomers (●) are hydrolyzed to ADP•Pi-actin (◉) as they flux through the actin filament, and disassemble as ADP-actin (O) at the pointed end.

free from the filament, ADP-G-actin monomers recycle their ADP for ATP to repeat the cycle.

The time required for an F-actin subunit to traverse a filament from the barbed to the pointed end provides estimates of the characteristic lifetime of the actin filament. Turnover is governed by the association and dissociation kinetics of actin at the filament ends, properties that depend heavily on the nucleotide profiles of subunits at the filament termini and internally on the polymer chains [32]. In purified actin networks, filament subunit recycling requires hours [37], but the pace can be accelerated to seconds or minutes in cells by the actions of associated actin binding proteins [1, 11, 38-41].

The actin cytoskeleton

In cells, actin filaments are linked together to form a three-dimensional support structure that fills the cytoplasmic space (Fig. I-2). This dense meshwork of actin polymer and bound regulatory proteins forms the actin cytoskeleton, which gives the cell shape, stiffness, and provides a mechanical scaffold that helps to fix the position of organelles and facillitate pathways for intracellular transport. The inter-filament spacing of the cortical actin cytoskeleton has been modeled as an orthogonal lattice with a pore size of

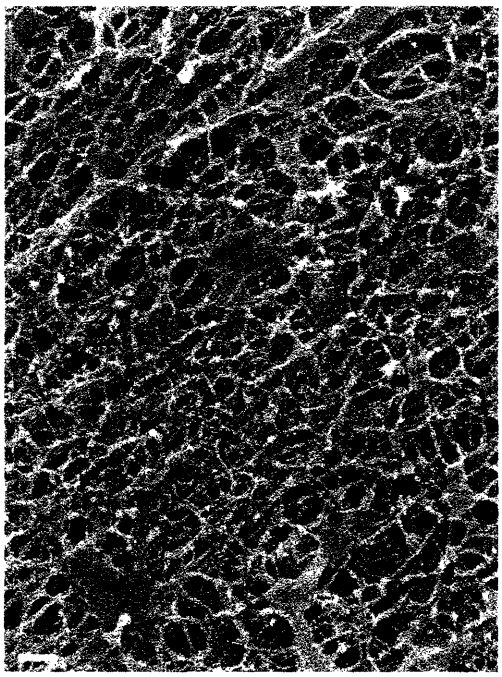

Fig. I-2. *The actin cytoskeleton.* Actin filaments are crosslinked together to form a dense meshwork of interconnected polymers. Many actin binding proteins are associated with this insoluble cellular fraction. Bar, 200 nm. Image courtesy of J. H. Hartwig.

20 – 100 nm [42, 43], through which the cell transports cytoplasmic solute and proteins. The cytoskeleton is organized by cross-linking, bundling, and branching proteins into functional subdomains based on their structure and dynamics. Some of the structures are relatively static, such as epithelial brush border microvilli, hair cell stereocilia, *Drosophila* neurosensory bristles, and non-muscle cell stress fibers [44], while others like lamellipodia, filopodia, and membrane ruffles are highly dynamic. The majority of cellular actin filaments are fixed in space by cross-linking proteins to form stiff gels [14]; however, there is some evidence that small actin filaments are able to diffuse through cytoskeletal pores [40] and are mobile near the plasma membrane [45].

Regulation of actin remodeling by actin binding proteins

In the cellular environment, a large cast of actin binding proteins establish spatial and temporal regulation of actin by influencing the unpolymerized and polymerized phases in order to tightly control the distribution, location, and kinetics of cytoplasmic actin [46]. The control mechanisms utilized by actin binding proteins can be generalized according

to their mechanism of action: barbed (gelsolin, capping protein) and pointed (tropomodulins, the Arp2/3 complex) end capping, barbed end anti-capping (Ena/VASPs), acceleration of filament depolymerization (ADF/cofilins), filament severing (gelsolin, ADF/cofilins), filament nucleation (the Arp2/3 complex), nucleotide exchange (profilin), and monomer sequestration (thymosins). Other actin binding proteins regulate cytoskeletal geometry by forming filament bundles (α-actinin), dendritic branches (the Arp2/3 complex), and orthogonal networks (filamins). To achieve the dynamic cycling rates and localized structural control of actin, many of these mechanisms behave synergistically [1, 32, 47, 48]. A few important actin binding proteins will be discussed here as examples of these general mechanisms of actin regulation.

Gelsolin

Gelsolin is an actin filament severing and barbed end capping protein [49]. When activated by μM calcium concentration, gelsolin binds to the side of an actin filament, interdigitates, and severs it with unmatched potency. After severing, gelsolin remains associated with the barbed filament end forming a tight cap. A severing/capping mechanism rapidly dissolves cytoskeletal networks by creating an increased number of short actin filaments that cannot anneal or rapidly elongate. Gelsolin can also initiate rapid actin filament polymerization and membrane protrusion through interactions with plasma membrane polyphosphoinositides that release gelsolin from the barbed ends [50, 51]. Gelsolin null mice exhibit deficiencies in wound healing, inflammation, and

thrombosis [52, 53]. Cells from these animals crawl poorly and organize pronounced stress fibers consistent with a diminished capability to sever actin filaments [52, 53]. Over-expression of gelsolin produces the opposite effect leading to increased membrane ruffling and chemotaxis [54]. Gelsolin also plays an important role in apoptosis as a substrate for caspase-3, which cleaves gelsolin to constituitively activate its severing function [55, 56]. In support, apoptotic cell death is delayed in cells that do not express gelsolin [56].

The Arp2/3 complex

The Arp2/3 complex binds to a preexisting actin filament, mimics a free barbed end, and nucleates a daughter filament at a 70° angle [57]. Nucleation by the Arp2/3 complex is activated by WASp/SCAR proteins [58] and may require the exposure of binding sites at barbed filament ends [59-61], although other reports maintain that nucleation can occur on the side of the parent filament [62-64]. The Arp2/3 complex also caps pointed filament ends with nM affinity [57], and is essential for rogue actin polymerization and the rocketing propulsion of the bacterial pathogens *Listeria* and *Shigella* [65]. Due to its ability to form a barbed end nucleation site, the Arp2/3 complex has been implicated in numerous models of cell membrane protrusion involving the formation of branched, dendritic actin networks [62, 66, 67]. However, branched actin filament networks created by the Arp2/3 complex alone are unlikely to account for the coherence of the leading edge of crawling cells, as the dendritic structures formed by the Arp2/3 complex are

unable to gel filament networks *in vitro* unless the potent actin filament cross-linking protein filamin is present [68].

ADF/cofilins

When barbed ends are capped, actin filament disassembly is slow, but it can be accelerated by actions of the ADF/cofilin protein family [69]. ADF/cofilin binds cooperatively to the sides of filaments [70], predominately at ADP-bound subunits which are in excess near the pointed filament end, and enhances the rate of pointed end subunit disassembly up to ~25-fold *in vitro* [71]. The depolymerization activity of ADF/cofilins is regulated by phosphorylation of serine-3. Phosphorylation of this residue by LIM kinase inactivates ADF/cofilin by inhibiting its ability to bind to actin filaments [72, 73]. This inhibition has been shown to be reversed by the Slingshot phosphatase [74]. Membrane phospholipids can also inactivate ADF/cofilins by inhibiting its ability to bind F-actin [75]. Kinetic analysis of actin filament dynamics *in vitro* reveals that accelerated filament turnover by ADF/cofilins produce net filament depolymerization in the presence of sequestering proteins [71], which, in cooperation with barbed end capping, has been postulated to account for the high rates of actin filament turnover observed *in vivo* [76]. ADF/cofilins have also been shown to be weak severing agents, fragmenting filaments near the pointed end, which increases end numbers and accelerates depolymerization if the newly formed barbed ends are capped [77-79] or polymerization if these ends remain free [80]. Recent studies support ADF/cofilin's proposed severing function, where local

uncaging of cofilin in cells increases barbed end exposure, F-actin content, locomotion, and determines the direction of cell migration [81].

Profilin

The intrinsic rate of nucleotide exchange on a free actin monomer can be accelerated by profilin, which binds to monomers in solution with high affinity [82], exchanges ADP for ATP ~140x faster than a monomer alone, and shuttles ATP-bound monomer to uncapped barbed ends [83, 84]. Profilin is inactivated by the membrane polyphosphoinositide PIP_2 [85]. Since the intrinsic rate of nucleotide exchange by actin during rapid filament turnover may be limiting in certain cases [32], profilin provides a mechanism to overcome this energetic barrier.

Ena/VASPs

Ena/VASPs interact with barbed filament ends at sites of actin assembly, such as the tips of lamelllipodia and filopodia, where they antagonize the activity of barbed end capping proteins, supporting F-actin assembly and causing filaments to grow longer and become less branched [86, 87]. This mechanism accounts for the diverse ability of these proteins to negatively regulate motility in fibroblasts [88], but accelerate the movement of *Listeria* in *in vitro* motility assays [65, 89]. The activity of Ena/VASP proteins are regulated by phosphorylation at serine 157 by cAMP dependent protein kinase [89, 90]. Phosphorylation at this site increases Ena/VASP binding to F-actin by about 40-fold.

Tropomodulins

Although most widely studied for their function capping the thin filaments of muscle sarcomeres, tropomodulins are also present in non-muscle cells where they cap actin filament pointed ends, a process that is dramatically enhanced in the presence of tropomyosins [91, 92]. The association of tropomodulins with pointed ends is transient, slowing polymerization at this end, which increases the levels of ADP-bound subunits at filament termini and leads to net depolymerization [93]. In endothelial cells, tropomodulin 3 expression negatively regulates cell movement, and results in a decrease in F-actin content and the number of free barbed ends [91], indicating that these events are regulated in a coordinated fashion during cell locomotion.

Thymosins

Thymosins are present in high concentrations in cells where they bind free monomers stoichiometrically and inhibit polymerization [94]. By sequestering cytoplasmic monomer at concentrations much higher than the critical concentration of purified actin, thymosins maintain large pools of unpolymerized actin available for the cell to incorporate into filaments as needed. A sequestered monomer has a higher affinity for the unpolymerized state than for polymerization at pointed actin filament ends, but not at barbed ends [94]. Therfore, as barbed ends are exposed, thymosin-sequestered monomer can polymerize specifically at these sites.

Filamins

Filamin family proteins are responsible for the creation and stabilization of actin filament networks [13]. Filamins are large, elongated, bivalent, flexible homodimers ~160 nm in length that bind and cross-link neighboring actin filaments into an orthogonal junction [95, 96]. Structurally, filamins are composed of an N-terminal actin binding domain followed by 24 repeat motifs having a β-barrel structure [97], where the terminal repeat at the C-terminus forms the dimerization domain [95, 98]. Filamins organize the cytoskeletal architecture from sites deep within the cell body up to the leading edge where they bind and affix the cytoskeleton to integral membrane proteins including β1 and β7 integrins and GP1bα [98, 99]. With a large and continually growing list of binding partners already discovered, filamins are likely to play a unique role as organizing centers for local cytoskeletal rearrangements [13].

Three filamin isoforms exist in humans, encoded by independent genes on different chromosomes and differentially expressed depending on the tissue of origin [100]. In non-muscle cells, filamin-A and filamin-B are the predominant isotypes [13], which abundantly localize to lamellipodia, promoting the formation of orthogonal filament arrays [14, 96], and also localize at the base of filopodia [101]. The importance of filamin-A in cytoskeletal organization and structure has been established in a natural occurring line of human melanoma cells that lack this protein [102, 103]. Despite expressing approximately wild-type levels of gelsolin, α-actinin, profilin, fodrin, and the Arp2/3 complex, filamin-A deficient cells are unable to crawl and have a surface replete

with spherical aneurysms (blebs) indicating a lack of cortical stability in the absence of FLNa [102, 103]. Rescuing these cells with filamin-A cDNA results in the reappearance of lamellar protrusions and membrane ruffles and restores a normal motile phenotype [103], as well as protecting them against apopototic cell death when mechanically stimulated on their surface by pulling on magnetic beads [104-106]. In humans, mutations of filamin-A, which is located on the X chromosome, result in severe congenital malformations of the brain, skeleton, viscera, and urogenital tract due to a putative gain of function effect [107]. Complete deletion of filamin-A is male embryonic lethal. Female filamin-A heterozygotes survive with the disease periventricular heterotopia, which is characterized by abnormal brain development, seizures, and vascular complications [108].

Cell crawling

To move, a cell must selectively build, compress, and destroy its actin-based structures in discrete regions. At the leading edge of a motile cell, actin polymerization drives membrane protrusion [109, 110]. As polymerization continues, actin filaments formed at the periphery transport into the cell's interior where they are depolymerized to recycle actin monomers for assembly elsewhere [10, 11, 38, 111, 112]. At steady state, cells crawl by balanced actin polymerization and depolymerization under the control of actin binding proteins [16, 76]. The ratio of actin monomer to polymer, the average cytoskeleton filament length, and the filament turnover time are determining factors that modulate the speed at which a cell moves across a substrate [1, 40]. For example, as

endothelial cells and fibroblasts crawl faster their filament turnover times and polymerized actin fractions decrease [1, 40]. The measured correlations between cell speed and actin dynamics provide strong evidence supporting a direct link between cytoskeleton remodeling and cell locomotion.

Fluorescence techniques for measuring actin dynamics

Actin dynamics can be measured in single cells with variable precision. Two analogous fluorescence techniques provide some of the best estimates of parameters that describe the dynamic nature of actin networks: photoactivation of fluorescence (PAF) and

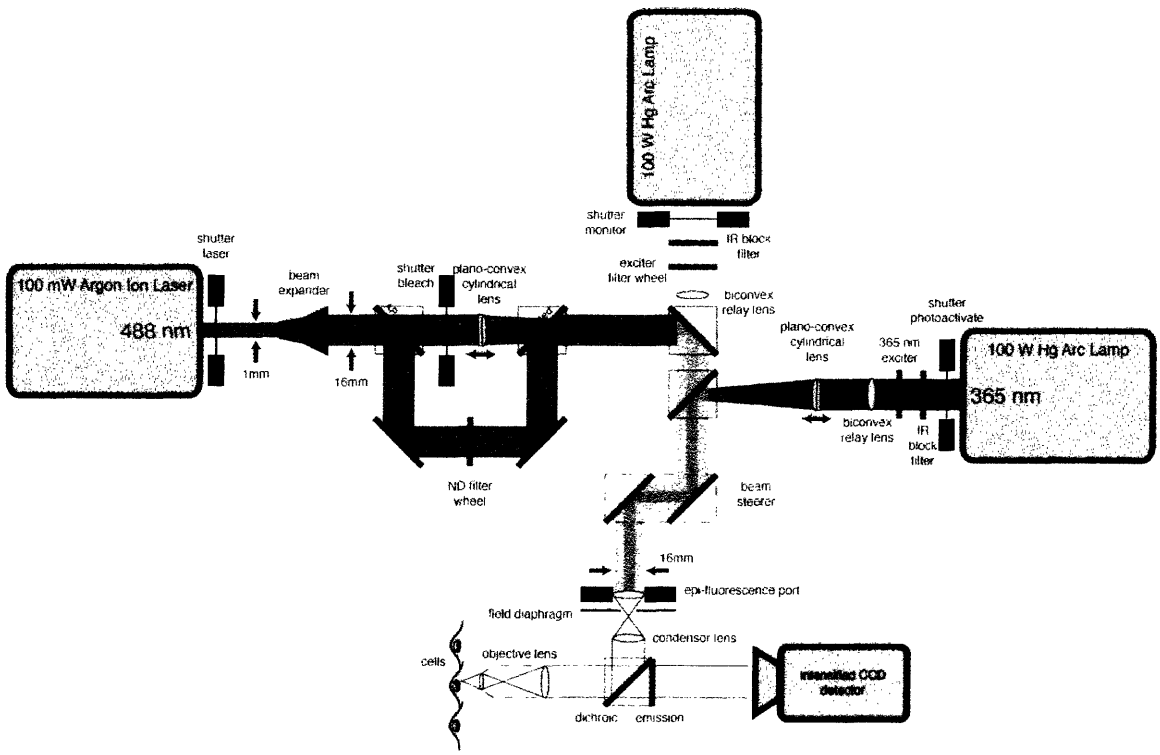

Fig. I-3. *Schematic design of a PAF/FRAP microscopy system.* Sample photoactivation or photobleaching is performed by two opposing light sources focused to a narrow rectangular band. Global excitation of the fluorophore for monitoring purposes is achieved with a third, perpendicular light source. Fluorescence emission is collected by a computer controlled intensified CCD camera.

fluorescence recovery after photobleaching (FRAP) (Fig. I-3). In PAF, a non-fluorescent, caged precursor actin molecule is selectively uncaged by exposure to ultraviolet (UV) light in a small spot or rectangular region within the cell [40, 113, 114]. FRAP is the inverse technique, in which the fluorescence of a labeled actin molecule is quenched with high-intensity light at the excitation wavelength of the fluorophores [115]. While PAF has inherent signal-to-noise advantages over FRAP [116], the advent of green fluorescent proteins and its colored variants are allowing new and exciting applications for FRAP technology using molecular fusion proteins [117]. Once the fluorescent actin derivative is uncaged or bleached, the fluorescence decay or recovery at the center of the photoactivated or photobleached region, respectively, is monitored over time. Using an interpretive model that describes the actin remodeling processes underlying the fluorescence evolution, appropriate physical parameters can be extracted and analyzed [116].

A mathematical description of actin dynamics

One mathematical model describing PAF- and FRAP-based actin dynamics, the Tardy Model, provides simultaneous estimates of the translational diffusion coefficient of actin monomer, the fraction of total actin polymerized, and the actin filament turnover time [116], and has been used to quantitate actin dynamics in various cell types such as endothelium, fibroblasts, and melanoma cells [1, 40], yielding results consistent with those previously published by other investigators [11, 38, 39, 41]. Although this model was developed to analyze cellular actin dynamics, the simplified rectangular cell

geometry and assumptions (e.g. homogeneous sample, no nucleus or organelles) inherent in the theory are equally suited for probing the dynamics of purified actin preparations.

The general mathematical problem defined by the Tardy Model involve one-dimensional, unsteady, coupled partial differential equations that describe actin monomer diffusion and filament turnover in a model cell. The general solution is represented as an infinite series for both actin monomer and filament concentrations. The result is a biphasic response, where the short-term dynamics are primarily due to monomer diffusion and the long-term to filament turnover, that depend strongly the ratio of the monomer diffusion and filament turnover times [116]. Under certain conditions when monomer diffusion is rapid compared to filament turnover, as typically is the case in purified actin solutions, the general solution to the long-term fluorescence can be simplified to a decaying exponential, where the y-intercept represents the 'immobile' fluorescence fraction and the decay constant is the filament turnover time [116].

Potential deleterious effects of photoactivation and photobleaching

While PAF and FRAP are generally non-invasive techniques that require only short exposures to light to initiate experiments, phototoxicity, photodissolution, and local heating of actin during uncaging, bleaching, and fluorescence excitation remain important factors to consider. These destructive processes can potentially induce actin filament and monomer crosslinking, denature actin protein structure, and/or break actin filaments. Estimation of the photoactivation (~100 kW/m^2) and excitation (~10 kW/m^2)

fluorescence intensities at the sample [118] classifies these light levels as low excitation intensities (< 5 MW/m^2) according to Vigers and colleagues [119]. At low light excitation levels, both actin and microtubules have the potential to fracture and dissolve after as short as ~1 min of continuous illumination [119, 120]. To mitigate these effects, light exposure must be minimized during sampling. Surface heating of the actin solution is less problematic, since even at the high laser intensities (> 5 MW/m^2) used to photobleach samples for FRAP experiments, the amount of sample heating is estimated to be less than 0.1°C [121]. Finally, the best evidence that F-actin phototoxicity is minimal after light exposure is measurements that photobleached or photoactivated actin filament lifetimes are similar to previously published values using alternative methods [16].

Endothelial cells

Endothelial cells, which line the inner surface of the vasculature, depend on proper actin cytoskeletal structure and dynamics. Situated at the barrier between flowing blood and soft tissue, the endothelium senses fluid forces and extracellular, soluble chemical signals in the blood to regulate macromolecule permeability, maintain vascular tone, and provide a surface resistant to blood clot formation [122]. Damage to the endothelial lining promotes thrombotic episodes, potentially resulting in myocardial infarction and stroke. In response to vascular wounding and signals promoting angiogenesis, endothelial cells are stimulated to move, redefining and remodeling their actin cytoskeletons. The fraction of total cellular actin incorporated into filaments, the lifetime of these filaments, the structure of the actin cytoskeleton, and the linkages between actin and cell-substrate

adhesion sites determine the cell's shape, stiffness, potential to crawl, and integrity of attachment to the artery wall, all of which affect endothelial function *in vivo*.

Endothelial cells are constantly subjected to mechanical forces that oscillate with variable magnitude and direction as blood is pumped over them during each cardiac cycle [122]. The hemodynamic environment and mechanical forces experienced by endothelial cells *in vivo* at different regions within the arterial system strongly influence their function [122] . The wall shear stress, one component of the applied force, has been shown to be particularly important in regulating endothelial cell function and has been postulated as a key parameter that modulates atherogenesis [122, 123]. Atherosclerotic lesions develop predominately at regions within the arterial tree where large fluctuations and gradients in the wall shear stress occur, such as highly curved or bifurcating blood vessels [124]. *In vitro* models of the *in vivo* environment have been used successfully for many years in order to decipher the mechanisms responsible for endothelial sensation and response to fluid flow [125-129].

The most striking aspect of the endothelial shear stress sensitivity is the marked shape change that occurs when shear stress is chronically applied to its apical surface [129]. In static culture, endothelial cells form a tightly packed, cobblestone monolayer. Subjecting these cells to laminar, steady fluid flow is sufficient to cause them to align and elongate in the direction of applied flow forming torpedo shapes and developing similarly oriented, prominent actin stress fibers [129, 130]. This occurs through a cascade of events that ultimately drives reorganization of the underlying actin filament network [122, 131]. These morphological changes are the eventual result of mechanisms that transduce

mechanical surface perturbations into intracellular chemical and molecular signals that impinge on the actin cytoskeleton [122, 123].

Endothelial cell actin dynamics in static culture

When a small region within an endothelial cell monolayer is denuded, adjacent cells migrate into the wound at speeds proportional to their distance from the wound edge [1]. The fastest cells are situated within the wound unimpeded by surrounding cells, while the slowest are far from the wound edge in the intact confluent monolayer. Filament turnover and polymer content correlate with cell speed such that the fastest cells contain the least amount of polymerized actin and exhibit the most rapid rates of filament turnover (Fig. I-4) [1]. While depolymerization coupled with accelerated filament turnover has been attributed to the ADF/cofilin family of actin binding proteins [69, 71], slower moving endothelial cells in static culture contain more F-actin associated cofilin. Since lack of

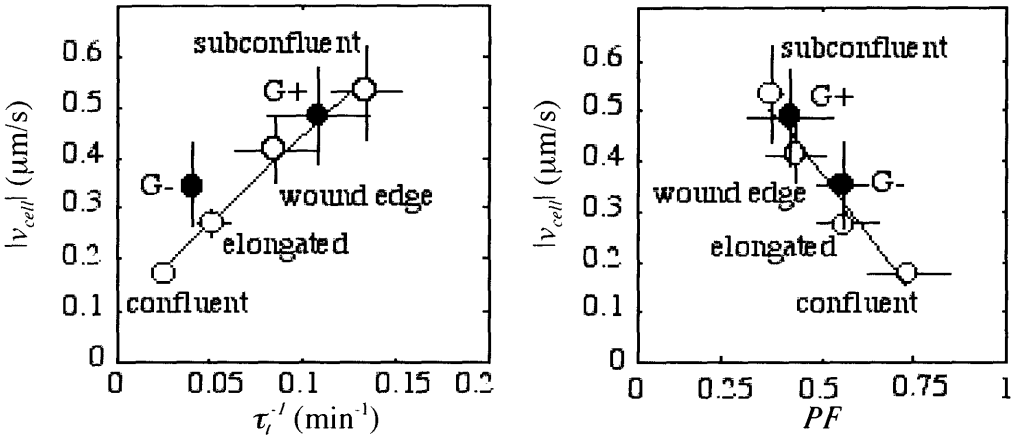

Fig. I-4. *Actin dynamics correlate with cell speed.* Endothelial cells that crawl faster have more rapid filament turnover rates (τ_t^{-1}) and less total actin polymerized (*PF*). Subconfluent mouse fibroblasts (●) that express (G+) or lack (G-) gelsolin follow a similar correlation. Adapted from reference [1].

gelsolin in dermal fibroblasts from gelsolin knockout mice slows their speed and actin dynamics in a similar fashion to endothelial cells, it has been postulated that the motile transition in endothelial cells is controlled by a gelsolin-mediated severing mechanism that liberates new pointed ends for ADF/cofilin to rapidly depolymerize [1].

References

1. McGrath, J.L., et al., *Regulation of the actin cycle in vivo by actin filament severing.* Proc Natl Acad Sci U S A, 2000. **97**(12): p. 6532-6537.
2. Oster, G.F., *On the crawling of cells.* J Embryol Exp Morphol, 1984. **83 Suppl**: p. 329-64.
3. Oster, G.F. and A.S. Perelson, *The physics of cell motility.* J Cell Sci Suppl, 1987. **8**: p. 35-54.
4. Oster, G., *Brownian ratchets: Darwin's motors.* Nature, 2002. **417**(6884): p. 25.
5. Evans, E., *New physical concepts for cell amoeboid motion.* Biophys J, 1993. **64**(4): p. 1306-22.
6. Lauffenburger, D.A. and A.F. Horwitz, *Cell migration: a physically integrated molecular process.* Cell, 1996. **84**(3): p. 359-69.
7. Lauffenburger, D.A., *Molecules, mechanics, and migration of cells.* Appl Mech Rev, 1994. **47**(6, pt 2): p. S287-S290.
8. Bray, D. and C. Thomas, *Unpolymerized actin in fibroblast and brain.* J Mol Biol, 1976. **16**: p. 1055-1069.
9. Carlsson, L., et al., *Profilin, a low molecular weight protein controlling actin polymerisability*, in *Contractile systems in non-muscle tissues*, S.V. Perry, A. Margreth, and R.S. Adelstein, Editors. 1976, Elsevier/North-Holland Biomedical Press: Amsterdam. p. 39-49.
10. Theriot, J.A. and T.J. Mitchison, *Comparison of actin and cell surface dynamics in motile fibroblasts.* J Cell Biol, 1992. **119**(2): p. 367-77.
11. Theriot, J.A. and T.J. Mitchison, *Actin microfilament dynamics in locomoting cells.* Nature, 1991. **352**(6331): p. 126-31.
12. Condeelis, J., *Are all pseudopods created equal?* Cell Motility and the Cytoskeleton, 1992. **22**: p. 1-6.
13. Stossel, T.P., et al., *Filamins as integrators of cell mechanics and signalling.* Nat Rev Mol Cell Biol, 2001. **2**(2): p. 138-45.
14. Hartwig, J.H. and P. Shevlin, *The architecture of actin filaments and the ultrastructural location of actin-binding protein in the periphery of lung macrophages.* J Cell Biol, 1986. **103**(3): p. 1007-20.
15. Wegner, A., *Head to tail polymerization of actin.* J Mol Biol, 1976. **108**(1): p. 139-50.
16. Zigmond, S.H., *Recent quantitative studies of actin filament turnover during cell locomotion.* Cell Motil Cytoskeleton, 1993. **25**(4): p. 309-16.

17. Janmey, P.A. and C. Chaponnier, *Medical aspects of the actin cytoskeleton.* Curr Opin Cell Biol, 1995. **7**(1): p. 111-7.

18. Elzinga, M., et al., *Complete amino-acid sequence of actin of rabbit skeletal muscle.* Proc Natl Acad Sci U S A, 1973. **70**(9): p. 2687-91.

19. Hightower, R.C. and R.B. Meagher, *The molecular evolution of actin.* Genetics, 1986. **114**(1): p. 315-32.

20. Pollard, T.D., *Actin.* Curr Opin Cell Biol, 1990. **2**(1): p. 33-40.

21. Vandekerckhove, J. and K. Weber, *At least six different actins are expressed in a higher mammal: an analysis based on the amino acid sequence of the amino-terminal tryptic peptide.* J Mol Biol, 1978. **126**(4): p. 783-802.

22. Herman, I.M., *Actin isoforms.* Curr Opin Cell Biol, 1993. **5**(1): p. 48-55.

23. Otterbein, L.R., P. Graceffa, and R. Dominguez, *The crystal structure of uncomplexed actin in the ADP state.* Science, 2001. **293**(5530): p. 708-11.

24. Kabsch, W., et al., *Atomic structure of the actin:DNase I complex.* Nature, 1990. **347**(6288): p. 37-44.

25. Carlier, M.F., D. Pantaloni, and E.D. Korn, *Fluorescence measurements of the binding of cations to high-affinity and low-affinity sites on ATP-G-actin.* J Biol Chem, 1986. **261**(23): p. 10778-84.

26. Frieden, C., D. Lieberman, and H.R. Gilbert, *A fluorescent probe for conformational changes in skeletal muscle G- actin.* J Biol Chem, 1980. **255**(19): p. 8991-3.

27. Carlier, M.F., D. Pantaloni, and E.D. Korn, *The effects of Mg2+ at the high-affinity and low-affinity sites on the polymerization of actin and associated ATP hydrolysis.* J Biol Chem, 1986. **261**(23): p. 10785-92.

28. Oosawa, F., *Size distribution of protein polymers.* J Theor Biol, 1970. **27**(1): p. 69-86.

29. Wegner, A. and J. Engel, *Kinetics of the cooperative association of actin to actin filaments.* Biophys Chem, 1975. **3**(3): p. 215-25.

30. Pollard, T.D., *Rate constants for the reactions of ATP- and ADP-actin with the ends of actin filaments.* J Cell Biol, 1986. **103**(6 Pt 2): p. 2747-54.

31. Korn, E.D., M.F. Carlier, and D. Pantaloni, *Actin polymerization and ATP hydrolysis.* Science, 1987. **238**(4827): p. 638-44.

32. Bindschadler, M., et al., *A mechanistic model of the actin cycle in cells.* Biophys J, 2004.

33. Bonder, E.M., D.J. Fishkind, and M.S. Mooseker, *Direct measurement of critical concentrations and assembly rate constants at the two ends of an actin filament.* Cell, 1983. **34**: p. 491-501.

34. Holmes, K.C., et al., *Atomic model of the actin filament.* Nature, 1990. **347**(6288): p. 44-9.

35. Milligan, R.A., M. Whittaker, and D. Safer, *Molecular structure of F-actin and location of surface binding sites.* Nature, 1990. **348**(6298): p. 217-21.

36. Amos, L.A., *Structure of muscle filaments studied by electron microscopy.* Annu Rev Biophys Biophys Chem, 1985. **14**: p. 291-313.

37. Selve, N. and A. Wegner, *Rate of treadmilling of actin filaments in vitro.* J Mol Biol, 1986. **187**(4): p. 627-31.

38. Wang, Y.L., *Exchange of actin subunits at the leading edge of living fibroblasts: possible role of treadmilling.* J Cell Biol, 1985. **101**(2): p. 597-602.

39. Theriot, J.A. and T.J. Mitchison, *Comparison of actin and cell surface dynamics in motile fibroblasts.* J Cell Biol, 1992. **119**(2): p. 367-77.

40. McGrath, J.L., et al., *Simultaneous measurements of actin filament turnover, filament fraction, and monomer diffusion in endothelial cells.* Biophys J, 1998. **75**(4): p. 2070-8.

41. Kreis, T.E., B. Geiger, and J. Schlessinger, *Mobility of microinjected rhodamine actin within living chicken gizzard cells determined by fluorescence photobleaching recovery.* Cell, 1982. **29**(3): p. 835-45.

42. Luby-Phelps, K., D.L. Taylor, and F. Lanni, *Probing the structure of cytoplasm.* J Cell Biol, 1986. **102**(6): p. 2015-22.

43. Satcher, R.L., Jr. and C.F. Dewey, Jr., *Theoretical estimates of mechanical properties of the endothelial cell cytoskeleton [see comments].* Biophys J, 1996. **71**(1): p. 109-18.

44. Bartles, J.R., *Parallel actin bundles and their multiple actin-bundling proteins.* Curr Opin Cell Biol, 2000. **12**(1): p. 72-8.

45. Sund, S.E. and D. Axelrod, *Actin dynamics at the living cell submembrane imaged by total internal reflection fluorescence photobleaching.* Biophys J, 2000. **79**(3): p. 1655-69.

46. dos Remedios, C.G., et al., *Actin binding proteins: regulation of cytoskeletal microfilaments.* Physiol Rev, 2003. **83**(2): p. 433-73.

47. Didry, D., M.F. Carlier, and D. Pantaloni, *Synergy between actin depolymerizing factor/cofilin and profilin in increasing actin filament turnover.* J Biol Chem, 1998. **273**(40): p. 25602-11.

48. Dufort, P.A. and C.J. Lumsden, *How profilin/barbed-end synergy controls actin polymerization: a kinetic model of the ATP hydrolysis circuit.* Cell Motil Cytoskeleton, 1996. **35**(4): p. 309-30.

49. Sun, H.Q., et al., *Gelsolin, a multifunctional actin regulatory protein.* J Biol Chem, 1999. **274**(47): p. 33179-82.

50. Janmey, P.A., et al., *Polyphosphoinositide micelles and polyphosphoinositide-containing vesicles dissociate endogenous gelsolin-actin complexes and promote actin assembly from the fast-growing end of actin filaments blocked by gelsolin.* J Biol Chem, 1987. **262**(25): p. 12228-36.

51. Hartwig, J.H., et al., *Thrombin receptor ligation and activated Rac uncap actin filament barbed ends through phosphoinositide synthesis in permeabilized human platelets.* Cell, 1995. **82**(4): p. 643-53.

52. Witke, W., et al., *Hemostatic, inflammatory, and fibroblast responses are blunted in mice lacking gelsolin.* Cell, 1995. **81**(1): p. 41-51.

53. Azuma, T., et al., *Gelsolin is a downstream effector of rac for fibroblast motility.* Embo J, 1998. **17**(5): p. 1362-70.

54. Cunningham, C.C., T.P. Stossel, and D.J. Kwiatkowski, *Enhanced motility in NIH 3T3 fibroblasts that overexpress gelsolin.* Science, 1991. **251**(4998): p. 1233-6.

55. Kwiatkowski, D.J., *Functions of gelsolin: motility, signaling, apoptosis, cancer.* Curr Opin Cell Biol, 1999. **11**(1): p. 103-8.

56. Kothakota, S., et al., *Caspase-3-generated fragment of gelsolin: effector of morphological change in apoptosis.* Science, 1997. **278**(5336): p. 294-8.

57. Mullins, R.D., J.A. Heuser, and T.D. Pollard, *The interaction of Arp2/3 complex with actin: nucleation, high affinity pointed end capping, and formation of branching networks of filaments.* Proc Natl Acad Sci U S A, 1998. **95**(11): p. 6181-6.

58. Machesky, L.M., et al., *Scar, a WASp-related protein, activates nucleation of actin filaments by the Arp2/3 complex.* Proc Natl Acad Sci U S A, 1999. **96**(7): p. 3739-44.

59. Falet, H., et al., *Importance of free actin filament barbed ends for Arp2/3 complex function in platelets and fibroblasts.* Proc Natl Acad Sci U S A, 2002. **99**(26): p. 16782-7.

60. Pantaloni, D., et al., *The Arp2/3 complex branches filament barbed ends: functional antagonism with capping proteins.* Nat Cell Biol, 2000. **2**(7): p. 385-91.

61. Ichetovkin, I., W. Grant, and J. Condeelis, *Cofilin produces newly polymerized actin filaments that are preferred for dendritic nucleation by the Arp2/3 complex.* Curr Biol, 2002. **12**(1): p. 79-84.

62. Amann, K.J. and T.D. Pollard, *The Arp2/3 complex nucleates actin filament branches from the sides of pre-existing filaments.* Nat Cell Biol, 2001. **3**(3): p. 306-10.

63. Amann, K.J. and T.D. Pollard, *Direct real-time observation of actin filament branching mediated by Arp2/3 complex using total internal reflection fluorescence microscopy*. Proc Natl Acad Sci U S A, 2001. **98**(26): p. 15009-13.

64. Carlsson, A.E., M.A. Wear, and J.A. Cooper, *End versus Side Branching by Arp2/3 Complex*. Biophys J, 2004. **86**(2): p. 1074-81.

65. Loisel, T.P., et al., *Reconstitution of actin-based motility of Listeria and Shigella using pure proteins*. Nature, 1999. **401**(6753): p. 613-6.

66. Pollard, T.D. and G.G. Borisy, *Cellular motility driven by assembly and disassembly of actin filaments*. Cell, 2003. **112**(4): p. 453-65.

67. Svitkina, T.M. and G.G. Borisy, *Arp2/3 complex and actin depolymerizing factor/cofilin in dendritic organization and treadmilling of actin filament array in lamellipodia*. J Cell Biol, 1999. **145**(5): p. 1009-26.

68. Nakamura, F., et al., *Comparison of filamin A-induced cross-linking and Arp2/3 complex- mediated branching on the mechanics of actin filaments*. J Biol Chem, 2002. **277**(11): p. 9148-54.

69. Bamburg, J.R., *Proteins of the ADF/cofilin family: essential regulators of actin dynamics*. Annu Rev Cell Dev Biol, 1999. **15**: p. 185-230.

70. McGough, A., et al., *Cofilin changes the twist of F-actin: implications for actin filament dynamics and cellular function*. J Cell Biol, 1997. **138**(4): p. 771-81.

71. Carlier, M.F., et al., *Actin depolymerizing factor (ADF/cofilin) enhances the rate of filament turnover: implication in actin-based motility*. J Cell Biol, 1997. **136**(6): p. 1307-22.

72. Arber, S., et al., *Regulation of actin dynamics through phosphorylation of cofilin by LIM- kinase [see comments]*. Nature, 1998. **393**(6687): p. 805-9.

73. Yang, N., et al., *Cofilin phosphorylation by LIM-kinase 1 and its role in Rac-mediated actin reorganization*. Nature, 1998. **393**(6687): p. 809-12.

74. Niwa, R., et al., *Control of actin reorganization by Slingshot, a family of phosphatases that dephosphorylate ADF/cofilin*. Cell, 2002. **108**(2): p. 233-46.

75. Yonezawa, N., et al., *Inhibition of the interactions of cofilin, destrin, and deoxyribonuclease I with actin by phosphoinositides*. J Biol Chem, 1990. **265**(15): p. 8382-6.

76. Carlier, M.F. and D. Pantaloni, *Control of actin dynamics in cell motility*. J Mol Biol, 1997. **269**(4): p. 459-67.

77. Du, J. and C. Frieden, *Kinetic studies on the effect of yeast cofilin on yeast actin polymerization*. Biochemistry, 1998. **37**(38): p. 13276-84.

78. Maciver, S.K., H.G. Zot, and T.D. Pollard, *Characterization of actin filament severing by actophorin from Acanthamoeba castellanii*. J Cell Biol, 1991. **115**(6): p. 1611-20.

79. Maciver, S.K., et al., *The effect of two actin depolymerizing factors (ADF/cofilins) on actin filament turnover: pH sensitivity of F-actin binding by human ADF, but not of Acanthamoeba actophorin*. Eur J Biochem, 1998. **256**(2): p. 388-97.

80. Condeelis, J., *How is actin polymerization nucleated in vivo?* Trends Cell Biol, 2001. **11**(7): p. 288-93.

81. Ghosh, M., et al., *Cofilin promotes actin polymerization and defines the direction of cell motility*. Science, 2004. **304**(5671): p. 743-6.

82. Perelroizen, I., et al., *Role of nucleotide exchange and hydrolysis in the function of profilin in actin assembly*. J Biol Chem, 1996. **271**(21): p. 12302-9.

83. Selden, L.A., et al., *Impact of profilin on actin-bound nucleotide exchange and actin polymerization dynamics*. Biochemistry, 1999. **38**(9): p. 2769-78.

84. Goldschmidt-Clermont, P.J., et al., *Mechanism of the interaction of human platelet profilin with actin*. J Cell Biol, 1991. **113**(5): p. 1081-9.

85. Lassing, I. and U. Lindberg, *Specific interaction between phosphatidylinositol 4,5-bisphosphate and profilactin*. Nature, 1985. **314**(6010): p. 472-4.

86. Krause, M., et al., *The Ena/VASP enigma*. J Cell Sci, 2002. **115**(Pt 24): p. 4721-6.

87. Bear, J.E., et al., *Antagonism between Ena/VASP proteins and actin filament capping regulates fibroblast motility*. Cell, 2002. **109**(4): p. 509-21.

88. Bear, J.E., et al., *Negative regulation of fibroblast motility by Ena/VASP proteins*. Cell, 2000. **101**(7): p. 717-28.

89. Laurent, V., et al., *Role of proteins of the Ena/VASP family in actin-based motility of Listeria monocytogenes*. J Cell Biol, 1999. **144**(6): p. 1245-58.

90. Gertler, F.B., et al., *Mena, a relative of VASP and Drosophila Enabled, is implicated in the control of microfilament dynamics*. Cell, 1996. **87**(2): p. 227-39.

91. Fischer, R.S., K.L. Fritz-Six, and V.M. Fowler, *Pointed-end capping by tropomodulin3 negatively regulates endothelial cell motility*. J Cell Biol, 2003. **161**(2): p. 371-80.

92. Fowler, V.M., *Tropomodulin: a cytoskeletal protein that binds to the end of erythrocyte tropomyosin and inhibits tropomyosin binding to actin*. J Cell Biol, 1990. **111**(2): p. 471-81.

93. Littlefield, R., A. Almenar-Queralt, and V.M. Fowler, *Actin dynamics at pointed ends regulates thin filament length in striated muscle*. Nat Cell Biol, 2001. **3**(6): p. 544-51.

94. Safer, D. and V.T. Nachmias, *Beta thymosins as actin binding peptides [published erratum appears in Bioessays 1994 Aug;16(8):590].* Bioessays, 1994. **16**(7): p. 473-9.

95. Hartwig, J.H. and T.P. Stossel, *Structure of macrophage actin-binding protein molecules in solution and interacting with actin filaments.* J Mol Biol, 1981. **145**(3): p. 563-81.

96. Hartwig, J.H., J. Tyler, and T.P. Stossel, *Actin-binding protein promotes the bipolar and perpendicular branching of actin filaments.* J Cell Biol, 1980. **87**(3 Pt 1): p. 841-8.

97. Fucini, P., et al., *Molecular architecture of the rod domain of the Dictyostelium gelation factor (ABP120).* J Mol Biol, 1999. **291**(5): p. 1017-23.

98. Gorlin, J.B., et al., *Human endothelial actin-binding protein (ABP-280, nonmuscle filamin): a molecular leaf spring.* J Cell Biol, 1990. **111**(3): p. 1089-105.

99. Pfaff, M., et al., *Integrin beta cytoplasmic domains differentially bind to cytoskeletal proteins.* J Biol Chem, 1998. **273**(11): p. 6104-9.

100. van der Flier, A. and A. Sonnenberg, *Structural and functional aspects of filamins.* Biochim Biophys Acta, 2001. **1538**(2-3): p. 99-117.

101. Ohta, Y., et al., *The small GTPase RalA targets filamin to induce filopodia.* Proc Natl Acad Sci U S A, 1999. **96**(5): p. 2122-8.

102. Cunningham, C.C., *Actin polymerization and intracellular solvent flow in cell surface blebbing.* J Cell Biol, 1995. **129**(6): p. 1589-99.

103. Cunningham, C.C., et al., *Actin-binding protein requirement for cortical stability and efficient locomotion.* Science, 1992. **255**(5042): p. 325-7.

104. Glogauer, M., et al., *The role of actin-binding protein 280 in integrin-dependent mechanoprotection.* J Biol Chem, 1998. **273**(3): p. 1689-98.

105. Kainulainen, T., et al., *Cell death and mechanoprotection by filamin a in connective tissues after challenge by applied tensile forces.* J Biol Chem, 2002. **277**(24): p. 21998-2009.

106. D'Addario, M., et al., *Cytoprotection against mechanical forces delivered through beta 1 integrins requires induction of filamin A.* J Biol Chem, 2001. **276**(34): p. 31969-77.

107. Robertson, S.P., et al., *Localized mutations in the gene encoding the cytoskeletal protein filamin A cause diverse malformations in humans.* Nat Genet, 2003. **33**(4): p. 487-91.

108. Fox, J.W., et al., *Mutations in filamin 1 prevent migration of cerebral cortical neurons in human periventricular heterotopia.* Neuron, 1998. **21**(6): p. 1315-25.

109. Mogilner, A. and G. Oster, *Cell motility driven by actin polymerization.* Biophys J, 1996. **71**(6): p. 3030-45.

110. Cooper, J.A., *The role of actin polymerization in cell motility.* Annu Rev Physiol, 1991. **53**: p. 585-605.

111. Welch, M.D., et al., *Actin dynamics in vivo.* Curr Opin Cell Biol, 1997. **9**(1): p. 54-61.

112. Watanabe, N. and T.J. Mitchison, *Single molecule speckle analysis of actin filament turnover in lamellipodia.* Science (submitted), 2001.

113. McCray, J.A. and D.R. Trentham, *Properties and uses of photoreactive caged compounds.* Annu Rev Biophys Biophys Chem, 1989. **18**: p. 239-70.

114. Lippincott-Schwartz, J., N. Altan-Bonnet, and G.H. Patterson, *Photobleaching and photoactivation: following protein dynamics in living cells.* Nat Cell Biol, 2003. **Suppl**: p. S7-14.

115. Reits, E.A. and J.J. Neefjes, *From fixed to FRAP: measuring protein mobility and activity in living cells.* Nat Cell Biol, 2001. **3**(6): p. E145-7.

116. Tardy, Y., et al., *Interpreting photoactivated fluorescence microscopy measurements of steady-state actin dynamics.* Biophys J, 1995. **69**(5): p. 1674-82.

117. Lippincott-Schwartz, J. and G.H. Patterson, *Development and use of fluorescent protein markers in living cells.* Science, 2003. **300**(5616): p. 87-91.

118. Ishihara, A., et al., *Photoactivation of caged compounds in single living cells: an application to the study of cell locomotion.* Biotechniques, 1997. **23**(2): p. 268-74.

119. Vigers, G.P., M. Coue, and J.R. McIntosh, *Fluorescent microtubules break up under illumination.* J Cell Biol, 1988. **107**(3): p. 1011-24.

120. Simon, J.R., et al., *Analysis of rhodamine and fluorescein-labeled F-actin diffusion in vitro by fluorescence photobleaching recovery.* Biophys J, 1988. **54**(5): p. 801-15.

121. Axelrod, D., *Cell surface heating during fluorescence photobleaching recovery experiments.* Biophys J, 1977. **18**(1): p. 129-31.

122. Davies, P.F., *Flow-mediated endothelial mechanotransduction.* Physiol Rev, 1995. **75**(3): p. 519-60.

123. Nerem, R.M., et al., *Hemodynamics and vascular endothelial biology.* J Cardiovasc Pharmacol, 1993. **21**(Suppl 1): p. S6-10.

124. Davies, P.F., *Spatial hemodynamics, the endothelium, and focal atherogenesis: a cell cycle link?* Circ Res, 2000. **86**(2): p. 114-6.

125. Bindschadler, M., et al., *A mechanistic model of the actin cycle.* Biophys J, 2004. **86**(5): p. 2720-39.

126. DePaola, N., et al., *Vascular endothelium responds to fluid shear stress gradients [published erratum appears in Arterioscler Thromb 1993 Mar;13(3):465].* Arterioscler Thromb, 1992. **12**(11): p. 1254-7.

127. Davies, P.F., et al., *Turbulent fluid shear stress induces vascular endothelial cell turnover in vitro.* Proc Natl Acad Sci U S A, 1986. **83**(7): p. 2114-7.

128. Helmlinger, G., et al., *Effects of pulsatile flow on cultured vascular endothelial cell morphology.* J Biomech Eng, 1991. **113**(2): p. 123-31.

129. Dewey, C.F., Jr., et al., *The dynamic response of vascular endothelial cells to fluid shear stress.* J Biomech Eng, 1981. **103**(3): p. 177-85.

130. Satcher, R., C.F. Dewey, Jr., and J.H. Hartwig, *Mechanical remodeling of the endothelial surface and actin cytoskeleton induced by fluid flow.* Microcirculation, 1997. **4**(4): p. 439-53.

131. Davies, P.F., et al., *Spatial relationships in early signaling events of flow-mediated endothelial mechanotransduction.* Annu Rev Physiol, 1997. **59**: p. 527-49.

Chapter II

Endothelial Actin Cytoskeleton Remodeling During Mechanostimulation with Fluid Shear Stress

Eric A. Osborn[1,2], Aleksandr Rabodzey[3], John H. Hartwig[2], and C. Forbes Dewey Jr.[4]

1. Division of Health Sciences and Technology, Harvard University - Massachusetts Institute of Technology, Cambridge MA 02139

2. Hematology Division, Brigham and Women's Hospital and Harvard Medical School, Boston MA 02115

3. Biological Engineering Division, Massachusetts Institute of Technology, Cambridge MA 02139

4. Department of Mechanical Engineering, Massachusetts Institute of Technology, Cambridge MA 02139

Work not performed by E. Osborn:

A. Rabodzey tracked endothelial cells and measured crawling speeds.

Abstract

Fluid shear stress stimulation induces endothelial cells to elongate and align in the direction of applied flow. Alignment requires 24 h of exposure to flow, but the cells respond within minutes to flow by diminishing their movements by 50%. Although movement slows, actin filament turnover times and the amount of polymerized actin in cells decreases, increasing actin filament remodeling in individual cells composing a confluent endothelial monolayer to levels used by disperse, non-confluent cells for rapid movement. Hours later, motility returns to pre-shear stress levels, but actin remodeling remains highly dynamic in many cells. We conclude that shear stress initiates a cytoplasmic actin remodeling response that is used to modify endothelial cell shape instead of bulk cell translocation.

Introduction

Atherosclerotic lesions develop at predictable locations in the arterial vascular network, primarily forming where vessels branch and bend while largely sparing nearby straight vessel segments [1]. Vessel bending and branching locally disturbs normal blood flow patterns, generating complex regions of flow separation and recirculation that alter the magnitude, direction, and frequency of forces applied to the vessel wall [2-4]. Endothelial cells, which line the vessel wall and function to regulate vascular homeostasis, are exquisitely sensitive to the forces produced by flowing blood [5-7]. The blood flow profiles present at atherogenic regions cause endothelial injury and chronic dysfunction, leading to the accumulation of lipids in the vessel wall that eventually form atherosclerotic plaques [8, 9].

One of the most obvious markers of endothelial dysfunction *in vivo* is a disorganization of cell shapes. Endothelial cells that populate atheroprotective regions are elongated into torpedo shapes that point into the direction of flow [10], while those located at atherogenic regions are more cuboidal [11]. These observations are reproduced *in vitro* by exposing primary endothelial cell cultures to fluid shear stress using different flow profiles [7, 12-14]. Such studies, combined with computational modeling efforts, have confirmed that it is the arterial regions with the lowest shear stress that correlate with aberrant endothelial cell shapes and are at greatest risk of atherosclerotic lesion development [9].

Although the mechanosensitive molecular mechanisms that determine shear stress-mediated endothelial shape change remain controversial, a growing body of evidence supports a decentralized, integrated signaling network in which cytoskeletal polymers transmit apical shear forces to membrane attachment sites where conformational changes in connected

proteins initiate signaling events [15]. Recently, heterogeneous μm-scale displacements of cytoskeletal structures have been described in endothelial cells that, when converted to strain maps, reveal an apical to basal gradient of force transmission [16]. Changes in the number, type, and structure of cytoskeletal connections will alter the location and magnitude of transmitted forces and may modify the specific endothelial phenotype, depending on the spatial and temporal microstimuli that each endothelial cell senses [17].

Of the three types of cytoskeletal polymers – actin filaments, intermediate filaments, and microtubules – that determine endothelial cell shape, actin filaments are the most abundant and are located in closest proximity to the cell membrane. Confluent endothelial cells assemble ~70% of their 100 μM total actin into a rich meshwork of just over 50,000 actin filaments that are on average ~3 μm long [18]. In the cell cortex, cross-linking proteins organize actin filaments into viscoelastic gels that connect to transmembrane proteins and signaling complexes located at intercellular and extracellular matrix adhesion sites. Of particular importance are the direct connections of actin filaments to β integrin tails by talin [19] and filamins [20], and to cadherins by vinculin and catenins [21]. During cell locomotion and shape change events, the actin cytoskeleton is extensively remodeled [18, 22], primarily by adding and subtracting subunits at free filament ends.

Investigators have extensively studied structural actin cytoskeletal remodeling in response to fluid shear stress in endothelial cells. Basally-located dense peripheral bundles of actin filaments (stress fibers) dissolve shortly after shear stress exposure only to reform hours later just under the apical membrane, aligned with the long axis of the cell [23-26]. The abundant microvilli present on the apical endothelial surface under static conditions disappear, leaving a smooth, glassy contour [23]. These structural alterations reduce the peak shear stresses imposed on individual cells [27, 28] and cause elongated endothelial

cells to become more resistant to micropipette surface deformations [29]. While these experiments reveal novel insights into the modification of cytoskeletal structures by fluid shear stress, the theory and experimental techniques used in these studies are of limited utility in understanding the dynamic nature of the actin cytoskeleton remodeling process. Experiments tracing tagged actin molecules in living endothelial cells are required to directly determine how actin distributes and remodels during fluid shear stress mechanostimulation.

This paper reports measurements of the temporal evolution of actin cytoskeleton remodeling in living endothelial cells stimulated with laminar, steady fluid flow using the complementary techniques of photoactivation of fluorescence (PAF) and fluorescence recovery after photobleaching (FRAP). These techniques allow us to simultaneously measure the amount of polymerized actin and the rate of actin filament subunit turnover in individual endothelial cells, which are then correlated with migration rate. We show for the first time that fluid shear stress rapidly enhances endothelial actin remodeling to levels measured in the most dynamic endothelial cells under static conditions. Increased filament subunit turnover precedes a drop in the amount of polymerized actin, revealing that net actin cytoskeleton depolymerization characterizes the earliest phase of the endothelial shear stress response. In contrast to endothelial cells in static culture that enhance actin remodeling in proportion to their rate of migration across a substrate [18], we find that the shear stress-induced enhancement of actin remodeling is initially decoupled from increased endothelial motility. While migration rates eventually recover to pre-shear stress levels, actin cytoskeletal remodeling remains activate in many endothelial cells after shear stress accommodation.

Results

Fluorescent actin analogs function similar to native actin in endothelial cells

Fluorescently tagged actin monomers were introduced into individual bovine aortic endothelial cells (BAECs) forming confluent monolayers for use as tracers of actin cytoskeltal dynamics in PAF and FRAP experiments. For PAF, BAECs were microinjected with caged-resorufin iodoacetamide-labeled rabbit muscle actin (CR-actin) at a final concentration estimated to account for < 2% of total actin and photoactivated. CR-actin has been shown previously to incorporate into the cytoskeleton of various cell types and function as a reliable marker during actin remodeling [18, 22]. FRAP studies were performed by photobleaching BAECs transiently transfected with a vector encoding a human β-actin EGFP fusion protein (EGFP-actin). EGFP-actin co-localizes with native actin filaments after staining with Alexa® 546 phalloidin in fixed and permeabilized BAECs (Fig. II-1 A), where it both concentrates at the cell cortex and incorporates into actin filament bundles spanning the cell. In living BAECs, EGFP-actin is diffusely present throughout the cell cytoplasm and becomes particularly enriched in regions of active membrane ruffling and lamellipodial extension (Videos 1 and 2, Supplemental materials).

Detergent treatment of confluent BAECs with Triton X-100 followed by high-speed centrifugation (>100,000 *g*) separates actin into soluble and insoluble fractions that represent bulk measurements of monomer and filament populations, respectively. Immunoblots of these fractions with an anti-GFP polyclonal antibody reveals that EGFP-actin is detectable only in transfected cells and partitions into the cytoskeleton in a similar ratio as compared with native actin (Fig. II-1 B). Densitometric analysis of these immunoblots shows that 51 ± 2% of EGFP-actin is Triton insoluble ($n = 4$), a value only

modestly lower than the 58 ± 6% Triton insoluble actin measured previously in confluent BAECs using similar techniques [18]. Using the total EGFP-actin mass present in whole cell lysates of BAECs, the fraction of total BAECs positive for EGFP-actin expression, and a 2×10^{-6} μl geometric estimate for the cytoplasmic volume, the average expression level was calculated to be ~0.6 pg EGFP-actin per cell. Since BAECs forming a confluent monolayer contain ~6.6 pg endogenous actin per cell [18], this corresponds to an average increase in the total actin content of ~10% per cell expressing the EGFP-actin vector. This level of overexpression is not likely to have a significant effect on global actin organization or dynamics, given the excess of actin monomer sequestering proteins present in non-muscle cells. Taken together, the evidence shows that the EGFP-actin fusion protein functions similar to endogenous actin in endothelial cells, a finding supported by the characterization of EGFP-actin expression in other cell types [30].

Shear stress alters the dynamics of actin remodeling in endothelial cells

We measured the temporal shear stress response of actin remodeling in BAECs with PAF and FRAP. Photobleached or photoactivated regions marked within BAECs change more rapidly after fluid shear stress mechanostimulation than those not exposed to fluid flow (Fig. II-2, A and B). Quantitation of the fluorescence recovery in FRAP experiments shows that mechanostimulation increases both the extent and rate of EGFP-actin fluorescence recovery into the depleted region (Fig. II-2 C). Since EGFP-actin is a tracer of actin cytoskeleton remodeling events, enhanced fluorescence photobleaching recovery kinetics indicate that actin remodeling is increased in BAECs after challenge with shear stress. PAF fluorescence decay measurements, the inverse of FRAP, provided quantitatively equivalent relationships between shear stress stimulation and enhanced fluorescence dynamics (data not shown).

Actin fluorescence recovery and decay curves are biphasic

The shape of the FRAP recovery curves indicates that the evolution of EGFP-actin fluorescence recovery into the depleted band is biphasic (Fig. II-2 C) and can be decomposed into fast (early) and slow (late) dynamic components. Previous work has shown that the fast dynamics primarily represent EGFP-actin monomer diffusion into the bleached region, while the slow dynamics depend on the rate of actin filament turnover as the bleached filaments replace non-fluorescent subunits with fluorescent ones, a process regulated by actin polymerization and depolymerization events [18, 31, 32]. A two-compartment model describing this biphasic behavior was used to interpret the fluorescence recovery into the photobleached or photoactivated region in FRAP and PAF experiments, respectively, allowing determination of the fraction of total actin that is polymerized and the average actin filament turnover time [32]. The polymerized fraction represents the percentage of total actin that is incorporated into filaments and is determined primarily by the relative amount of fast and slow fluorescence dynamics. In endothelial cells, actin filament dynamics are not limited by the rate of monomer diffusion [31], which is very rapid, and therefore the slow dynamics are primarily determined by the filament turnover time, the inverse of the filament subunit turnover rate.

Endothelial cells respond rapidly to shear stress by net depolymerization of their cytoskeletons

At baseline under static culture conditions, previous studies have shown that BAECs forming confluent monolayers maintain 73 ± 11% of their total actin in polymer and turnover actin filaments slowly with an average of 38.9 ± 11 minute lifetimes [18]. We confirm these measurements in the current study. Using PAF and FRAP, respectively, with CR-actin and EGFP-actin, we find that individual BAECs forming confluent monolayers

polymerize 68 ± 12% of their total actin and have average filament lifetimes of 35.2 ± 7.1 min prior to shear stress exposure (n = 10). Treatment with 1 μM jasplakinolide, a potent cell membrane permeant actin polymerizing agent, for 30 min increases the percent of actin polymerized to 95 ± 4% and halts actin filament turnover (n = 10), indicating that nearly all of the EGFP-actin expressed in BAECs is functional.

Individual BAECs in a confluent monolayer respond to 12 dyn/cm^2 fluid shear stress first by increasing their rate of actin filament turnover. While filament lifetimes decrease in a majority of cells minutes after applying shear stress (Fig. II-3 A), there is large cell-to-cell variability. Despite the individuality of the specific response, as a population the average filament turnover time in confluent BAECs decreases to a minimum of 12.2 ± 10.0 min between 30 and 60 minutes after shear stress stimulation. This level of actin filament turnover is similar to the most rapid turnover rates measured previously in the fastest moving endothelial cells [18]. Filament turnover times remain low for ≥6 h after the onset of fluid shear mechanostimulation (Fig. II-3 B).

The initial decrease in the average lifetime of cytoplasmic actin filaments after shear stress stimulation is followed by a net loss of polymerized actin. Despite the apparent individual variability in the enhancement of filament turnover, all BAECs show net depolymerization of their cytoskeletons in response to a shear stress challenge (Fig. II-3 C). At 30 to 60 minutes after shear stress application when actin filament turnover times are at a minimum, the percentage of total actin polymerized decreases to an average value of 43 ± 10% per endothelial cell. While the filament turnover time stabilizes at this lower value, the amount of actin polymer continues to fall, reaching a minimum amount of 34 ± 4% after approximately 3 to 3.5 hours of shear stress stimulation (Fig. II-3 D, $p < 0.01$ compared to the 30 – 60

min time period). At 5 hours, the polymer content tends to recover slightly to 55 ± 19%, but remains below pre-shear stress levels.

Actin remodeling is transiently decoupled from motility during shear stress exposure

Because endothelial cell motility correlates positively with enhanced filament turnover and decreased polymer content under static conditions [18], we examined the movement of endothelial cells to determine whether this relationship holds during shear stress-induced actin cytoskeleton remodeling. In the absence of fluid shear stress, BAECs crawl at the relatively slow rate of 0.35 ± 0.09 μm/min. Instead of accelerating motility in response to accelerated actin dynamics, shear stress exposed BAECs transiently decrease their rate of translocational movement after starting fluid flow (Fig. II-4). The slowing in movement occurs on the same time scale that bulk actin remodeling reaches a maximum, decreasing to a minimum speed of 0.14 ± 0.04 μm/min at 30 to 60 min after shear stress exposure and then remaining decreased for an additional 5 h. This is in stark contrast to measurements of actin remodeling in sparse endothelial cells under no-flow conditions, where non-confluent endothelial cells move ~3-fold faster with depleted F-actin content and accelerated subunit turnover rates [18]. Experiments on human umbilical vein and mouse lung endothelial cells handled under identical conditions show a similar shear stress-dependent decrease in cell speed on the same time scale (data not shown), implying that these observations are not species or cell line specific.

Actin remodeling remains enhanced in many endothelial cells after shear stress-induced endothelial shape change

In the presence of continual shear stress stimulation, BAECs become elongated and aligned in the direction of fluid flow in an accommodation response to the applied force. In individual BAECs, the shear stress-induced actin remodeling response is highly variable. While the polymerized fraction recovers to near pre-shear stress levels in most cells, some BAECs continue to have enhanced rates of actin filament subunit turnover, while others are more dynamically stable (Fig. II-5 A). This reveals that there is less correlation between polymer content and filament turnover in shear stress accommodated BAECs, as compared to the relationship observed in unstressed cells.

Despite the nature of the shear stress response in individual aligned cells, as a population shear stress accommodated BAECs maintain relatively enhanced levels of actin remodeling (Fig. II-5 B). The polymerized fraction falls slightly short of returning to pre-shear stress levels, averaging 57 ± 13% between 22 and 24 h, or ~10% less polymer than is present under static conditions. The filament turnover time during the same period recovers to a lesser extent at 26.0 ± 19.7 min, with the large variability representing differences in the activation of individual cells.

Discussion

We have measured the temporal dynamics of the actin cytoskeleton that underlie the dramatic shape change response of endothelial cells during exposure to fluid shear stress. We show that shear stress is a potent stimulator of actin filament turnover and leads to significant depolymerization of the cytoskeleton within minutes. In direct contrast to endothelial cells under static conditions where actin dynamics, shape change, and motility are tightly coupled, the cellular energy expended for shear stress-induced actin remodeling is thus largely funneled to effect shape change over movement, which transiently slows during the first 30 min of shear stress exposure. Later, as the cytoskeleton remodels and the cell changes shape, motility recovers but many of the cells remain in a partially activated state of actin remodeling that depends on the individual cell measured, even after morphological accommodation to the applied force. Based on this work, we define three temporal phases of dynamic actin cytoskeleton remodeling during shear stress stimulation that each likely utilize a unique combination of actin-based mechanisms.

Short term response to shear stress (0 – 30 min)

Actin cytoskeleton remodeling reaches maximum levels ~30 min after shear stress stimulation. In confirmation of previous work using bulk DNase assays on endothelial cell lysates [33], we find that shear stress-induced actin remodeling results in net cytoskeletal depolymerization. In addition, we report that endothelial cytoskeletal depolymerization occurs in response to accelerated actin filament turnover.

For purified actin, filament turnover depends primarily on the distribution of filament lengths, the number of free filament ends available for subunit exchange, and the rate of subunit addition and loss from these ends. Attempts to isolate the individual influences

modulating filament turnover are difficult, but recent comprehensive efforts modeling the kinetics of the actin cycle are providing new insights into the relative importance of these processes [34]. These efforts have shown that, as actin cycling becomes more dynamic, it tends towards the depolymerized state [34], as observed in our studies. In cells, actin binding proteins, often with overlapping mechanisms of action, modulate these parameters and provide multiple access points at which the cell can influence filament turnover. Complicating matters further, different combinations of these parameters can produce ostensibly similar effects on filament turnover. However, for filament turnover-mediated depolymerization, the rate-limiting factor is the loss of subunits from the pointed filament end [35]. In this case, mechanisms that influence pointed end kinetics and exposure, but do not alter barbed end capping, can result in depolymerization of the actin cytoskeleton and a net loss of polymerized actin.

The most obvious depolymerization mechanism is to increase the rate of subunit dissociation from the pointed ends of actin filaments. ADF/cofilins perform this function *in vitro* by accelerating the kinetics of ADP-filament subunit depolymerization up to ~25-fold [35]. The depolymerization activity of ADF/cofilin is regulated by phosphorylation of serine-3. Phosphorylation of this residue by LIM kinase inactivates ADF/cofilin by inhibiting its ability to bind to actin filaments [36, 37]. This inhibition has been shown to be reversed by the Slingshot [38] and TEST2 phosphatases.

Although cofilin dephosphorylation is attractive, evidence as to the role ADF/cofilins play in the initial shear stress response is inconclusive. The Rho GTPases Rac, Rho, and Cdc42, which activate LIM kinase, are differentially activated within the first 15 min of shear stress [39-41] and there is a progressive cofilin phosphorylation and inactivation beginning at ~30 min after shear stress initiation [42]. Since the burst of shear stress-induced filament

turnover and depolymerization occurs during the 30 min time interval prior to cofilin deactivation, cofilin activity may be important in this process. However, to sustain this new equilibrium of diminished polymer with a higher filament subunit cycling rate, cofilin must remain active or other mechanisms must be called into play. Results in endothelial cells under static conditions suggest there may not be a simple one-to-one correspondance between cofilin activation and increased filament turnover. Endothelial cells in a confluent monolayer under static conditions have ample amounts of F-actin associated cofilin but maintain high polymer fractions with slow rates of filament turnover [18]. Furthermore, cofilin association with the actin cytoskeleton actually decreases in endothelial cells with the most dynamic actin cytoskeletons and fastest rates of movement [18].

Increasing the number of free pointed filament ends available for disassembly is another way to accelerate actin filament turnover to cause net depolymerization in populations of actin filaments. This can be accomplished passively by spontaneous mechanical filament fragmentation or actively by filament severing, filament nucleation and release, and/or pointed end uncapping. Of these mechanisms, fragmentation and severing are at an advantage over uncapping or nucleation and release for mediating rapid depolymerization events in that they increase the number of free filament ends while simultaneously decreasing filament lengths. *In vitro*, actin filaments spontaneously fragment and anneal [43], a process which may be accelerated *in vivo* by fluid shear stress if the forces imposed on the cross-linked filament network exceed the mechanical strength of the individual filament. Theoretical estimates predict that this is unlikely [44].

A more plausible way to rapidly generate an increased number of short actin filaments is by active filament severing [45]. ADF/cofilin and the gelsolin family of proteins are the most widely studied filament severing proteins, and of the two, gelsolin is the most potent [46,

47]. The severing activity of gelsolin is calcium regulated [46]. Since one of the earliest responses to fluid shear stress is a transient oscillatory rise in free cytoplasmic calcium concentrations [48, 49] and cytoplasmic calcium chelation blocks shear stress-induced depolymerization in bulk endothelial lysates [33], gelsolin-mediated actin filament severing may also be important during the initial shear stress response. Under static conditions, however, gelsolin and cofilin appear to work synergistically to regulate endothelial cell actin dynamics and movement [18], and therefore both activities may be important during the shear stress response.

The accessibility of pointed filament ends may also be modulated in cells. Tropomodulin-3 caps actin filament pointed ends, and when overexpressed negatively regulates endothelial cell motility under static conditions [50]. The Arp2/3 complex can also cap pointed ends, however its major response is the formation of dendritic branching structures by *de novo* nucleation from the barbed filament end [51]. These branches can then release from the sides of filaments to create new free pointed filament ends.

Relationship between shear stress-induced actin remodeling and endothelial cell motility

The factors contributing to the migrational properties of individual endothelial cells are complicated, depending on the origin of the cells, the type of substrate, and, most importantly, the density of cells on the surface. Endothelial cells are more motile in sparse culture presumably because they establish few contacts with their neighbors. When cells incorporate into a confluent monolayer, they diminish their movements and slow their cytoplasmic actin filament turnover rate [18]. We have found that the application of shear stress further decreases the rate of endothelial migration in these confluent monolayers in confirmation of Blackman et al. [52], but in contrast to others [53]. Since subconfluent

endothelial cells respond differently to fluid shear stress, by increasing cell speed [54-56], it is possible that the studies reporting increased cell speed following shear stress were less densely confluent and quiescent than in our study.

Under static conditions, endothelial cells have an upper limit on their rates of movement and the bulk dynamics of their cytoskeletons, where movement and dynamics are directly coupled [18]. The observation that motility slows and remains depressed for hours after fluid shear stress stimulation before recovering, while actin remodeling is enhanced, reveals that actin remodeling is initially decoupled from productive motility in shear stress stimulated endothelium. Increased intercellular and/or substrate adhesion is one possible means to achieve this decoupling, since adhesion is an important determinant of cell speed [57]. Alternatively, the connections between actin filaments and transmembrane adhesion molecules may change, such as that shown for increased filamin binding to β integrin tails which negatively regulates cell movement [58]. Regulation of myosin-based cell contraction may also be important in this process.

Actin dynamics during the phase of decreased endothelial cell movement (1 – 6 h)

After the initial phase of the shear stress response characterized by net cytoskeletal depolymerization, a new steady state of actin remodeling is achieved where the polymer fractions remain low and the filament turnover times are enhanced, but with reduced cell motility. This phase requires different mechanisms to maintain, e.g. one that promotes enhanced filament turnover without a net change in actin polymer content. Since most studies have focused on early and late end points, data to support a mechanism during this intermediate phase of the actin response is limited. A portion of total cofilin is phosphorylated and therefore inactivated at 2 h after shear stress [42]. Cap G, a member of the gelsolin superfamily that caps barbed ends but does not sever filaments, becomes

increasingly associated with the cytoskeleton after shear stress exposure, beginning at 2 h and remaining elevated over static controls at 24 h [59]. Since cells vigorously protect the number of barbed ends exposed, this work implies that shear stress exposed endothelial cells contain an increased number of actin filaments, a finding consistent with observations that average actin filament lengths decrease in endothelial cells with fast actin dynamics under static conditions [18]. Additionally, since Cap G capping events are calcium dependent, basal calcium levels may be chronically elevated as compared to no flow conditions; however, studies examining the long term calcium response after shear stress exposure have yet to be performed. In steady state filament populations of the same length undergoing no net polymerization, kinetic modeling predicts that filament turnover is accelerated to the greatest extent by simultaneously increasing the off rate of ADP-subunits at the pointed filament end, the rate of Pi dissociation from ADP•Pi-subunits after ATP hydrolysis, and the combination of accelerated ATP/ADP exchange rates on actin monomers with shuttling of these ATP-monomers to the barbed filament end [34]. Additional investigations must be performed at the intermediate stages of the shear stress-induced endothelial shape change response to address the complex regulatory events controlling actin remodeling during this phase.

Actin remodeling in shear stress accomodated endothelium (~24 h)

We measure that shear stress accommodated endothelial cell actin cytoskeletons do not completely recovery to their pre-stressed state, but rather, despite their return to baseline cell speed, these cells reach a new steady state of slightly decreased polymer fraction with highly variable rates of filament turnover. The observation that the amount of polymerized actin after 24 h shear stress is less than unstressed cells reveals that increased cytoskeletal polymer content is not required to resist shear stress forces in chronically stimulated

endothelium; rather, it is the architectural organization of the cytoskeleton that is optimized. The large variability in the rate of filament turnover, even in cells with similar elongated shapes and polymer fractions, suggests that cytoskeletal rearrangement is a continuous, heterogeneous response of the endothelial cell to comply with the force pattern imposed on its surface and maintain its optimized morphology [27, 28].

The observation that the endothelial response to shear stress is heterogeneous at the level of the individual cell is consistent with heterogeneous subcellular spatial differences in fluid shear stress stimulation on the endothelial surface [17]. Since the endothelial surface of an individual cell is wavy, not smooth, topographic differences determined by the submembrane actin filament network architecture create microvariations in the fluid profile (and hence the fluid shear stress) that locally change the distribution of shear stress [27, 28]. Remodeling of actin is an important mechanism for the cell to regulate the stress it experiences by optimizing its structure against the mechanical load on its surface as well as altering its connections with molecules at the membrane surface that may participate in signaling events. In this way, depending on their surface topography, neighboring endothelial cells in a confluent monolayer can have radically different phenotypes given their specific force stimulation. Indeed, this is observed *in vivo* where endothelial cell shape and arterial atherogenicity are markedly different between cells located just a few cell diameters away from each other. Therefore, changes in the actin network structure and connections mediated by remodeling events may have a significant impact on cellular mechanotransduction and the atherogenic process.

Materials and methods

Reagents

pEGFP human β-actin, purified recombinant GFP, and anti-GFP polyclonal antibody were obtained from Clontech; DMEM, Lipofectin®, Opti-MEM® I, and Leibovitz's L-15 Media were obtained from Invitrogen; Alexa® 546 phalloidin, Alexa® 488 dextran, and jasplakinolide were obtained from Molecular Probes; anti-actin monoclonal antibody was obtained from Sigma-Aldrich; HRP-labeled goat anti-mouse secondary antibody was obtained from Bio-Rad Laboratories.

Cell culture, microinjection, and transfection

Primary BAECs were purchased from VEC Technologies and cultured in uncoated flasks in low glucose DMEM supplemented with 10% FCS and 100 U/ml penicillin and streptomycin. For experiments, BAECs between passages two and ten were plated on glass coverslips coated with 0.1% gelatin.

CR-actin was synthesized according to the method of Theriot and Mitchison [22], diluted to 1 mg/ml in Injection Buffer (1mM Hepes, 0.2 mM $MgCl_2$, 0.5 mM ATP, pH 7.4) containing 5 μM Alexa® 488 dextran (10 kD), and microinjected into BAECs. Prior to experiments, microinjected BAECs were allowed to recover for 1 hour.

EGFP-actin was transfected into 70% confluent BAECs using a ratio of 2 μg/ml cDNA to 20 μl/ml Lipofectin® diluted in serum-free Opti-MEM® I and incubated for 5 h at 37°C and 5% CO_2 after which the transfection solution was replaced with normal growth media. BAECs expressed detectable levels of EGFP-actin by 48 hours after transfection, and were

used for experiments between 48 and 72 hours. The transfection efficiency was 13 ± 4% of total BAECs, measured by counting the number of positively reporting cells in paired DIC and fluorescent images at 72 hours post-transfection ($n = 8$).

Immunofluorescence

BAECs were fixed with 4% paraformaldehyde for 20 min at RT, followed by permeabilization with 0.2% Triton X-100 in PBS for 5 min. Samples were incubated with 1 μM Alexa® 546 phalloidin for 10 min to stain actin filaments, washed three times in PBS, and mounted (Aqua Polymount; Polysciences) onto glass microscope slides. Images were digitally recorded with a cooled CCD camera (Orca II ER; Hamamatsu) on a Nikon Eclipse TE2000 microscope with a 63X oil immersion objective and MetaMorph® software (Universal Imaging Corporation).

SDS-PAGE and immunoblotting

BAECs were grown to confluence in 60 mm Petri dishes, extracted with 200 μl of Triton Lysis Buffer (60 mM Pipes, 25 mM Hepes, 10 mM EGTA, 2 mM $MgCl_2$, 1% Triton X-100, 1mM PMSF, 1μM phallacidin, and 0.1 mg/ml aprotinin, leupeptin, and benzamidine, pH 6.9) at 4°C, and collected from the surface using a rubber scraper. Samples were solubilized with equal amounts of SDS-PAGE Sample Buffer in total for whole cell lysates or after separation into Triton soluble and insoluble fractions by cetrifugation for 30 min at 215,000 g and 4°C. Triton soluble and insoluble fractions were matched for total protein, loaded on a modified 11% acrylamide Laemmli slab gel [60], and separated by SDS-PAGE. Whole cell lysates were loaded at 50% of the matched total protein value. Proteins were transferred to PVDF membranes (Millipore) for 60 min using a Trans-Blot® cell (Bio-Rad Laboratories) at 100V. PVDF membranes were blocked in PBS with 0.02% Tween 20 and

5% Carnation nonfat dry milk, pH 7.4. Blocked membranes were incubated with a 1:1000 dilution of primary antibody for 1 h at RT, washed three times with PBS, and probed with a 1:5000 dilution of HRP-labeled goat anti mouse secondary antibody for 1 h. Washed membranes were developed using SuperSignal® West Pico Chemiluminescent Substrate (Pierce Biotechnology), digitized, and densitometrically analyzed. For GFP immunoblots, purified recombinant GFP standards were used to quantitate the amount of GFP present.

Shear stress

Steady, laminar shear stress at 12 dyn/cm^2 was applied to confluent BAECs using a parallel plate flow chamber as previously described [49]. Briefly, the chamber consisted of two stainless steel plates maintained at 37°C by a copper heating block that were separated by a 0.5 mm silicone sheet (Allied Biomedical) with a 5 × 50 mm rectangular section removed to create a flow channel. Confluent BAECs grown overnight on a 25 mm diameter coverslip coated with 0.1% gelatin were placed in a recess milled into the surface of the bottom stainless steel plate and the flow chamber was assembled. A Materflex® peristaltic pump (Cole-Parmer) was used to pump DMEM containing 10% FCS at 37°C and 5% CO_2 from a reservoir through the flow chamber. A second sealed reservoir was placed between the pump and the flow chamber to eliminate pulsations. Since the flow through the channel can be approximated as two-dimensional fully developed laminar flow with a parabolic velocity profile, the wall shear stress was determined as a linear function of the volume flow rate pumped through the chamber.

PAF and FRAP

PAF and FRAP experiments were performed on individual BAECs forming confluent monolayers contained within a parallel plate flow chamber using a Zeiss Axiovert 405M

microscope with a 100X oil immersion objective. For PAF, BAECs microinjected with CR-actin were located by a co-injected Alexa® 488 dextran volumetric tracer and the CR-actin was photoactivated in a 7 – 10 μm wide strip spanning the cell width using the 365 nm line of a mercury arc lamp as previously described [31]. For FRAP, a 1 – 2 μm wide band was photobleached across one dimension of individual BAECs expressing EGFP-actin with a 100 mW argon ion laser (Melles Griot) at 488 nm. The photoactivation and photobleaching times were < 1 s for PAF and FRAP experiments. The evolution of fluorescence at the center of the photoactivated or photobleached region was measured over time and analyzed with a two-compartment mathematical model describing actin monomer and polymer dynamics as previously described [31, 32]. Control experiments were performed under static conditions, after which fluid flow was initiated and experiments were performed during shear stress stimulation at selected times up to 24 h. For certain static control experiments, BAECs were incubated with 1 μM jasplakinolide for 30 min at 37°C prior to photobleaching.

Motility

Cell motility was measured by quantitative time lapse video microscopy. Digital images of BAECs within confluent monolayers were captured every 2 min under static conditions and during exposure to 12 dyn/cm^2 fluid shear stress for 24 h on a Zeiss IM-35 microscope with a 10X phase contrast objective and CCD camera (C2400-77; Hamamatsu). Mean-square-displacements were calculated by tracking nuclear trajectories in each video frame. Root-mean-square cell speed was determined by fitting mean-square-displacements to a formula describing cell dispersion as a function of time and cell persistence as previously described [18, 61].

Online supplemental material

Time lapse video of a subconfluent BAEC expressing EGFP-actin was digitally captured every 2 s for 5 min with an Orca II ER CCD camera on a Nikon Eclipse TE2000 microscope using a 63X oil immersion objective and MetaMorph® software. At each time point, paired DIC and fluorescent images were recorded. During the video, the cell was maintained at 37°C using a temperature controller (Harvard Apparatus) in Leibovitz's L-15 Media without phenol red supplemented with 10% FCS.

Acknowledgments

We are grateful for many clarifying discussion with James McGrath and Thomas Stossel. We thank Michael Gimbrone and the Vascular Research Laboratory at Brigham and Women's Hospital for their generous help with the cell culture and shear stress experiments. Support for this research was provided by the National Institutes of Health (HL54145). E. A. Osborn is a Whitaker Foundation Graduate Fellow.

Abbreviations list

BAECs, bovine aortic endothelial cells; CR-actin, caged resorufin iodoacetamide-labeled actin; PAF, photoactivation of fluorescence

References

1. Caro, C.G., J.M. Fitz-Gerald, and R.C. Schroter, *Arterial wall shear and distribution of early atheroma in man.* Nature, 1969. **223**(211): p. 1159-60.
2. Stehbens, W.E., *Letter: Hemodynamics and atherosclerosis.* Exp Mol Pathol, 1974. **20**(3): p. 412-5.
3. Zarins, C.K., et al., *Carotid bifurcation atherosclerosis. Quantitative correlation of plaque localization with flow velocity profiles and wall shear stress.* Circ Res, 1983. **53**(4): p. 502-14.
4. Ku, D.N. and D.P. Giddens, *Pulsatile flow in a model carotid bifurcation.* Arteriosclerosis, 1983. **3**(1): p. 31-9.
5. Davies, P.F., *Flow-mediated endothelial mechanotransduction.* Physiol Rev, 1995. **75**(3): p. 519-60.
6. Davies, P.F., et al., *Spatial relationships in early signaling events of flow-mediated endothelial mechanotransduction.* Annu Rev Physiol, 1997. **59**: p. 527-49.
7. Dewey, C.F., Jr., et al., *The dynamic response of vascular endothelial cells to fluid shear stress.* J Biomech Eng, 1981. **103**(3): p. 177-85.
8. Gimbrone, M.A., Jr., et al., *Endothelial dysfunction, hemodynamic forces, and atherogenesis.* Ann N Y Acad Sci, 2000. **902**: p. 230-9; discussion 239-40.
9. Malek, A.M., S.L. Alper, and S. Izumo, *Hemodynamic shear stress and its role in atherosclerosis.* Jama, 1999. **282**(21): p. 2035-42.
10. Cornhill, J.F., et al., *Quantitative study of the rabbit aortic endothelium using vascular casts.* Atherosclerosis, 1980. **35**(3): p. 321-37.
11. Goode, T.B., et al., *Aortic endothelial cell morphology observed in situ by scanning electron microscopy during atherogenesis in the rabbit.* Atherosclerosis, 1977. **27**(2): p. 235-51.
12. Davies, P.F., et al., *Turbulent fluid shear stress induces vascular endothelial cell turnover in vitro.* Proc Natl Acad Sci U S A, 1986. **83**(7): p. 2114-7.
13. Helmlinger, G., et al., *Effects of pulsatile flow on cultured vascular endothelial cell morphology.* J Biomech Eng, 1991. **113**(2): p. 123-31.
14. DePaola, N., et al., *Vascular endothelium responds to fluid shear stress gradients [published erratum appears in Arterioscler Thromb 1993 Mar;13(3):465].* Arterioscler Thromb, 1992. **12**(11): p. 1254-7.
15. Helmke, B.P. and P.F. Davies, *The cytoskeleton under external fluid mechanical forces: hemodynamic forces acting on the endothelium.* Ann Biomed Eng, 2002. **30**(3): p. 284-96.
16. Helmke, B.P., A.B. Rosen, and P.F. Davies, *Mapping mechanical strain of an endogenous cytoskeletal network in living endothelial cells.* Biophys J, 2003. **84**(4): p. 2691-9.

17. Davies, P.F., J. Zilberberg, and B.P. Helmke, *Spatial microstimuli in endothelial mechanosignaling*. Circ Res, 2003. **92**(4): p. 359-70.

18. McGrath, J.L., et al., *Regulation of the actin cycle in vivo by actin filament severing*. Proc Natl Acad Sci U S A, 2000. **97**(12): p. 6532-6537.

19. Calderwood, D.A. and M.H. Ginsberg, *Talin forges the links between integrins and actin*. Nat Cell Biol, 2003. **5**(8): p. 694-7.

20. Stossel, T.P., et al., *Filamins as integrators of cell mechanics and signalling*. Nat Rev Mol Cell Biol, 2001. **2**(2): p. 138-45.

21. Wheelock, M.J. and K.R. Johnson, *Cadherin-mediated cellular signaling*. Curr Opin Cell Biol, 2003. **15**(5): p. 509-14.

22. Theriot, J.A. and T.J. Mitchison, *Actin microfilament dynamics in locomoting cells*. Nature, 1991. **352**(6331): p. 126-31.

23. Satcher, R., C.F. Dewey, Jr., and J.H. Hartwig, *Mechanical remodeling of the endothelial surface and actin cytoskeleton induced by fluid flow*. Microcirculation, 1997. **4**(4): p. 439-53.

24. Franke, R.P., et al., *Induction of human vascular endothelial stress fibres by fluid shear stress*. Nature, 1984. **307**(5952): p. 648-9.

25. Barbee, K.A., P.F. Davies, and R. Lal, *Shear stress-induced reorganization of the surface topography of living endothelial cells imaged by atomic force microscopy*. Circ Res, 1994. **74**(1): p. 163-71.

26. Galbraith, C.G., R. Skalak, and S. Chien, *Shear stress induces spatial reorganization of the endothelial cell cytoskeleton*. Cell Motil Cytoskeleton, 1998. **40**(4): p. 317-30.

27. Barbee, K.A., et al., *Subcellular distribution of shear stress at the surface of flow-aligned and nonaligned endothelial monolayers*. Am J Physiol, 1995. **268**(4 Pt 2): p. H1765-72.

28. Satcher, R.L., Jr., et al., *The distribution of fluid forces on model arterial endothelium using computational fluid dynamics*. J Biomech Eng, 1992. **114**(3): p. 309-16.

29. Sato, M., N. Ohshima, and R.M. Nerem, *Viscoelastic properties of cultured porcine aortic endothelial cells exposed to shear stress*. J Biomech, 1996. **29**(4): p. 461-7.

30. Ballestrem, C., B. Wehrle-Haller, and B.A. Imhof, *Actin dynamics in living mammalian cells*. J Cell Sci, 1998. **111**(Pt 12): p. 1649-58.

31. McGrath, J.L., et al., *Simultaneous measurements of actin filament turnover, filament fraction, and monomer diffusion in endothelial cells*. Biophys J, 1998. **75**(4): p. 2070-8.

32. Tardy, Y., et al., *Interpreting photoactivated fluorescence microscopy measurements of steady-state actin dynamics*. Biophys J, 1995. **69**(5): p. 1674-82.

33. Morita, T., et al., *Role of Ca2+ and protein kinase C in shear stress-induced actin depolymerization and endothelin 1 gene expression*. Circ Res, 1994. **75**(4): p. 630-6.

34. Bindschadler, M., et al., *A mechanistic model of the actin cycle in cells.* Biophys J, 2004. **86**(5).

35. Carlier, M.F., et al., *Actin depolymerizing factor (ADF/cofilin) enhances the rate of filament turnover: implication in actin-based motility.* J Cell Biol, 1997. **136**(6): p. 1307-22.

36. Arber, S., et al., *Regulation of actin dynamics through phosphorylation of cofilin by LIM- kinase [see comments].* Nature, 1998. **393**(6687): p. 805-9.

37. Yang, N., et al., *Cofilin phosphorylation by LIM-kinase 1 and its role in Rac-mediated actin reorganization.* Nature, 1998. **393**(6687): p. 809-12.

38. Niwa, R., et al., *Control of actin reorganization by Slingshot, a family of phosphatases that dephosphorylate ADF/cofilin.* Cell, 2002. **108**(2): p. 233-46.

39. Wojciak-Stothard, B. and A.J. Ridley, *Shear stress-induced endothelial cell polarization is mediated by Rho and Rac but not Cdc42 or PI 3-kinases.* J Cell Biol, 2003. **161**(2): p. 429-39.

40. Tzima, E., et al., *Activation of Rac1 by shear stress in endothelial cells mediates both cytoskeletal reorganization and effects on gene expression.* Embo J, 2002. **21**(24): p. 6791-800.

41. Tzima, E., et al., *Activation of integrins in endothelial cells by fluid shear stress mediates Rho-dependent cytoskeletal alignment.* Embo J, 2001. **20**(17): p. 4639-47.

42. Lin, T., et al., *Rho-ROCK-LIMK-cofilin pathway regulates shear stress activation of sterol regulatory element binding proteins.* Circ Res, 2003. **92**(12): p. 1296-304.

43. Nakaoka, Y. and M. Kasai, *Behaviour of sonicated actin polymers: adenosine triphosphate splitting and polymerization.* J Mol Biol, 1969. **44**(2): p. 319-32.

44. Satcher, R.L., Jr. and C.F. Dewey, Jr., *Theoretical estimates of mechanical properties of the endothelial cell cytoskeleton.* Biophys J, 1996. **71**(1): p. 109-18.

45. Hartwig, J.H., *Mechanisms of actin rearrangements mediating platelet activation.* J Cell Biol, 1992. **118**(6): p. 1421-42.

46. Sun, H.Q., et al., *Gelsolin, a multifunctional actin regulatory protein.* J Biol Chem, 1999. **274**(47): p. 33179-82.

47. Bamburg, J.R., *Proteins of the ADF/cofilin family: essential regulators of actin dynamics.* Annu Rev Cell Dev Biol, 1999. **15**: p. 185-230.

48. Blackman, B.R., L.E. Thibault, and K.A. Barbee, *Selective modulation of endothelial cell [Ca2+]i response to flow by the onset rate of shear stress [In Process Citation].* J Biomech Eng, 2000. **122**(3): p. 274-82.

49. Shen, J., et al., *Fluid shear stress modulates cytosolic free calcium in vascular endothelial cells.* Am J Physiol, 1992. **262**(2 Pt 1): p. C384-90.

50. Fischer, R.S., K.L. Fritz-Six, and V.M. Fowler, *Pointed-end capping by tropomodulin3 negatively regulates endothelial cell motility.* J Cell Biol, 2003. **161**(2): p. 371-80.

51. Pollard, T.D. and G.G. Borisy, *Cellular motility driven by assembly and disassembly of actin filaments.* Cell, 2003. **112**(4): p. 453-65.

52. Blackman, B.R., G. Garcia-Cardena, and M.A. Gimbrone, Jr., *A new in vitro model to evaluate differential responses of endothelial cells to simulated arterial shear stress waveforms*. J Biomech Eng, 2002. **124**(4): p. 397-407.

53. Dieterich, P., et al., *Quantitative morphodynamics of endothelial cells within confluent cultures in response to fluid shear stress*. Biophys J, 2000. **79**(3): p. 1285-97.

54. Masuda, M. and K. Fujiwara, *Morphological responses of single endothelial cells exposed to physiological levels of fluid shear stress*. Front Med Biol Eng, 1993. **5**(2): p. 79-87.

55. Li, S., et al., *The role of the dynamics of focal adhesion kinase in the mechanotaxis of endothelial cells*. Proc Natl Acad Sci U S A, 2002. **99**(6): p. 3546-51.

56. Shiu, Y.T., et al., *Rho mediates the shear-enhancement of endothelial cell migration and traction force generation*. Biophys J, 2004. **86**(4): p. 2558-65.

57. Palecek, S.P., et al., *Integrin-ligand binding properties govern cell migration speed through cell-substratum adhesiveness*. Nature, 1997. **385**(6616): p. 537-40.

58. Calderwood, D.A., et al., *Increased filamin binding to beta-integrin cytoplasmic domains inhibits cell migration*. Nat Cell Biol, 2001. **3**(12): p. 1060-8.

59. Pellieux, C., et al., *Cap G, a gelsolin family protein modulating protective effects of unidirectional shear stress*. J Biol Chem, 2003. **278**(31): p. 29136-44.

60. Laemmli, U.K., *Cleavage of structural proteins during the assembly of the head of bacteriophage T4*. Nature, 1970. **227**(259): p. 680-5.

61. Othmer, H.G., S.R. Dunbar, and W. Alt, *Models of dispersal in biological systems*. J Math Biol, 1988. **26**(3): p. 263-98.

Figure legends

Figure II-1. **EGFP-actin localization and distribution in endothelial cells.** (A) BAECs expressing a human β-actin EGFP fusion protein 60 h after transfection were fixed, permeabilized with Triton X-100, and stained with Alexa® 546 phalloidin to label total actin filaments. The condition for each panel is labeled next to the image. Arrowheads in the merged image indicate co-localization of EGFP-actin and phalloidin fluorescence on a long F-actin bundle. Bar, 10 μm. (B) Confluent monolayers of BAECs transfected with EGFP-actin (+) or control (-) were extracted in 0.2% Triton X-100 and either separated into Triton soluble supernatant (s) and Triton insoluble pellet (p) by centrifugation or maintained as total cell lysates (t). Immunoblots of GFP or actin are shown in the top and bottom panels, respectively.

Figure II-2. **Endothelial cell fluorescent actin dynamics are modified by 12 dyn/cm^2 fluid shear stress.** (A and B) Panels of fluorescence images from representative FRAP and PAF experiments on individual BAECs in a confluent monolayer under static conditions or exposed to shear stress for (A) 30 min or (B) 1 h. (A) FRAP experiments were performed on BAECs transfected with EGFP-actin. (B) For PAF experiments, BAECs were microinjected with CR-actin. Photobleaching and photoactivation were performed at 0 s. For images of BAECs exposed to shear stress, the direction of applied fluid flow is from left to right. Bars, 10 μm. (C) FRAP fluorescence recovery curves measured at the center of the photobleached band for the cells shown in (A) under static conditions (red circles) or after exposure to shear stress for 30 min (green triangles).

Figure II-3. **Short term shear stress response of endothelial cell actin remodeling.** (A) Filament turnover time and (C) polymer fraction measured during the first hour of shear

stress stimulation with PAF (red triangles) and FRAP (green circles) in individual BAECs within a confluent monolayer. Fluid shear stress was applied to BAECs at 0 min. The grey dashed lines represent average values for the combined PAF and FRAP data. (B and D) PAF and FRAP data measured in individual BAECs was averaged in 30 min intervals over 6 h after exposure to 12 dyn/cm^2 fluid shear stress beginning at 0 h (mean ± SD, $n \geq 5$). $p \leq 0.05$ for data from (B) 0 to 6 h and (D) 0 to 5 h in comparisons with static control, *t* test.

Figure II-4. **Endothelial cell motility during shear stress stimulation.** Digitized time-lapse video images of confluent BAECs were recorded under static conditions and after exposure to fluid shear stress starting at 0 h and the root-mean-square cell speed calculated. Cell speeds are were grouped into 30 min intervals and averaged (mean ± SD, $n = 25$).

Figure II-5. **Actin remodeling response of endothelial cells after accommodation to shear stress.** (A) 24 h after the application of shear stress, BAECs become elongated and aligned in the direction of applied fluid flow (left to right). FRAP experiments on two representative elongated, aligned BAECs after ~24 h of shear stress exposure are shown in the fluorescence panels, where green represents EGFP-actin. Photobleaching was performed at 0 s. Fluorescence recovery curves for cell 1 (green triangles) and cell 2 (red circles) are shown to the right of the fluorescence panels. Analysis of these recovery curves reveals that both cells contain ~50% polymerized actin despite a 10-fold faster rate of filament turnover in cell 1. Bar, 10 μm. (B and C) Averages of polymer fraction and filament turnover time measured in individual BAECs within a confluent monolayer under static conditions or after exposure to fluid shear stress for 22 – 24 h (mean ± SD, $n = 23$). *, $p \leq 0.05$, comparisons with static control, *t* test.

Online supplemental material

BAEC expressing EGFP-actin crawling across a glass surface. (Video 1) Time lapse DIC video of a subconfluent BAEC expressing EGFP-actin 48 h after transfection. (Video 2) Corresponding time lapse fluorescence video of the same cell, where green represents EGFP-actin fluorescence. Frames were captured every 2 s for a total of 5 min. The video frame rate is 10 frames/s. Bars, 10 μm.

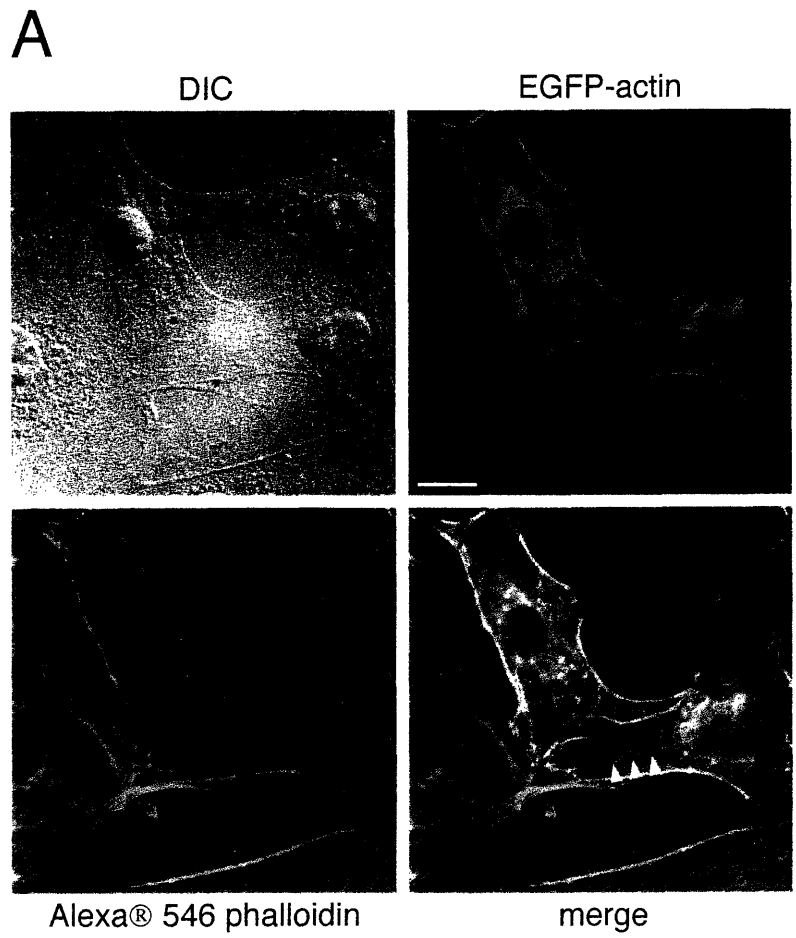

Figure II-1, Osborn et al.

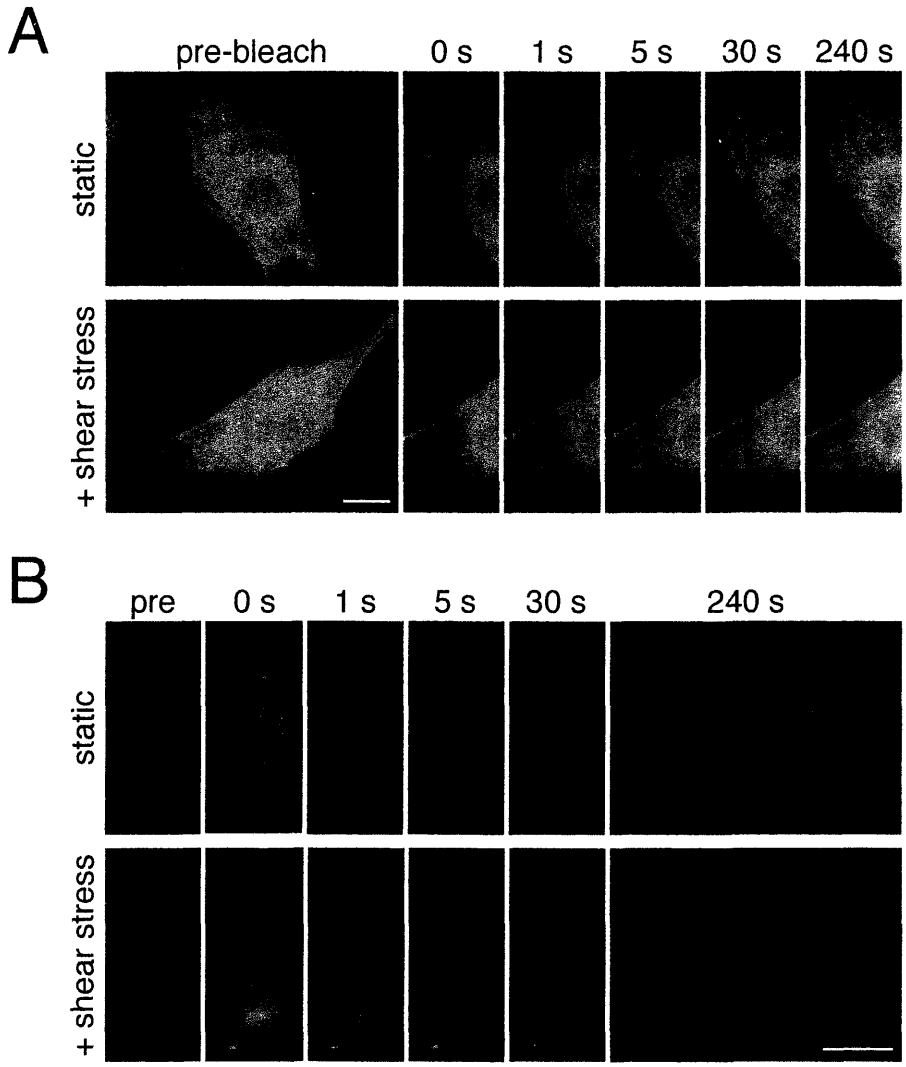

Figure II-2, Osborn et al.

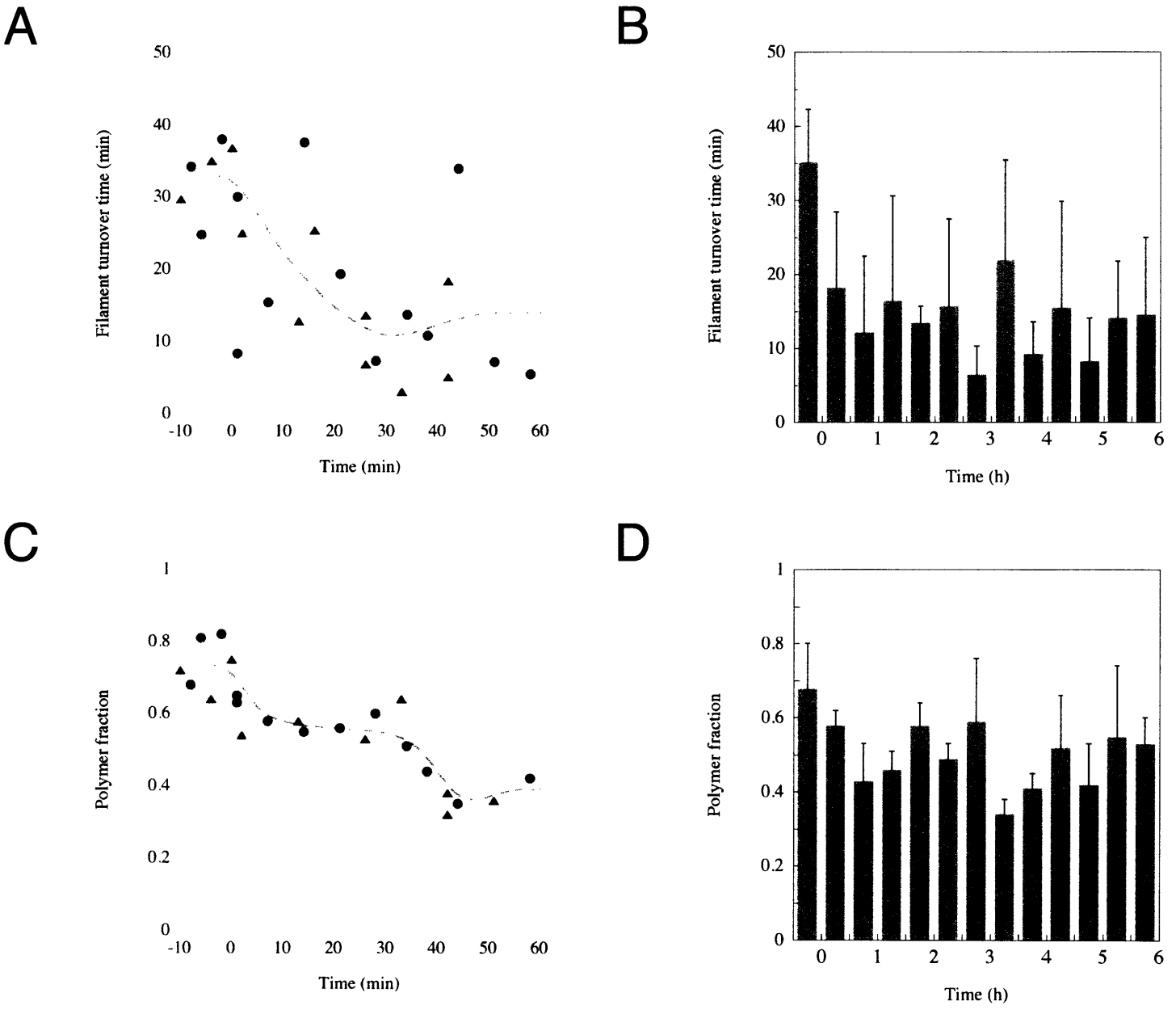

Figure II-3, Osborn et al.

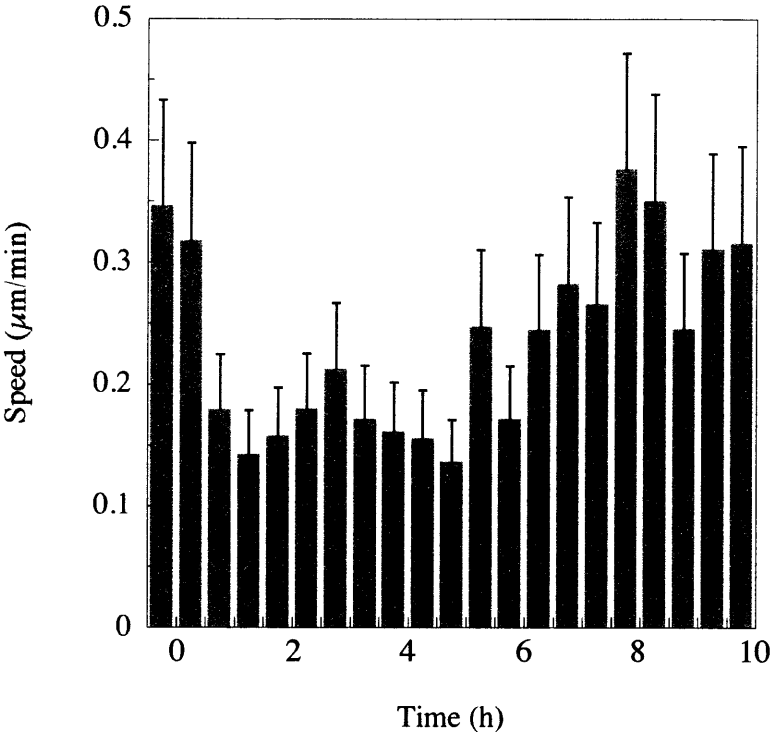

Figure II-4, Osborn et al.

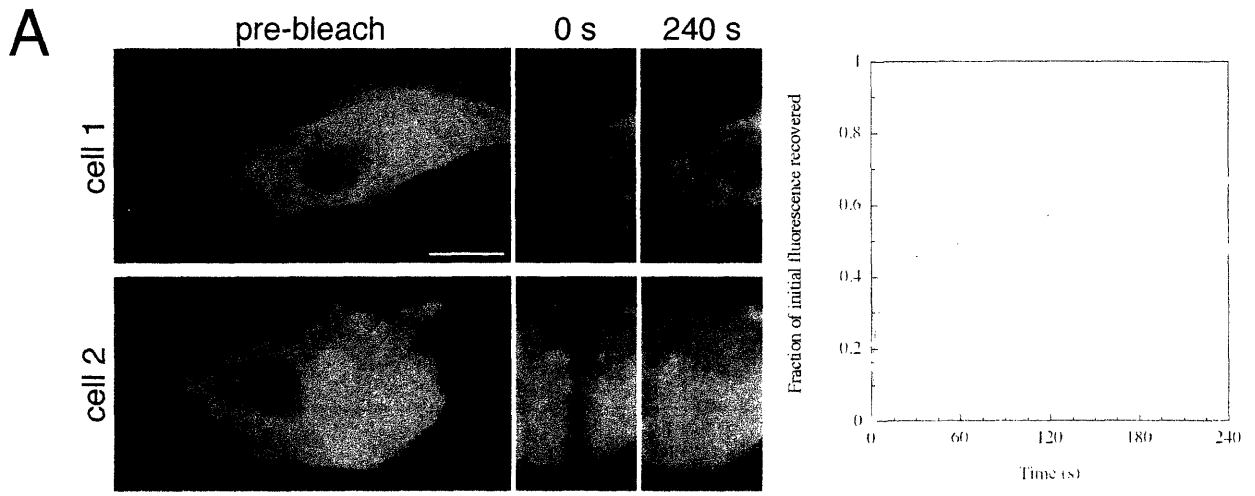

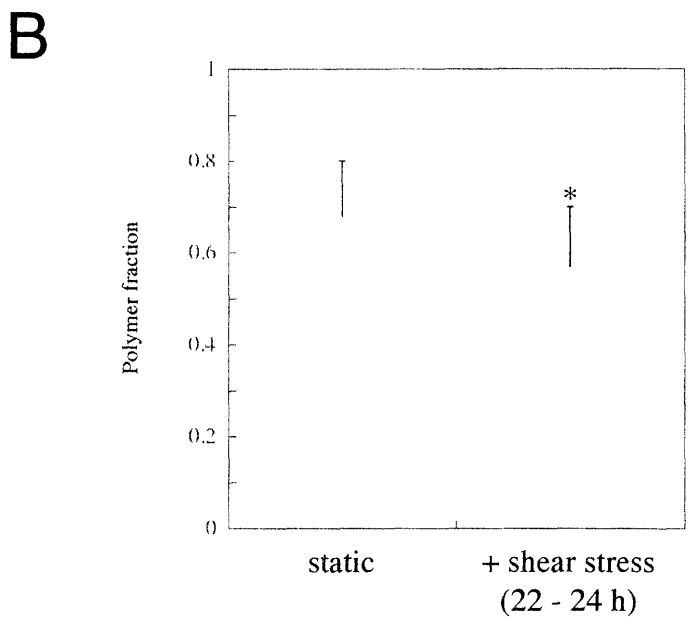

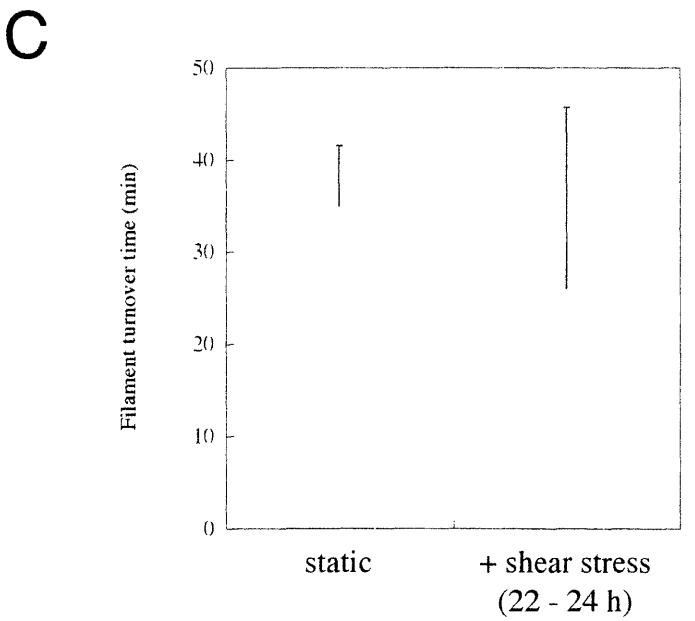

Figure II-5, Osborn et al.

Chapter III

Filamin Cross-linking Stabilizes Actin Filament Dynamics

Eric A. Osborn[1,2], James L. McGrath[3], Fumihiko Nakamura[2], Sarah K. Chalos[4], Michael Schleicher[5], C. Forbes Dewey Jr.[4], and John H. Hartwig[2]

1. Division of Health Sciences and Technology, Harvard University - Massachusetts Institute of Technology, Cambridge MA 02139

2. Hematology Division, Brigham and Women's Hospital and Harvard Medical School, Boston MA 02115

3. Department of Biomedical Engineering, University of Rochester, Rochester NY 14642

4. Department of Mechanical Engineering, Massachusetts Institute of Technology, Cambridge MA 02139

5. Adolph-Butenandt-Institut Zellbiologie, Ludwig-Maximilians-Universität, 80336 München Germany

Work not performed by E. Osborn:

F. Nakamura purified filamin-A proteins and performed F-actin co-sedimentation and gel point assays.

M Schleicher purified ddFLN.

Summary

Non-muscle cell shape change and motility depend primarily on the dynamics and distribution of cross-linked cytoplasmic actin polymer. We determine the steady state dynamics of purified actin filament networks in the entangled state and after orthogonal cross-linking with filamins using a novel, non-perturbing fluorescence system. Human filamin A or *Dictyostelium discoidium* filamin slow actin filament tunover by ~50% and recruit much of a significant population of actin oligomers that we measure are present in polymerized purified actin solutions into the immobile filament fraction. Surprisingly, these observations occur at very low stoichiometry to actin, approximately requiring only one filamin molecule bound per actin filament, similar to the amount required for actin filament gelation *in vitro*. Networks formed with filamin truncates localize this activity to the actin binding domain and reveal that dimerization and orthogonal cross-linking are not required for dynamic stabilization. Re-expression of filamin A with or without the actin binding domain in human melanoma cells that naturally lack this protein support the findings in purified actin networks. These results indicate that filamin cross-linking stabilizes filament dynamics by slowing filament subunit cycling rates and by either decreasing spontaneous filament fragmentation or promoting filament annealing.

Introduction

Actin filaments fill the cytoplasmic space of cells, determining cellular morphology, and provide motility through coordinated remodeling events. Certain actin-regulatory proteins govern the dynamic nature of actin by controlling the kinetics and access of monomers to filament ends, nucleating or severing filaments, sequestering monomers, or altering monomer nucleotide exchange [1, 2]. Other proteins cross-link adjacent actin filaments, creating structures that ultimately define the architecture and mechanical properties of cytoplasm [3, 4].

One cross-linking protein family, the filamins, are essential for non-muscle cell motility [5-7]. The most extensively studied family member is human Filamin A (FLNa[1]), which self-associates at its C-terminus to form a large (560 kDa) flexible homodimer [8]. FLNa organizes actin filaments into orthogonal networks by linking neighboring filaments together with its N-terminal actin binding domains [8, 9], and affixes the network to the plasma membrane through specific glycoprotein interactions at the C-terminus [10]. With many binding partners now described that may modulate its activity, FLNa participates in signaling cascades by spatially collecting and concentrating signaling proteins near the plasma membrane, possibly as an organizing center for local actin network rearrangements [3].

A homologous protein to FLNa found in amoeba, *Dictyostelium discoidium* filamin (ddFLN) has been shown to be an effective actin filament crosslinking protein *in vitro* that is essential to *Dictyostelium* cortical actin network structure [11-16]. ddFLN is a miniature version of the human counterpart, self-associating to form elongated dimers that bind adjacent actin filaments and assembling a three-dimensional filament network analogous to

FLNa [17, 18]. Cells that lack ddFLN exhibit defects in motility, chemotaxis, and phagocytosis [11, 14, 15] that can be rescued by ddFLN re-expression [16].

While most studies investigating cross-linking protein function have focused on their architectural and mechanical influences on actin filament networks, even in the highly cross-linked gel state, actin filaments are not static cellular structures, but exhibit dynamic 'turnover' through addition and loss of monomeric subunits from their ends [19, 20]. Therefore, direct binding interactions between cross-linking proteins and actin filaments may also influence the local dynamic stability and kinetic properties of the individual filaments composing the structures they create. Indeed, evidence that the actin filament bundling proteins α-actinin and the 30 kDa *Dictyostelium discoidium* actin-bundling protein slow actin filament depolymerization *in vitro* have been suggested to account for at least some portion of the remarkable stability of extracted, Triton-insoluble actin cytoskeletons [21-23]. Determining the influence of cross-linking on actin filament dynamics in individual cells will allow further understanding of the stability of subcellular structural domains of the cytoskeleton.

Here, we use a combination of reconstituted, purified actin network experiments and cellular studies to determine the effects of the filamin family of actin filament cross-linking proteins on the dynamics of actin networks. We develop a novel photoactivation of fluorescence (PAF) system for studying reconstituted, purified actin filament network dynamics based on simple physical relations governing purified actin filaments. This system measures the dynamics of steady state filament networks *in situ* with only minimal light perturbation, a clear advantage over other techniques that require mechanical sample manipulation and extrapolation of transient measurements to infer steady state dynamics. Using this system, we observe that polymerized solutions of purified actin filaments turnover very slowly and

contain a population of oligomers in excess of the amount of monomeric actin. Compared to these entangled filament networks, orthogonal cross-linking of actin filaments with filamins further decreases their rate of filament turnover and immobilizes a large percentage of the rapidly diffusing oligomers, an observation that, similar to the stoichiometries needed for actin filament gelation [24], only requires ~1 filamin molecule bound per actin filament. Using truncated filamin proteins, we localize these effects to the actin binding domain, independent of filamin dimerization and actin filament cross-linking activities. In support of the measurements in reconstituted actin networks, we show with PAF and fluorescence recovery after photobleaching (FRAP) that filament subunit cycling decreases in human melanoma cells spontaneously lacking FLNa when full-length FLNa is restored, but not if FLNa lacks the actin binding domain.

Experimental procedures

Caged resorufin iodoacetamide-labeled actin (CR-actin)

CR-actin was synthesized according to the method of Theriot and Mitchison [19]. Prior to labeling, rabbit muscle actin isolated as previously described [25] was further purified to remove contamination by Cap Z [26] with fast protein liquid chromatography on a Superose 6 column (Amersham Biosciences) and verified to be Cap Z free by immunoblotting with a polyclonal antibody that recognizes both the α and β subunits of Cap Z. Purified CR-actin was diluted to 70 μM in Buffer A (2 mM Tris-HCl, 0.2 mM $CaCl_2$, 0.5 mM β-mercaptoethanol, 0.5 mM ATP, pH 7.4), frozen in liquid nitrogen, and stored at –80 °C. The day before experiments, CR-actin was thawed, diluted to 10 μM in Buffer A, and placed at 4 °C overnight in the dark to equilibrate. Equilibrated CR-actin was centrifuged at 300,000 × *g* for 30 min at 4 °C and the supernatant was removed and stored in the depolymerized form at 4 °C.

Functionally, CR-actin is polymerization competent and rivals the assembly rate, lag time, and steady state fluorescence of equivalent experiments with unlabeled actin in a fluorescence-based actin assembly assay (data not shown). Briefly, these experiments were performed by mixing equal parts of monomeric CR-actin and 10% pyrene-labeled G-actin at a final concentration of 2 μM in Buffer B (10 mM Tris-HCl, 2 mM $MgCl_2$, 100 mM KCl, 0.1 mM EGTA, 0.5 mM β-mercaptoethanol, 0.5 mM ATP, pH 7.4) and monitoring the change in pyrene-actin fluorescence as actin filaments polymerize with a luminescence spectrometer (model LS-50B; PerkinElmer) at excitation and emission wavelengths of 366 nm and 388 nm, respectively.

Filamin purification

FLNa-ΔN153, a fusion protein lacking the first 153 amino acids of FLNa, was prepared using the polymerase chain reaction. A cDNA fragment encoding FLNa-ΔN153 was amplified using pFASTBAC FLNa [24] as the template, a forward primer, GAAGAGCTCATGTGGGACGAGGAGGAGGATG, containing a *Sac*I site, and a reverse primer, CACACTCGGTGCCCACCTTCACTTC. The 1.3 kbp of the amplified fragment was purified, *Sac*I/*Bst*BI-digested, ligated into the *Sac*I(*SstI*)/*Bst*BI(*Nsp*V) sites of the pFASTBAC1 vector (Invitrogen) to generate pFASTBAC1-ΔN153/*Bst*BI, and confirmed by sequencing. The 3'-site of FLNa cDNA was prepared by cutting pREP4 FLNa [27] with *Bst*BI and *Xba*I, and subsequently ligated into the pFASTBAC1-ΔN153/*Bst*BI opened with *Bst*BI and *Xba*I to create pFASTBAC1 FLNa-ΔN153.

FLNa-ΔC112, a fusion protein lacking 112 amino acids at the C-terminus, was prepared by cutting pREP4-FLNa-ΔC112 [27] (prepared in dam$^+$*E.coli*) with *Cla*I and *Xba*I, and ligated into the pFASTBAC1 FLNa (prepared in dam$^+$*E.coli*) after opening with *Cla*I and *Xba*I, thereby generating pFASTBAC1 FLNa-ΔC112.

Human recombinant FLNa, FLNa-ΔN153, and FLNa-ΔC112 were expressed using a Baculovirus Expression System (Invitrogen) in Sf9 insect cells and purified as previously described [24]. ddFLN was purifed from AX2 cells as detailed elsewhere [28]. All purified filamins were stored in aliquots at –80 °C.

F-actin co-sedimentation

Purified FLNa or FLNa-ΔN153 was incubated with or without 10 μM G-actin for 1 h at 23 °C in PHEM buffer (60 mM PIPES, 25 mM Hepes, 10 mM EGTA, 2 mM $MgCl_2$, pH 6.9)

containing 0.75% Triton X-100, followed by centrifugation at 100,000 × *g* for 20 min. Pellets were resuspended in the starting assay volume and equal volumes of supernatants and pellets were loaded onto 9% SDS-polyacrylamide slab gels where the proteins were electrophoretically separated and then visualized by staining with Coomassie Brilliant Blue.

Measurement of filament network gelation

Filamin-induced network gelation was determined using a miniature falling ball viscometer [29]. 2 μM rabbit muscle G-actin was polymerized by adding Buffer B in the presence of different concentrations of FLNa, FLNa-ΔC112, FLNa-ΔN153, or ddFLN. The mixtures were immediately drawn into vertically positioned 100 μl glass micropipettes (Fisher Scientific) and incubated at 23 °C for 60 min. Apparent viscosity was calculated by measuring the time required for a 0.7 mm diameter stainless steel ball to fall 5 cm in the micropipette.

Critical concentration

The steady state critical concentration of CR-actin, unlabeled actin, or unlabeled actin with 1:20 FLNa was determined by measuring the 24 h fluorescence of F-actin solutions at different concentrations containing a 1:5 mixture of 10% pyrene-labeled actin and CR-actin in Buffer B at 23 °C with a PerkinElmer luminescence spectrophotometer. Samples of unlabeled actin and unlabeled actin with FLNa were polymerized *de novo* at the appropriate final concentration, whereas CR-actin samples were prepared from serial dilutions of a 2 μM F-actin solution.

Reconstitution of purified actin filament networks

Rectangular, borosilicate glass microcapillary tubes (Friedrich and Dimmock) of dimensions 0.05 mm × 0.5 mm × 50 mm were sealed onto the end of a 100 μl glass micropipette with melted wax. A 1 ml syringe fitted with a two-way stopcock was connected to the other end of the micropipette by a length of silicone tubing and used to load the microcapillary tubes with the purified protein solutions. Prior to sample loading, the microcapillary tubes were coated with 1 mg/ml BSA for 2 min at 37°C to block actin adsorption to the glass surface. At this BSA concentration, < 1% of total actin was detected bound to the glass surface by SDS-polyacrylamide gel electrophoresis and Coomassie Brilliant Blue staining (data not shown). CR-actin was diluted to 2 μM in either Buffer A for G-actin experiments or Buffer B to induce actin polymerization for filament studies, and loaded into the BSA coated microcapillary tubes. For experiments including additional purified proteins, different concentrations of phallacidin, FLNa, ddFLN, FLNa-ΔN153, or FLNa-ΔC112 were mixed with CR-actin prior to sample loading. The tube was released from the micropipette by breaking it above the wax seal and the ends were sealed with seal-ease® clay (Beckton Dickinson). CR-actin was allowed to reach steady state (overnight) at room temperature in the dark.

Cell culture, motility, microinjection, and transfection

Human melanoma cells were cultured as previously described [5] in minimal essential medium (Invitrogen) supplemented with 8% newborn calf serum, 2% fetal bovine serum, and 100 U/ml penicillin/streptomycin. 0.5 mg/ml G_{418} (Invitrogen) was added to the growth media of FLNa expressing cells. For experiments, human melanoma cells were plated at ~30% confluence on uncoated glass coverslips. Cell motility was measured by quantitative time lapse video microscopy as previously described [20].

CR-actin was diluted to 1 mg/ml in Injection Buffer (1mM Hepes, 0.2 mM $MgCl_2$, 0.5 mM ATP, pH 7.4) containing 5 μM Alexa® 488 dextran (10 kDa; Molecular Probes), and microinjected into melanoma cells. Prior to experiments, microinjected melanoma cells were allowed to recover for 1 hour.

A plasmid encoding a fusion protein of human β-actin and enhanced green fluorescent protein (EGFP-actin; Clontech) was transfected into 70% confluent melanoma cells using a ratio of 2 μg/ml cDNA to 6 μl/ml Lipofectamine-2000® (Invitrogen) diluted in serum-free Opti-MEM® I (Invitrogen) and incubated for 5 h at 37°C and 5% CO_2 after which the transfection solution was replaced with normal growth media. Melanoma cells expressed detectable levels of EGFP-actin by 48 hours after transfection, and were used for experiments between 48 and 72 hours. The transfection efficiency was ~15% (data not shown).

Reconstituted actin network theory and simulations

In PAF experiments on steady state reconstituted actin networks, monomer diffusion, filament diffusion, and filament turnover determine the fluorescence decay of photoactivated bands of actin. Since the photoactivated band is bounded above and below by the microcapillary tube wall, diffusion is limited to one-dimension on a time scale of $\tau_D \sim \omega^2/D_\xi$, where ω is the band width and D_ξ is the diffusion coefficient for ξ = m or f, representing monomers or filaments, respectively. For ω = 100 μm and D_m = 71.5 $\mu m^2/s$ [30], monomer diffuses from the band within minutes. Regardless of whether filaments diffuse by worm-like reptation [31, 32] or similar to rigid rods [33], the mobility of filaments above a critical length along their longest contours are orders of magnitude less than monomer, with proportionately longer diffusion times.

Despite the complexity of the actin cycle, filaments turnover by a net flux of subunits from the 'barbed' to the 'pointed' filament end, where, at steady state, subunit assembly must exactly balance disassembly [34]. When filaments are long and turnover is slow compared to the rate of ATP hydrolysis on subunits, filament turnover is limited primarily by the rate of ADP-bound subunit dissociation at the pointed end (k_{pD}^-), expressed as $\tau_t \sim L_{avg}/k_{pD}^-$, where L_{avg} is the number-average filament length. As an upper limit, a 2 μm actin filament with $k_{pD}^- = 0.3$ s^{-1} [35] will completely recycle subunits in ~40 min.

Since monomer diffusion is markedly faster than both filament diffusion and turnover, filament dynamics dominate the long-term fluorescence evolution in photoactivated bands, starting only minutes after photoactivation. Additionally, since filament diffusion, but not turnover, depends on ω, filament turnover exclusively dominates the long-term fluorescence dynamics when ω becomes large. To test these limits, simulations of PAF experiments were performed for different values of ω to generate theoretical spatial fluorescence intensity profiles across the width of the photoactivated band using a dual-compartment mathematical model describing diffusion and turnover [36] in Matlab (version 5.2.1; The Mathworks) on a Macintosh G4 computer (Apple) with $\tau_\tau = 40$ min and $D_f = 1.8$ μm^2/s (calculated from [33] for a 2 μm rigid rod). 30 μm wide simulations exhibit spatial intensity profiles that simultaneously broaden, the hallmark of filament diffusion, and decay, a product of filament diffusion and turnover (Fig. III-1*A*). Simulations of 230 μm photoactivated bands show spatial fluorescence profiles that decay over time without broadening (Fig. III-1*B*), indicating the slow rate of filament diffusion from the photoactivated band as predicted.

PAF and FRAP

PAF and FRAP experiments were performed with a microscopy system that was modified from a previous design [37] to include an additional illumination path for photobleaching at 488 nm with a 100 mW argon ion laser (543-AP; Melles Griot). For melanoma cells, PAF and FRAP studies were performed essentially as previously described [20, 37] and analyzed with a two-compartment mathematical model that simultaneously determines the polymerized fraction (PF), the filament turnover time (τ_t), and the monomer diffusion coefficient (D_m) [36]. During the experiments, melanoma cells were maintained at 37 °C using a temperature controller (Harvard Apparatus) in Leibovitz's L-15 Media (Invitrogen) without phenol red supplemented with 10% FCS. For certain controls, melanoma cells were pre-treated with 1 μM jasplakinolide (Molecular Probes) for 30 min at 37 °C prior to photobleaching.

For PAF experiments on reconstituted actin networks, CR-actin was photoactivated by a 5 – 10 s 365 nm light pulse to produce a 30 μm or 230 μm wide rectangular region spanning the microcapillary tube and images were captured over time with a Gen III Image Intensifier (VS4-1845; Video Scope) and CCD camera (C2400-77; Hamamatsu) on a Zeiss IM-35 microscope using a 16X multi-immersion objective (NA = 0.5). The evolution of fluorescence at the center and across the width of the photoactivated region was measured with NIH Image software (developed at the U.S. National Institutes of Health and available on the Internet at http://rsb.info.nih.gov/nih-image/), corrected for photobleaching as detailed elsewhere [37] using a rate constant of 38.5 s, and stored for later analysis (see below). All reconstituted actin network experiments were performed at 23 °C.

Monomer diffusion coefficients were calculated from PAF experiments on unpolymerized CR-actin using the diffusive component of the two-compartment model [36] by setting $\tau_t =$

∞ to eliminate filament turnover and $PF = 0$ such that the entire actin pool is unpolymerized. Filament turnover times were calculated from the long-term fluorescence decay of PAF experiments in reconstituted actin networks using a simplified version of the two-compartment model [36], in which the fluorescence decay was fit by an exponential of the form $F^* = F(t)/F_o = Ie^{-t/\tau_t}$, where I is the 'immobile' fluorescence fraction and F_o is the initial fluorescence intensity; however, for this interpretation to be valid, three conditions must be satisfied. The first condition, $\omega << \ell$, is satisfied since $\omega \leq 230$ μm and ℓ = 50 mm, the length of the microcapillary tube. The second condition, $\beta << \pi^2/(1+\gamma)$, where $\beta = \tau_D/\tau_t$ and γ is the ratio of polymerized to monomeric actin (~10 for pure actin), is satisfied given that we measure $\beta \leq 0.1$ for all experiments (data not shown). The final condition is that filament diffusion, visualized as photoactivated band broadening, must contribute a negligible amount to the fluorescence decay. This condition was considered satisfied if the photoactivated band did not exceed 10% of its original width, calculated from filtered spatial fluorescence intensity profiles as the distance between points at opposite edges of the band that were 50% of the maximum profile intensity.

Actin cycle kinetic model

Results obtained from reconstituted actin network experiments were analyzed and compared with predictions from a comprehensive mechanistic model describing the steady state actin cycle [34], available on the Internet at http://mcgrathlab.urmc.rochester.edu/actincycle/. For computations, the total actin concentration was c_a = 2 μM, barbed and pointed ends were completely uncapped ($\alpha = \beta = 1$), profilin and β4-thymosin activities were disabled (P = B = 0), and a random hydrolysis model was assumed. Using experimental measurements of L_{avg} and PF, either the filament length or filament concentration was fixed and k_{pD}^- was

manipulated to simulate PAF experiments on reconstituted actin networks with and without filamin according to our estimates of this parameter from experimentally determined actin filament lifetimes. The critical concentration ($1-c_f/c_a$), polymer fraction (c_f/c_a), average filament length (c_f/n), and filament lifetime ($\tau_l = L_{avg}/\bar{q}$) predicted by the model were compared to experimental observations. Here, c_f is the F-actin concentration, n is the concentration of actin filaments, and $\bar{q}$ is the subunit flux through filaments.

Fluorescence measurement of actin assembly

Melanoma cells were grown on 0.1% gelatin coated borosilicate glass tubes to a desired density in standard culture medium, detergent extracted with 0.1% Triton X-100, and the assembly of 1 μM pyrene-labeled actin on free cytoskeletal filament ends was assayed as previously described [20]. Experiments were repeated in the presence of 2 μM cytochalasin B to determine cellular barbed and pointed end content as detailed elsewhere [38]. Cell density was calculated in control glass tubes maintained in parallel culture by trypsinizing the cells from the surface and counting them with a hemocytometer.

Measurement of actin filament lengths

In reconstituted actin networks, the number-average filament length $L_n = (\sum n_i \ell_i)/(\sum n_i)$, where n_i is the number of actin filaments at length ℓ_i, was determined for each experiment by negative staining with 2% uranyl acetate and electron microscopy as previously described [8] on samples prepared in parallel to those loaded into microcapillary tubes for PAF studies. This technique was chosen over others because it requires no pipetting steps during sample manipulation and therefore minimizes artifacts from filament fragmentation. Negatively stained actin filaments were visualized at 5000X and 25000X on a transmission electron microscope (model JEM-1200EX; JEOL) with an accelerating voltage of 80 kV.

Photographic negatives were digitized, further magnified, and the contour lengths of at least 100 actin filaments were measured using NIH Image. Filaments in which both ends could not be discriminated were skipped. The shortest actin filament measured was 0.15 μm (~54 monomers); filaments 0.2 μm long were routinely measured. The weight-average filament length, $L_w = \left(\sum n_i \ell_i^2\right) / \left(n_i \ell_i\right)$, was calculated and used to determine the polydispersity index (L_n / L_w) to characterize the spread of the filament length distribution.

In melanoma cell cytoskeletons, the average filament length was calculated with $L_{avg} = \left(N_A PF m_a\right) / \left(aMn_f\right)$, where N_A is Avagadro's constant, PF is the polymer fraction, a = 370 monomers per μm filament length [39], M = 42 kDa for monomeric actin [40], and n_f is the number of filaments per cell. The actin mass per cell (m_a) was calculated as 11% of total cellular protein [5] using a bicinchoninic acid protein assay (Pierce Biotechnology).

Immunofluorescence

BAECs were fixed with 2% formaldehyde for 20 min at 23 °C, followed by permeabilization with 0.2% Triton X-100 in PBS for 5 min. Samples were incubated with 1 μM Alexa® 546 phalloidin for 10 min to stain actin filaments, washed three times in PBS, and mounted (Aqua Polymount; Polysciences) onto glass microscope slides. Images were digitally recorded with a cooled CCD camera (Orca II ER; Hamamatsu) on a Nikon Eclipse TE2000 microscope with a 63X oil immersion objective and MetaMorph® software (Universal Imaging Corporation).

Results

Monomer diffusion and the amount of polymerized actin in reconstituted networks

PAF experiments with unpolymerized actin establish the diffusivity of CR-actin monomer as D_m = 58 ± 24 μm^2/s in a low salt (Buffer A) aqueous solution at 23 °C. This measurement is consistent with published values by other investigators of D_m = 49 – 81 μm^2/s using dynamic light scattering and FRAP [30, 41-44]. Uncaged monomeric actin diffuses from a 230 μm wide fluorescent region within seconds, and the entire photoactivated band is uniformly dispersed minutes following photoactivation (Fig. III-2). Given this time course, monomer diffusion from the photoactivated band is ≥ 95% complete by ~5 min following photoactivation; therefore, subsequent fluorescence changes in the photoactivated band result from filament dynamics.

To determine whether CR-labeling and cross-linking affect the distribution between unpolymerized and polymerized actin, we measure the critical concentration required for actin filament self-assembly using classical techniques. In a high salt (Buffer B) aqueous solution at 23 °C, the critical concentration of CR-actin is 0.18 ± 0.03 μM (Fig. III-3), a value that is similar to unlabeled actin (0.15 ± 0.01 μM) and in good agreement with published reports for other labeled and unlabeled actins [45, 46]. In the presence of FLNa cross-linker at actin gelling concentrations, the critical concentration is 0.19 ± 0.01 μM (Fig. III-3). Since the critical concentration is essentially unaffected by filament cross-linking, entangled and cross-linked reconstituted actin networks contain equivalent fractions of total actin polymerized, calculated as $PF = (c_a - c_c)/c_a \cong 0.92$, where $c_a = 2\ \mu$M, the total actin concentration.

Actin dynamics in reconstituted networks of entangled purified filaments

To establish experimental conditions where filament turnover dominates filament diffusion in the long-term fluorescence decay, we examine different widths of photoactivated bands based on the predicted time scales of these two processes (see experimental procedures). For 30 μm wide photoactivated bands, the fluorescence simultaneously decays as the band broadens (Fig. III-4*A*), a relationship that reflects both filament diffusion and turnover in mathematical simulations (Fig. III-1*A*). In contrast, the fluorescence liberated within 230 μm wide photoactivated bands decays over time without an appreciable increase in width (Fig. III-4*A*), as predicted in simulations where filament turnover dominates (Fig. III-1*B*).

Interpreting the center-line fluorescence intensities, we measure that the fraction of immobile actin is 0.65 ± 0.03 and 0.65 ± 0.02 in 30 μm and 230 μm wide photoactivated bands, respectively (Fig. III-4*B*). If all filaments were immobile, the immobile fraction would equal the polymer fraction. Since the polymer fraction greatly exceeds the immobile fraction, the difference represents a population of oligomers that diffuse on the same time scale as actin monomers. For filaments to diffuse rapidly, they must be composed of few subunits, since longer, rod-like filaments are significantly less mobile than globular monomers. Experimentally, it has been observed that 10-mer filaments diffuse similar to rigid rods [47], indicating that the oligomers we detect in entangled filament networks are likely < 10 subunits (~27 nm) in length.

From experiments with 230 μm wide photoactivated bands where filament turnover dominates, we measure that purified filament turnover occurs slowly with an average lifetime of 6.1 ± 0.7 h (Fig. III-4*C*). To validate whether the fluorescence decay is due to filament turnover, CR-actin was polymerized to steady state in the presence of equimolar phallacidin, a compound that reduces the critical concentration at both filament ends to nearly zero [48].

With phallacidin, nearly all of the actin becomes immobilized (0.98 ± 0.02) and photoactivated bands of CR-actin show only marginal fluorescence decay 6 h after photoactivation (data not shown), corresponding to extremely long filament turnover times (Fig. III-4, *B* and *C*). These results are consistent with the stabilizing effect of phallacidin-F-actin subunit complexes, which promote increased incorporation of actin monomers into polymer and decrease the recycling rate of filament subunits [48].

The number-average actin filament length measured from electron micrographs of negatively stained actin filaments is 2.1 ± 1.8 μm in purified filament networks. The distribution of filament lengths is broad with a polydispersity index of 0.58 and skewed towards shorter filaments (Fig. III-4*D*), consistent with the exponential distributions observed in other studies and by different methods [8, 49-51]. As expected, adding phallacidin causes filaments to significantly lengthen to 3.4 ± 1.5 μm in comparison to actin alone ($p < 0.01$) and results in a length distribution that is more compact (data not shown), characterized by a polydispersity index of 0.84.

Effect of cross-linking on reconstituted network actin dynamics

Unlike entangled networks, 30 μm photoactivated bands of CR-actin assembled in the presence of purified human FLNa or ddFLN fail to broaden with time (Fig. III-5*A*). Since photoactivated filament diffusion is greatly hindered in the presence of cross-linker, we directly measure the filament turnover time from the long-term fluorescence decay over a range of FLNa concentrations to determine the effects of filamin-mediated cross-linking on the dynamic cycling of filament subunits. At a ratio of 1 FLNa per 500 actin monomers, there is a sharp increase in the average filament lifetime to 12.0 ± 1.0 h (Fig. III-5*B*), corresponding to a ~50% decrease in the filament turnover rate compared to purified filaments in the entangled state ($p < 0.01$). The addition of more cross-linker does not

further increase the filament turnover time, which remains slowed to a similar extent up to a molar ratio of 1:5 FLNa to actin monomers. Given the low stoichiometry, the dose-response relationship suggests that relatively few FLNa molecules are required to maximally decrease the rate of purified filament turnover.

In addition to its stabilizing effect on filament turnover, FLNa binding to actin filaments dose-dependently increases the immobile fluorescence fraction (Fig. III-5*C*), bringing it closer to the total polymer content measured directly from the critical concentration of CR-actin and implying that oligomers become trapped within the cross-linked network. Despite the requirement of at least 1 FLNa per 800 actin monomers to induce network gelation (Fig. III-3, *inset*), we observe that even at low stoichiometries the addition of FLNa to reconstituted networks tends to immobilize more actin than without cross-linker. In filament gels above a molar ratio of 1 FLNa to 500 actin monomers, the percentage of immobile actin increases on average by ~15 – 20% over actin alone ($p < 0.05$). At the highest concentration tested, the immobile fraction reaches a maximum average value of 0.87 ± 0.03 when 1 FLNa molecule is present for every 5 actin monomers.

Similar to the observations with FLNa, we measure that reconstituted actin networks cross-linked with 1:100 or 1:20 purified ddFLN exhibit longer filament turnover times and have more of their actin immobilized when compared to actin alone (Fig. III-5, *B* and *C*). At a molar ratio to actin of 1:20, ddFLN cross-linked filaments contain 0.85 ± 0.02 of their F-actin in the immobile fluorescence pool ($p < 0.01$) and slowly turnover subunits in 8.7 ± 1.4 h. Since ddFLN and FLNa similarly affect purified actin remodeling, stabilization of actin dynamics and oligomer trapping may be a general property of filamin family proteins.

To further understand the fate of oligomers immobilized by filamins, we compare the lengths of actin filaments in cross-linked and entangled filament networks. In the presence

of FLNa or ddFLN the percentage of filaments < 1 μm decreases from ~30% in entangled networks to ~5% after cross-linking (Fig. III-5, *D* and *E*), resulting in an increase in the number-average length to 3.5 ± 1.8 μm and 2.4 ± 1.2 μm for FLNa and ddFLN, respectively, and more compact filament length distributions (polydispersity indices ~0.80). While some lengthening of filaments is expected in cross-linked networks since turnover slows, this can only explain a portion of the lengthening effect, implying that filamins either decrease filament fragmentation by quenching the spontaneous generation of oligomers or enhance oligomer annealing onto the free ends of longer filaments in the network.

Localization of the stabilizing effect of filamins on purified actin dynamics

To investigate whether stabilization of actin dynamics and oligomeric incorporation depend on FLNa-mediated filament cross-linking and/or F-actin subunit binding, we employ amino acid truncates of the full-length FLNa molecule that lack either actin-binding capacity (FLNa-ΔN153) or the ability to self-associate into dimers (FLNa-ΔC112). In a F-actin co-sedimentation assay, FLNa-ΔN153 is absent from the pellet after centrifugation at 100,000 × g in contrast to the full-length FLNa molecule (Fig. III-6*A*), revealing that FLNa-ΔN153 is unable to bind F-actin. Both truncated FLNa molecules, even at high stoichiometry to actin, do not form stiff gels (Fig. III-6*B*), as demonstrated by classic gel point measurements.

In reconstituted actin networks, FLNa-ΔC112 slows filament turnover to 15.4 ± 0.3 h compared to measurements on entangled actin filaments ($p < 0.01$) but FLNa-ΔN153 does not (Fig. III-6*C*), thus localizing this activity to the actin binding domain. Similarly, only the FLNa-ΔC112 truncate retains the ability to immobilize oligomers (Fig. III-6*D*), indicating that filamin dimerization and filament cross-linking activities are not required to stabilize filament turnover and trap oligomers.

Rate constants for filament turnover in entangled and cross-linked filament networks

We use a first-order treadmilling model to estimate the F-actin disassembly kinetics at the pointed filament end. While the true nature of actin cycling is more complex, the treadmilling model of filament turnover is valid for actin concentrations near the critical concentration of ATP-bound subunits at the pointed end (~0.6 μM), similar to that used in these studies [35, 45, 46]; under these circumstances, filament elongation is observed exclusively at the barbed end [52]. Of the three F-actin subunit species (ATP-, ADP•Pi-, and ADP-bound) that dissociate from pointed ends, the predominate species is ADP-bound actin [34] since purified filament turnover is slow and the filaments are relatively long at steady state in reconstituted actin networks. For a steady state treadmilling model, by definition, monomer assembly at the barbed end must exactly balance disassembly at the pointed end. Therefore, we use the simple relationship $\tau_t = L_{avg}/k_{pD}^-$ to estimate k_{pD}^-, the dissociation rate constant for ADP-bound subunits from the pointed end. Since our technique determines actin filament subunit disassembly rates in a true steady state actin network free from mechanical perturbation, it therefore provides the best estimates to date of steady state rate constants.

Using this relationship we estimate that $k_{pD}^- = 0.042 \pm 0.005$ s^{-1} for purified actin filaments, consistent with the lowest values reported by other investigators in purified actin preparations [53]. For cross-linked actin networks with 1 FLNa or ddFLN per 100 actin monomers, the treadmilling model predicts that k_{pD}^- decreases to 0.031 ± 0.008 s^{-1} and 0.027 ± 0.004 s^{-1}, respectively. Since the rates are indistinguishable, these homologous proteins likely utilize similar mechanisms to slow filament subunit loss. However, because

treadmilling is an incomplete description of the complex kinetic events governing actin cycling, these values may represent an upper limit for k_{pD}^{-}.

To address these issues and validate our experimental findings, we use a comprehensive mathematical model that provides a complete kinetic description of the steady state actin cycle [34] to simulate our data and derive parameters that describe purified actin remodeling (Table III-1). At a constant filament concentration, decreasing k_{pD}^{-} results in a marked increase in actin filament lifetimes, as observed in our studies including filamin cross-linker; but, in contrast to our measurements, changing k_{pD}^{-} produces little change in the average filament length. Holding filament length constant and decreasing k_{pD}^{-} also results in longer filament lifetimes, which further increase if filaments lengthen. These results indicate that changes in k_{pD}^{-} alone cannot account for the significantly longer filaments present in cross-linked networks, in support of a filamin-mediated fragmentation/annealing mechanism to explain these observations. In addition, these simulations show that the predicted polymer fraction, and therefore the critical concentration, are not only similar to our experimental measurements, but are relatively insensitive to changes in k_{pD}^{-} of this magnitude, confirming our observations.

Effect of FLNa on cellular actin dynamics

It has been well established that human melanoma cells discovered to spontaneously lack FLNa expression (hereafter referred to as M2 cells) translocate poorly compared to their FLNa rescued counterparts (A7 cells) [5]. Our results confirm this work, as we measure that A7 cells crawl at a speed of 0.34 ± 0.17 μm/min, while the net movement of M2 cells is undetectable in our assay. Despite a failure to move efficiently, M2 cells rapidly form and

retract large blebs from their surfaces that are lost in A7 cells. We sought to determine the basis for the FLNa- M2 cell's uncontrolled protrusive behavior.

M2 and A7 cells were microinjected with CR-actin or transfected with EGFP-actin such that their actin dynamics may be probed with PAF or FRAP, respectively. For PAF experiments, CR-actin incorporates into the actin cytoskeleton where it functions as a reliable tracer of actin remodeling events [19, 20]. For FRAP studies, EGFP-actin co-localizes extensively with F-actin, as visualized by Alexa®-546 phalloidin staining, in fixed, detergent extracted M2 and A7 cells (Fig. III-7*A*). The actin fluorescence pattern observed in M2 cells is more homogeneous and diffuse than that of the FLNa-expressing A7 cells, which localize actin to the cortical region at the cell edge. In contrast to A7 cells whose periphery is replete with filopodia, the periphery of M2 cells contains numerous circular fluorescent rings of EGFP-actin, which in living M2 cells expressing EGFP-actin are identified as spherical blebs that rapidly extend and retract from the cell surface (supplemental videos *A* and *B*).

Since previous reports reveal that M2 and A7 cell F-actin content is time-dependent after plating and correlates inversely with cytoplasmic stability measured by the presence of surface blebbing [5], we use PAF and FRAP to measure actin dynamics in these cells before (24 h) and after (≥ 72 h) the surfaces of melanoma cells have stabilized. In confirmation of previous work [6, 54], we measure that the F-actin content increases in M2 and A7 cells residing on the substrate for a longer period of time and that FLNa- M2 cells consistently polymerize more of their total actin than FLNa+ A7 cells (Fig. III-7*B*), reaching a polymer fraction of 0.62 ± 0.04 and 0.49 ± 0.03, respectively, ≥ 72 h after plating. C1 melanoma cells that do not express detectable FLNa by immunoblot (data not shown) support the M2 cell observations since they also contain more actin polymer than A7 cells. Pre-treatment of M2 and A7 cells for 30 min with 1 μM jasplakinolide, a potent

cell membrane permeant actin polymerizing agent, elevates the polymer fractions in excess of 90% in both phenotypes, indicating that nearly all of the expressed EGFP-actin is functional.

Despite their lack of efficient translational locomotion, we measure that M2 cells exhibit similar filament lifetimes when compared to their FLNa expressing A7 counterparts (Fig. III-7*C*). During the phase when their surfaces are most unstable ~24 h after plating, M2 cells turnover filaments more rapidly than A7 cells, with lifetimes of 6.6 ± 1.2 min. Despite their radically different motile phenotypes and distributions of monomer and polymer, eventually M2 and A7 cells achieve equivalent ~18 min filament lifetimes.

While other cell types increase their actin remodeling in proportion to their crawling speed [20], melanoma cells lacking FLNa do not follow this convention. To better understand actin dynamics in these two cell lines, we determine the average length of cellular actin filaments from measurements of pointed end numbers in permeabilized cells and total actin content (Table III-2). Biochemical assays measuring the rate of pyrene-labeled actin assembly onto Triton X-100 permeabilized cell cytoskeletons reveal that M2 cells contain ~60% less pointed filament ends per cell (44,700 ± 11,900) than A7 cells. While the number of free pointed ends is the best estimate of the total number of actin filaments per cell, this value may underestimate the filament number if a significant portion of pointed filament ends are capped by tropomodulins [55] or the Arp2/3 complex [56]. Not surprisingly, A7 cells also have fewer filaments with uncapped barbed ends, 5,210 ± 1,530. The average lengths of actin filaments comprising the cytoskeletal network in M2 and A7 cells averge average 4.7 μm and 1.4 μm, respectively, calculated from the polymer fraction, filament number, and total actin mass per melanoma cell[2]. These results suggest that M2

cells increase the average lengths of their actin filaments in an attempt to create more rigid networks and restore the mechanical stability that FLNa imparts to their actin cytoskeleton.

A first-order model of steady state actin filament dynamics predicts that F-actin subunit loss from the filament end is directly proportional to the length of the actin filament undergoing depolymerization. Our findings show that M2 cells compensate for FLNa loss by increasing both basal filament concentration and filament length. Since both melanoma cell phenotypes exhibit nearly identical filament turnover times, and if we assume that the cells are on average at a steady state, then to turnover at the same rate the longer filaments that populate the M2 cell cytoskeleton must depolymerize significantly faster than those in the A7 cell, implying that filaments lose subunits ~3X faster in the absence of FLNa. While a steady state assumption is not likely to be true in cells, the correlation between FLNa expression and filament turnover stabilization observed in reconstituted actin networks holds in the melanoma cells.

To determine whether the actin binding activity of FLNa is required to stabilize actin dynamics in M2 cells as observed in reconstituted networks, we use M2 cell clones stably transfected with a human FLNa cDNA lacking the actin binding domain (C5 cells), which was generated by removing amino acids 23 – 233 near the N-terminus of full-length FLNa [57]. Loss of actin binding ability does not rescue C5 melanoma cells from the M2 phenotype; C5 cells continue to produce blebs at their surface and do not productively crawl (supplemental video *C*). We measure that C5 cells have turnover times and polymer fractions similar to M2 cells, indicating that it is the actin binding activity of filamin that promotes the stability of filament turnover, consistent with the loss of turnover stabilizing function observed in reconstituted networks with FLNa truncates that are unable to bind F-actin.

Discussion

Filamins have long been recognized as important organizers of the cytoskeletal architecture, linking filaments into three-dimensional lattices that govern cell mechanics and shape. We reveal an additional role for filamins as modulators of actin filament dynamic stability and kinetics. Along with their potent gelation activity, filamins slow the rate of actin filament turnover to further stabilize filaments in cross-linked actin networks. In addition, filamins immobilize oligomers present in purified actin preparations, incorporating them into existing filaments which grow longer than would be predicted solely for decreased rates of cycling, revealing that filamins promote annealing and/or decrease spontaneous fragmentation of filaments. These properties occur at low stoichiometries, only requiring ~1 FLNa molecule bound per actin filament. Filamin-induced filament stabilization may play an important role in cell movement and shape change by stabilizing existing cytoplasmic gels in the bulk cytoskeleton and newly formed networks at the active sites of membrane protrusion in the cell cortex.

Significance of the purified protein PAF system for studying reconstituted actin networks

Here, we utilize PAF for the first time to analyze actin remodeling in purified reconstituted actin networks at steady state. In these experiments, the long-term fluorescence in photoactivated bands of actin decays due to two competing mechanisms that rearrange the actin network – filament diffusion and filament turnover – which can be isolated from each other simply by using different widths of photoactivated bands. This system measures the dynamics of steady state actin filament networks *in situ* with only minimal light perturbation, which represents a clear advantage over previous techniques relying on

mechanical sample manipulations and extrapolation of transient measurements to infer steady state dynamics. Under certain conditions, this system can be used to estimate the pointed end ADP-bound subunit dissociation rate constant, a range of published values dor purified actin that currently span an order of magnitude. Parameters describing actin dynamics that are obtained with this purified system can then be tested against theoretical actin model predictions and values obtained in cellular experiments to further understand the mechanisms by which actin regulatory proteins influence actin remodeling. In this work, we have evaluated the effect of two orthogonal filament cross-linking proteins, ddFLN and FLNa, on purified actin dynamics in reconstituted networks as a model system for understanding aspects of the cellular actin cytoskeleton.

Cross-linking stabilizes actin filament turnover

Forming a gel with ddFLN or FLNa hinders diffusion in 30 μm wide photoactivated bands of CR-actin and unexpectedly, these cross-linked actin gels also exhibit decreased rates of filament turnover, but only if the actin binding activity of filamin is intact. The actin-binding domain of filamin binds multiple actin monomers in the long-pitch helix groove of actin filaments as evidenced by competition of filamin-actin binding by tropomyosin [58] and by the stoichiometry of filamin-actin binding [59]. When actin polymerizes in the presence of FLNa, perpendicular branching of actin filaments occurs producing X- and T-shaped junctions as filaments are recruited into the actin network by filamin. At T-junctions, pointed filament ends abut the sides of other filaments [8]. As monomeric subunits cycle from entrapped filaments in the actin network, filaments shorten from their pointed ends and eventually encounter bound filamin molecules. Binding of overlapping adjacent F-actin subunits at the pointed ends of actin filaments by filamin could stabilize these ends, reducing ADP-F-actin subunit dissociation and decreasing the filament cycling rates. Since

FLNa and ddFLN share homologous actin binding domains, and the estimated dissociation constants are indistinguishable, these sequence related but structurally different proteins function similarly.

Experiments in melanoma cells with or without FLNa reveal a similar relationship between the presence of FLNa and the cycling rate of actin filaments given a model based on first-order turnover kinetics. The effect of FLNa expression on actin filament length and number as determined here with PAF and biochemical actin nucleation experiments is also directly observable by electron microscopy [54]. M2 cells attempt to compensate for their deficient ability to gel actin filaments by increasing their polymer fraction and actin filament lengths in order to increase the rigidity of their actin network. They also may activate accessory actin binding proteins to accelerate actin filament turnover rates to levels observed in cells expressing FLNa that have much shorter actin filaments on average. The stabilizing effect of FLNa on the actin network in A7 cells may decrease the turnover rate of actin filaments, as observed in cross-linked reconstituted actin networks of purified actin and FLNa.

In confirmation of measurements in the reconstituted networks, experiments in melanoma cells expressing FLNa truncates lacking the actin binding domain behave phenotypically and dynamically identical to M2 cells, indicating the importance of actin binding activity for filamin-induced filament stabilization. Since the vast majority of FLNa binding partners interact near the C-terminus [3], signaling intermediates acting through FLNa in M2 cells expressing the FLNa actin binding truncate are unable to compensate for loss of FLNa binding; however, without the actin binding domain FLNa is likely unable to localize to appropriate subcellular domains.

Filamins may function as a molecular 'clutch'

In many other cell types, the pace of actin dynamics correlates positively with the speed of cell movement [20]. Straying from this relationship, loss of FLNa in melanoma cells eliminates cell movement but actin cycling continues unimpeded at an enhanced rate since M2 cells must turnover significantly longer filaments. At the other end of the spectrum, one report reveals that increased binding of FLNa to β–integrin tails negatively regulates cell motility [60], implying a parabolic relationship between cell crawling behavior and levels of cytoplasmic FLNa, as observed previously in M2 cell clones induced to express different amounts of FLNa [5]. In this way, we observe that FLNa is an important coupling factor between actin remodeling and productive cellular locomotion, and may engage and disengage the dynamic cytoskeleton similar to a molecular 'clutch' to regulate cell translocation. While there is evidence that phosphorylation modulates filamin's activity [61-64], the regulatory mechanisms controlling the interactions of filamin with the cytoskeleton remain largely unknown.

Filamins trap actin oligomers in reconstituted actin networks by altering filament fragmentation and/or annealing

Filaments diffuse in purified actin solutions, but at different rates depending on their length. Since polymerization is unregulated in purified actin preparations, the steady state filament length distribution is polydisperse, containing filaments with a wide range of mobilities. Some filaments are small enough to diffuse similar to actin monomers, and therefore are excluded from the immobile fraction of longer filaments in PAF experiments. Published studies provide ample evidence for the existence of populations of stable actin oligomers in purified actin solutions [30, 41, 42, 65, 66], which when isolated by gel filtration were identified primarily to be actin dimers [30].

We measure the presence of a significant population of oligomers in steady state purified F-actin preparations, a large fraction of which disappear after filamin binding. Oligomer trapping by filamins occurs without an appreciable change in the amount of monomeric actin, as determined by the critical concentration. Since filaments grow longer and the length distribution changes in the presence of cross-linker, these oligomers are incorporated into the immobile fraction. The slowing of F-actin subunit turnover by filamins could theoretically cause filaments to grow longer, but kinetic modeling predicts an insignificant change in filament length under our conditions. Therefore, to increase filament length significantly as observed in our studies, filamins must either stabilize filaments against breakage or promote the annealing of oligomers onto filament ends.

The spectrin superfamily of cross-linking proteins influence the dynamic stability of cytoplasmic gels

Other investigators have implicated cross-linking proteins as mediators of actin filament stability in an attempt to explain the remarkable longevity of portions of the actin cytoskeleton following detergent extraction [22, 23]. Compared to the size and functional diversity of this broad class of proteins, relatively few studies, all with filament bundling proteins at high stoichiometries to actin, have been performed to address the influence of filament cross-linking proteins on actin dynamics [21, 23]. The effects of filamin observed here occur at doses well below those employed in these studies on well-defined steady state networks with purified proteins.

Members of the spectrin superfamily of actin cross-linking proteins (β-spectrin, dystrophin, filamin, fimbrin, plectin, α-actinin, and utrophin) are structurally diverse but contain conserved actin binding regions at their NH_2-termini [4] which complex with F-actin through calponin homology domains [67]. Spectrin, α-actinin, and filamin have a single

actin binding region with two calponin homology domains, one that is required for filament binding and one that is not required but may increase the binding affinity [68, 69]. While similarities exist between their actin binding regions, many of these related proteins are believed to have additional F-actin interaction sites and/or the ability to modulate their calponin homology domains to express differential functions [70]. Regardless of their plasticity, we observe that both FLNa and ddFLN, two closely related proteins, decrease the rate of purified filament turnover to similar extents. Since α-actinin and 30 kD *Dictyostelium* actin bundling protein also slow depolymerization, other proteins in the spectrin superfamily may share similar filament stabilization mechanisms.

Compared to filaments bundles which disassemble slowly [71], dynamic cellular structures like lamellipodia, filopodia, and membrane ruffles likely require a different set of cross-linking proteins with unique properties to form, such as the Arp2/3 complex and filamin. However, despite expressing nearly wild-type levels of gelsolin, α-actinin, profilin, fodrin, and the Arp2/3 complex, among others, M2 cells develop a continuous array of abnormal spherical protrusions from their surface are unable to crawl [5, 54]. Therefore, actin filaments organized into high-angle dendritic arrays and parallel bundles by the Arp2/3 complex and α-actinin, respectively, are insufficient to stabilize the cortical cytoplasm of these cells. Rescuing M2 cells with FLNa repairs these defects [5]. We conclude that one aspect of this repair mechanism may involve the dynamic stabilization of actin filaments by FLNa.

Acknowledgments

Special thanks to Dr. Lisa Flanagan for generously providing the human melanoma cells. We would also like to thank Dr. Thomas P. Stossel for critically reviewing this manuscript and his insightful comments. Support for this research was provided by the National Institutes of Health (HL56993, J. H. Hartwig; HL54145, C. F. Dewey, Jr.). E. A. Osborn is a Whitaker Foundation Graduate Fellow.

References

1. Stossel, T.P., et al., *Cell crawling two decades after Abercrombie.* Biochem Soc Symp, 1999. **65**: p. 267-80.
2. dos Remedios, C.G., et al., *Actin binding proteins: regulation of cytoskeletal microfilaments.* Physiol Rev, 2003. **83**(2): p. 433-73.
3. Stossel, T.P., et al., *Filamins as integrators of cell mechanics and signalling.* Nat Rev Mol Cell Biol, 2001. **2**(2): p. 138-45.
4. Dubreuil, R.R., *Structure and evolution of the actin crosslinking proteins.* Bioessays, 1991. **13**(5): p. 219-26.
5. Cunningham, C.C., et al., *Actin-binding protein requirement for cortical stability and efficient locomotion.* Science, 1992. **255**(5042): p. 325-7.
6. Cunningham, C.C., *Actin polymerization and intracellular solvent flow in cell surface blebbing.* J Cell Biol, 1995. **129**(6): p. 1589-99.
7. Fox, J.W., et al., *Mutations in filamin 1 prevent migration of cerebral cortical neurons in human periventricular heterotopia.* Neuron, 1998. **21**(6): p. 1315-25.
8. Hartwig, J.H., J. Tyler, and T.P. Stossel, *Actin-binding protein promotes the bipolar and perpendicular branching of actin filaments.* J Cell Biol, 1980. **87**(3 Pt 1): p. 841-8.
9. Hartwig, J.H. and P. Shevlin, *The architecture of actin filaments and the ultrastructural location of actin-binding protein in the periphery of lung macrophages.* J Cell Biol, 1986. **103**(3): p. 1007-20.
10. Gorlin, J.B., et al., *Human endothelial actin-binding protein (ABP-280, nonmuscle filamin): a molecular leaf spring.* J Cell Biol, 1990. **111**(3): p. 1089-105.
11. Brink, M., et al., *A Dictyostelium mutant lacking an F-actin cross-linking protein, the 120-kD gelation factor.* J Cell Biol, 1990. **111**(4): p. 1477-89.
12. Condeelis, J., J. Salisbury, and K. Fujiwara, *A new protein that gels F-actin in the cell cortex of D. discoidium.* Nature, 1981. **292**: p. 161-3.
13. Condeelis, J., et al., *Properties of the 120,000- and 95,000-dalton actin-binding proteins from Dictyostelium discoideum and their possible functions in assembling the cytoplasmic matrix.* J Cell Biol, 1984. **99**(1 Pt 2): p. 119s-126s.
14. Cox, D., et al., *Targeted disruption of the ABP-120 gene leads to cells with altered motility.* J Cell Biol, 1992. **116**(4): p. 943-55.
15. Cox, D., et al., *Genetic deletion of ABP-120 alters the three-dimensional organization of actin filaments in Dictyostelium pseudopods.* J Cell Biol, 1995. **128**(5): p. 819-35.
16. Cox, D., et al., *Re-expression of ABP-120 rescues cytoskeletal, motility, and phagocytosis defects of ABP-120- Dictyostelium mutants.* Mol Biol Cell, 1996. **7**(5): p. 803-23.

17. Fucini, P., et al., *The repeating segments of the F-actin cross-linking gelation factor (ABP-120) have an immunoglobulin-like fold.* Nat Struct Biol, 1997. **4**(3): p. 223-30.

18. Fucini, P., et al., *Molecular architecture of the rod domain of the Dictyostelium gelation factor (ABP120).* J Mol Biol, 1999. **291**(5): p. 1017-23.

19. Theriot, J.A. and T.J. Mitchison, *Actin microfilament dynamics in locomoting cells.* Nature, 1991. **352**(6331): p. 126-31.

20. McGrath, J.L., et al., *Regulation of the actin cycle in vivo by actin filament severing.* Proc Natl Acad Sci U S A, 2000. **97**(12): p. 6532-6537.

21. Zigmond, S.H., R. Furukawa, and M. Fechheimer, *Inhibition of actin filament depolymerization by the Dictyostelium 30,000-D actin-bundling protein.* J Cell Biol, 1992. **119**(3): p. 559-67.

22. Watts, R.G. and T.H. Howard, *Role of tropomyosin, alpha-actinin, and actin binding protein 280 in stabilizing Triton insoluble F-actin in basal and chemotactic factor activated neutrophils.* Cell Motil Cytoskeleton, 1994. **28**(2): p. 155-64.

23. Cano, M.L., et al., *Mechanisms responsible for F-actin stabilization after lysis of polymorphonuclear leukocytes.* J Cell Biol, 1992. **116**(5): p. 1123-34.

24. Nakamura, F., et al., *Comparison of filamin A-induced cross-linking and Arp2/3 complex- mediated branching on the mechanics of actin filaments.* J Biol Chem, 2002. **277**(11): p. 9148-54.

25. Spudich, J.A. and S. Watt, *The regulation of rabbit skeletal muscle contraction. I. Biochemical studies of the interaction of the tropomyosin-troponin complex with actin and the proteolytic fragments of myosin.* J Biol Chem, 1971. **246**(15): p. 4866-71.

26. Casella, J.F., E.A. Barron-Casella, and M.A. Torres, *Quantitation of Cap Z in conventional actin preparations and methods for further purification of actin.* Cell Motil Cytoskeleton, 1995. **30**(2): p. 164-70.

27. Ohta, Y., et al., *The small GTPase RalA targets filamin to induce filopodia.* Proc Natl Acad Sci U S A, 1999. **96**(5): p. 2122-8.

28. Condeelis, J. and M. Vahey, *A calcium- and pH-regulated protein from Dictyostelium discoideum that cross-links actin filaments.* J Cell Biol, 1982. **94**(2): p. 466-71.

29. MacLean-Fletcher, S.D. and T.D. Pollard, *Viscometric analysis of the gelation of Acanthamoeba extracts and purification of two gelation factors.* J Cell Biol, 1980. **85**(2): p. 414-28.

30. Lanni, F. and B.R. Ware, *Detection and characterization of actin monomers, oligomers, and filaments in solution by measurement of fluorescence photobleaching recovery [published erratum appears in Biophys J 1989 Jul;56(1):following 222].* Biophys J, 1984. **46**(1): p. 97-110.

31. Kas, J., et al., *F-actin, a model polymer for semiflexible chains in dilute, semidilute, and liquid crystalline solutions.* Biophys J, 1996. **70**(2): p. 609-25.

32. Kas, J., H. Strey, and E. Sackmann, *Direct imaging of reptation for semiflexible actin filaments.* Nature, 1994. **368**(6468): p. 226-9.

33. Doi, M. and S.F. Edwards, *The theory of polymer dynamics*. 1986, Oxford [Oxfordshire]

New York: Clarendon Press ;

Oxford University Press. xiii, 391 p.

34. Bindschadler, M., et al., *A mechanistic model of the actin cycle*. Biophys J, 2004. **86**(5): p. 2720-39.

35. Pollard, T.D., *Rate constants for the reactions of ATP- and ADP-actin with the ends of actin filaments*. J Cell Biol, 1986. **103**(6 Pt 2): p. 2747-54.

36. Tardy, Y., et al., *Interpreting photoactivated fluorescence nicroscopy measurements of steady-state actin dynamics*. Biophys J, 1995. **69**(5): p. 1674-82.

37. McGrath, J.L., et al., *Simultaneous measurements of actin filament turnover, filament fraction, and monomer diffusion in endothelial cells*. Biophys J, 1998. **75**(4): p. 2070-8.

38. Hartwig, J.H., *Mechanisms of actin rearrangements mediating platelet activation*. J Cell Biol, 1992. **118**(6): p. 1421-42.

39. Huxley, H.E., *Electron Microscope Studies on the Structure of Natural and Synthetic Protein Filaments from Striated Muscle*. J Mol Biol, 1963. **77**: p. 281-308.

40. Elzinga, M., et al., *Complete amino-acid sequence of actin of rabbit skeletal muscle*. Proc Natl Acad Sci U S A, 1973. **70**(9): p. 2687-91.

41. Newman, J., et al., *Presence of oligomers at subcritical actin concentrations*. Biochemistry, 1985. **24**: p. 1538-1544.

42. Mozo-Villarias, A. and B.R. Ware, *Actin oligomers below the critical concentration detected by fluorescence photobleaching recovery*. Biochem, 1985. **24**: p. 1544-48.

43. Montague, C., K.W. Rhee, and F.D. Carlson, *Measurement of the translational diffusion constant of G-actin by photon correlation spectroscopy*. J Muscle Res Cell Motil, 1983. **4**(1): p. 95-101.

44. Tait, J.F. and C. Frieden, *Polymerization and gelation of actin studied by fluorescence photobleaching recovery*. Biochemistry, 1982. **21**(15): p. 3666-74.

45. Korn, E.D., M.F. Carlier, and D. Pantaloni, *Actin polymerization and ATP hydrolysis*. Science, 1987. **238**(4827): p. 638-44.

46. Bonder, E.M., D.J. Fishkind, and M.S. Mooseker, *Direct measurement of critical concentrations and assembly rate constants at the two ends of an actin filament*. Cell, 1983. **34**(2): p. 491-501.

47. Doi, Y. and C. Frieden, *Actin polymerization. The effect of brevin on filament size and rate of polymerization*. J Biol Chem, 1984. **259**(19): p. 11868-75.

48. Wieland, T. and H. Faulstich, *Amatoxins, phallotoxins, phallolysin, and antamanide: the biologically active components of poisonous Amanita mushrooms*. CRC Crit Rev Biochem, 1978. **5**(3): p. 185-260.

49. Oosawa, F., *Size distribution of protein polymers*. J Theor Biol, 1970. **27**(1): p. 69-86.

50. Kawamura, M. and K. Maruyama, *A further study of electron microscopic particle length of F-actin polymerized in vitro*. J Biochem (Tokyo), 1972. **72**(1): p. 179-88.

51. Burlacu, S., P.A. Janmey, and J. Borejdo, *Distribution of actin filament lengths measured by fluorescence microscopy*. Am J Physiol, 1992. **262**(3 Pt 1): p. C569-77.

52. Wegner, A., *Head to tail polymerization of actin*. J Mol Biol, 1976. **108**(1): p. 139-50.

53. Janmey, P.A. and T.P. Stossel, *Kinetics of actin monomer exchange at the slow growing ends of actin filaments and their relation to the elongation of filaments shortened by gelsolin*. J Muscle Res Cell Motil, 1986. **7**(5): p. 446-54.

54. Flanagan, L.A., et al., *Filamin A, the Arp2/3 complex, and the morphology and function of cortical actin filaments in human melanoma cells*. J Cell Biol, 2001. **155**(4): p. 511-8.

55. Fischer, R.S., K.L. Fritz-Six, and V.M. Fowler, *Pointed-end capping by tropomodulin3 negatively regulates endothelial cell motility*. J Cell Biol, 2003. **161**(2): p. 371-80.

56. Mullins, R.D., J.A. Heuser, and T.D. Pollard, *The interaction of Arp2/3 complex with actin: nucleation, high affinity pointed end capping, and formation of branching networks of filaments*. Proc Natl Acad Sci U S A, 1998. **95**(11): p. 6181-6.

57. Kainulainen, T., et al., *Cell death and mechanoprotection by filamin a in connective tissues after challenge by applied tensile forces*. J Biol Chem, 2002. **277**(24): p. 21998-2009.

58. Maruyama, K. and K. Ohashi, *Tropomyosin inhibits the interaction of F-actin and filamin*. J Biochem (Tokyo), 1978. **84**(4): p. 1017-9.

59. Hartwig, J.H. and T.P. Stossel, *Structure of macrophage actin-binding protein molecules in solution and interacting with actin filaments*. J Mol Biol, 1981. **145**(3): p. 563-81.

60. Calderwood, D.A., et al., *Increased filamin binding to beta-integrin cytoplasmic domains inhibits cell migration*. Nat Cell Biol, 2001. **3**(12): p. 1060-8.

61. Goldmann, W.H., *p56(lck) Controls phosphorylation of filamin (ABP-280) and regulates focal adhesion kinase (pp125(FAK))*. Cell Biol Int, 2002. **26**(6): p. 567-71.

62. Vadlamudi, R.K., et al., *Filamin is essential in actin cytoskeletal assembly mediated by p21-activated kinase 1*. Nat Cell Biol, 2002. **4**(9): p. 681-90.

63. Glogauer, M., et al., *The role of actin-binding protein 280 in integrin-dependent mechanoprotection*. J Biol Chem, 1998. **273**(3): p. 1689-98.

64. Ohta, Y. and J.H. Hartwig, *Actin filament cross-linking by chicken gizzard filamin is regulated by phosphorylation in vitro*. Biochemistry, 1995. **34**(20): p. 6745-54.

65. Lanni, F., D.L. Taylor, and B.R. Ware, *Fluorescence photobleaching recovery in solutions of labeled actin*. Biophys J, 1981. **35**(2): p. 351-64.

66. Pardee, J.D. and J.A. Spudich, *Mechanism of K+-induced actin assembly*. J Cell Biol, 1982. **93**(3): p. 648-54.

67. Stradal, T., et al., *CH domains revisited.* FEBS Lett, 1998. **431**(2): p. 134-7.

68. Carugo, K.D., S. Banuelos, and M. Saraste, *Crystal structure of a calponin homology domain.* Nat Struct Biol, 1997. **4**(3): p. 175-9.

69. Way, M., B. Pope, and A.G. Weeds, *Evidence for functional homology in the F-actin binding domains of gelsolin and alpha-actinin: implications for the requirements of severing and capping.* J Cell Biol, 1992. **119**(4): p. 835-42.

70. Galkin, V.E., et al., *The utrophin actin-binding domain binds F-actin in two different modes: implications for the spectrin superfamily of proteins.* J Cell Biol, 2002. **157**(2): p. 243-51.

71. Kreis, T.E., B. Geiger, and J. Schlessinger, *Mobility of microinjected rhodamine actin within living chicken gizzard cells determined by fluorescence photobleaching recovery.* Cell, 1982. **29**(3): p. 835-45.

72. Cantiello, H.F., et al., *Actin-binding protein contributes to cell volume regulatory ion channel activation in melanoma cells.* J Biol Chem, 1993. **268**(7): p. 4596-9.

Footnotes

[1]*Abbreviations used are*: FLNa, filamin A; ddFLN, *Dictyostelium discoidium* filamin; F-actin, filamentous actin; G-actin, monomeric actin; PAF, photoactivation of fluorescence; CR-actin, caged resorufin iodoacetamide-labeled actin; *PF*, polymer fraction; τ_t, filament turnover time; D_m, monomer diffusion coefficient; c_c, critical concentration; k_{pD}^-, pointed end ADP-bound F-actin subunit dissociation rate constant

[2]Actin accounts for 11% of the total cellular protein mass in melanoma cells, independent of FLNa expression [5]. Therefore, from total protein measurements, the total actin mass is 4.0 ± 0.3 pg/cell and 3.9 ± 0.2 pg/cell in M2 and A7 cells, respectively, assuming that ~20% of the cell volume is non-cytoplasmic using previous measurements of M2 (2.45 pl) and A7 (2.57 pl) cell volumes [72].

Figure legends

Figure III-1. **Simulations of PAF experiments with 30 μm and 230 μm wide photoactivated bands.** *A*, spatial fluorescence profiles across the width of a 30 μm wide or *B*, 230 μm wide photoactivated band were simulated using a two-compartment mathematical model that provides a mathematically description of combined diffusion and turnover. For 30 μm wide photoactivated bands, filament diffusion and turnover occur on a similar time scale. For 230 μm wide photoactivated bands, filament diffuse on a slower time scale than subunits turnover. The *insets* show measurements of the width of the photoactivated band at half-maximum fluorescence intensity over time. In both simulations, $PF = 0.95$, $D_f = 1.8$ $\mu m^2/s$, and $\tau_t = 40$ min.

Figure III-2. **Actin monomer diffusion from a 230 μm wide photoactivated band.** *A*, microcapillary tubes loaded with 2 μM monomeric CR-actin were photoactivated and image sequences captured to monitor the fluorescence evolution at the band center-line (arrowhead) and across the width (arrow). *B*, spatial fluorescence profiles spanning the photoactivated band. *C*, Fluorescence intensity measured at the center of the photoactivated region, used to calculate D_m, the diffusion coefficient of actin monomers. For this experiment, $D_m = 57$ $\mu m^2/s$.

Figure III-3. **Steady state critical concentration of CR-actin and the effect of filamin cross-linking.** Actin (blue circles), actin with 1:20 FLNa (green squares), or CR-actin (red triangles) was mixed with 10% pyrene-labeled actin, incubated at 23 °C for 24 h, and the steady state fluorescence measured as a function of increasing total actin concentration (for each condition, $n = 3$). The critical concentration is the minimum concentration of actin required for filament formation. The *inset* shows apparent viscosity of actin networks measured with a miniature falling ball assay after polymerization with different

concentrations of human recombinant FLNa. The sharp increase in apparent viscosity at ~1 FLNa to 800 actin monomers is operationally defined as the gel point.

Figure III-4. **Characterization of actin dynamics in reconstituted networks of purified, entangled actin filaments.** *A*, 2 μM CR-actin was polymerized in microcapillary tubes with or without equimolar phallacidin, photoactivated in 30 μm or 230 μm wide regions across one-dimension of the tube, and images were collected for analysis. The fluorescence intensity was measured at the center of the band for mathematically interpretation and across the width (arrows) to identify evidence of band broadening due to fluorescent filament diffusion. *B*, the low-mobility fraction represents the fraction of fluorescent actin that remains $\geq$ 5 min after photoactivation after the high mobility components have escaped. *C*, the fluorescence decay constant was determined from an exponential curve fit, which for 230 μm bands, represents the filament turnover time of purified actin filaments (for each width band, $n \geq 6$). *D*, the lengths of purified actin filaments were measured (n = 2,631) by tracing the contours of individual filaments from digitized electron micrographs of negatively stained filaments, a representative image of which is shown in the *inset*. Bar, 200 nm.

Figure III-5. **Filamin-induced cross-linking stabilizes reconstituted actin network dynamics.** *A*, image sequences from PAF experiments on 2 μM CR-actin polymerized in the presence of either 1:20 human recombinant FLNa or ddFLN. *B*, the filament turnover time and *C*, low-mobility fraction were measured from center-line photoactivated band fluorescence intensities at increasing ratios of filamin to actin (for each condition, $n \geq 5$). *D* and *E*, actin filament lengths were measured (for each condition, $n \geq 100$) in cross-linked reconstituted networks from electron micrographs of negatively stained filaments under identical conditions to PAF experiments. Bars, 200 nm.

Figure III-6. **Actin binding, but not dimerization or cross-linking, is required for filamin-mediated dynamic stabilization of purified actin filaments.** *A*, 10 μM G-actin was polymerized in the presence of different concentrations of purified recombinant full-length FLNa or FLNa-ΔN153, which lacks 153 amino acids at the N-terminus overlapping the putative actin binding domain. After centrifugation, co-sedimentation of FLNa or FLN-ΔN153 with F-actin was determined by Coomassie Brilliant Blue staining of SDS-polyacrylamide gel electrophoresed supernatants (S) and pellets (P). *B*, measurements of the apparent viscosity of actin polymerized in the presence of different concentrations of FLNa (black circles), FLNa-ΔN153 (green squares), or FLNa-ΔC112 (red triangles) in which the dimerization domain at repeat 24 of FLNa was deleted (for each condition, $n = 5$). *C* and *D*, PAF experiments on reconstituted actin networks with 2 μM CR-actin polymerized in the absence or presence of 1 molecule of FLNa, ddFLN, FLNa-ΔC112, or FLNa-ΔN153 per 20 actin monomers were analyzed and the filament turnover times and low-mobility fractions calculated from the center-line fluorescence intensities in photoactivated bands.

Figure III-7. **FLNa modulates actin dynamics in melanoma cells.** *A*, M2 and A7 cells expressing a human β-actin EGFP fusion protein ~65 h after transfection were fixed, permeabilized with 0.2% Triton X-100, and stained with Alexa® 546 phalloidin to label total actin filaments. The condition for each panel is labeled above each image column. Bar, 10 μm. *B* and *C*, PAF and FRAP experiments were performed with CR-actin or EGFP-actin on melanoma cells that do not express FLNa (M2 and C1 cells), express full-length FLNa (A7 cells), or express a FLNa construct with the actin binding domain removed (C5 cells), and the fluorescence decay or recovery intensities were mathematically interpreted to determine the actin polymer fraction and average filament turnover time.

Supplemental videos

M2 cell expressing EGFP-actin. (Video *A*) Time lapse DIC video of a FLNa- M2 cell expressing EGFP-actin 48 h after transfection. (Video *B*) Corresponding time lapse fluorescence video of the same cell, where green represents EGFP-actin fluorescence. Frames were captured every 2 s for a total of 5 min. The video frame rate is 10 frames/s. Bars, 10 μm.

M2 cells expressing a FLNa truncate lacking the actin binding domain. (Video *C*) Time lapse DIC video of a C5 cell 18 - 24 h after plating. Frames were captured every 2 min for a total of 6 h. The video frame rate is 10 frames/s. Bar, 10 μm.

Tables

Table III-1. *Predictions of purified actin dynamics with a mechanistic model of the actin cycle*. Using a comprehensive model of the actin cycle [34], reconstituted network experiments were simulated by either fixing n or L_{avg} and altering k_{pD}^{-} to mimic filamin-induced slowing of filament turnover. For simulations, the total actin concentration was 2 μM, pointed and barbed filament ends were 100% uncapped, and profilin and β4-thymosin were inactivated. The filament concentration in reconstituted networks was calculated from experimental measurements of the critical concentration and the number-average filament length. Boxes shaded gray indicate parameters that were held constant during the simulation. τ_t, filament turnover time; *PF*, polymer fraction; c_c, critical concentration; n, filament concentration; L_{avg}, average filament length; k_{pD}^{-}, pointed end ADP-bound F-actin subunit dissociation rate.

Simulated experiment	n (μM)	L_{avg} (μm)	k_{pD}^{-} (s^{-1})	τ_t (h)	*PF*	c_c (μM)
actin	1.70	2.94	0.035	16.3	0.93	0.15
actin + 1:100 FLNa	1.70	2.98	0.023	29.5	0.94	0.13
actin	2.41	2.06	0.035	12.8	0.92	0.16
actin + 1:100 FLNa	2.45	2.06	0.023	23.6	0.94	0.13
actin + 1:100 FLNa	1.90	2.67	0.023	27.5	0.94	0.13
actin + 1:100 FLNa	1.47	2.98	0.023	32.5	0.94	0.13

Table III-2. *Characterization of filament ends and lengths in melanoma cell cytoskeletons.* Melanoma cells were permeabilized with 0.1% Triton X-100, 1 μM pyrene-labeled actin was added, and the change in fluorescence was measured over time as fluorescent actin assembles onto free filament nuclei within the cytoskeleton matrix. Experiments were repeated in the presence of 2 μM cytochalasin B to preferentially block barbed ends. Assuming the number of pointed ends represents the number of filaments, the average filament length (L_{avg}) populating melanoma cytoskeletons was calculated. Errors are reported as S.E.

	Pointed end nuclei per cell	*Barbed end nuclei per cell*	*% free barbed ends per cell*	L_{avg} (μm)
M2 cells	44,700 ± 11,900	5,210 ± 1,530	11.7	4.7
A7 cells	114,000 ± 25,100	16,200 ± 2,080	14.2	1.4

A

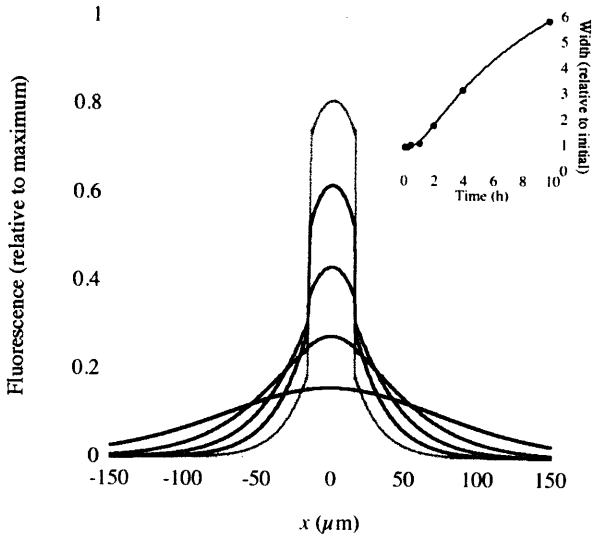

B

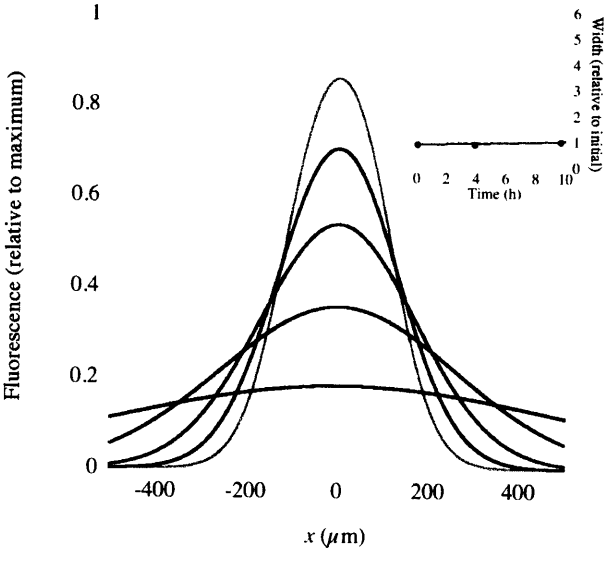

Figure III-1, Osborn et al.

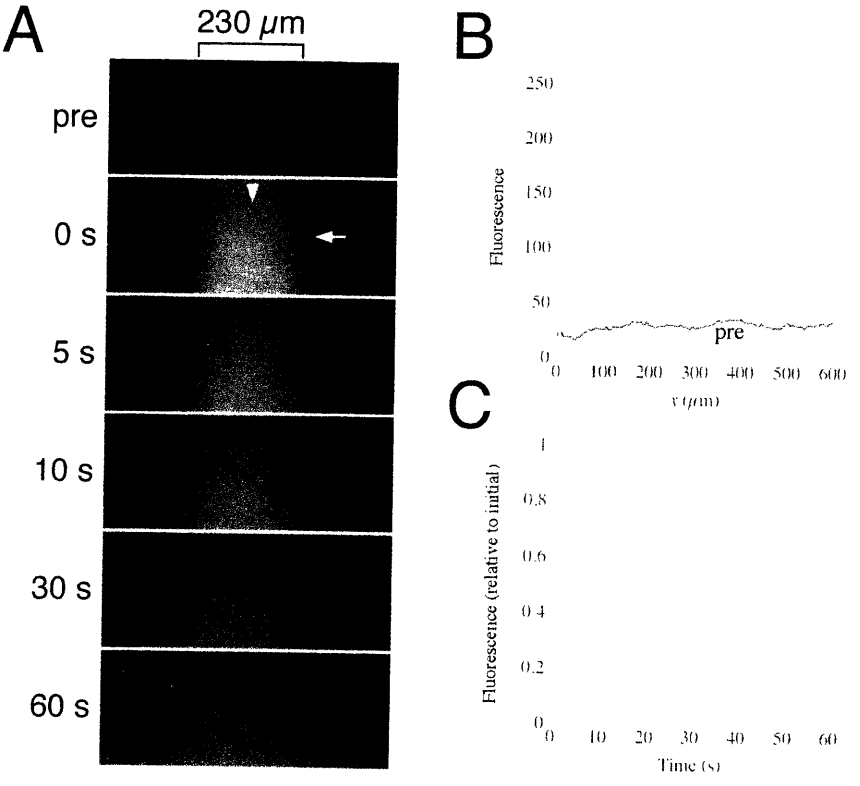

Figure III-2, Osborn et al.

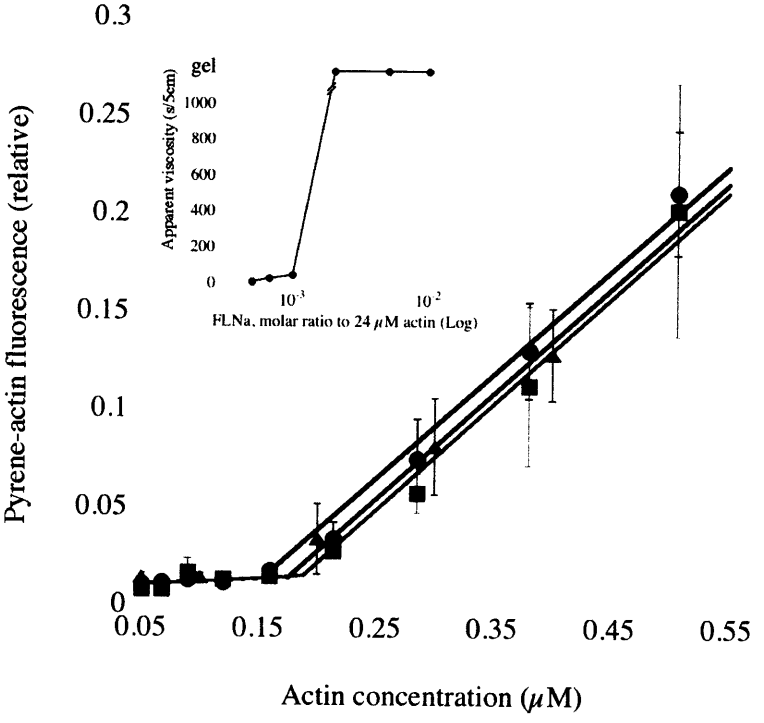

Figure III-3, Osborn et al.

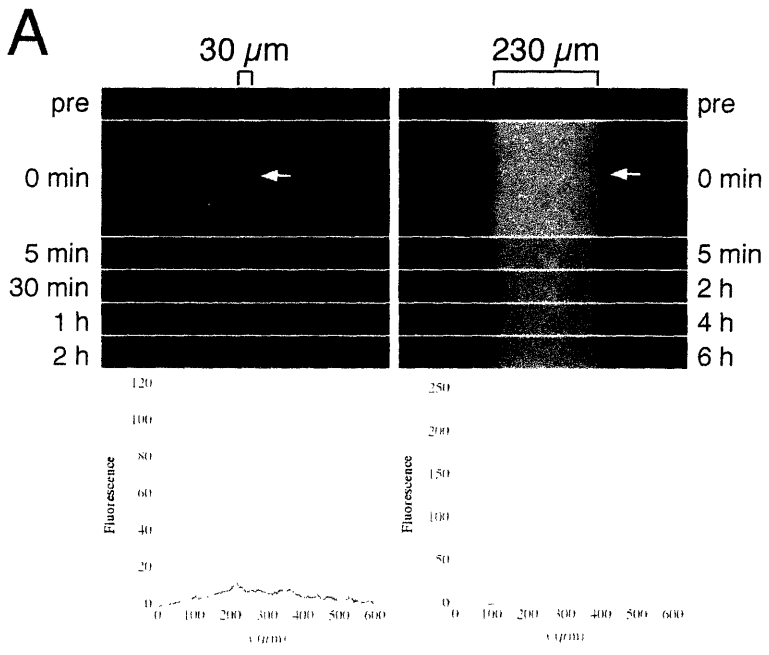

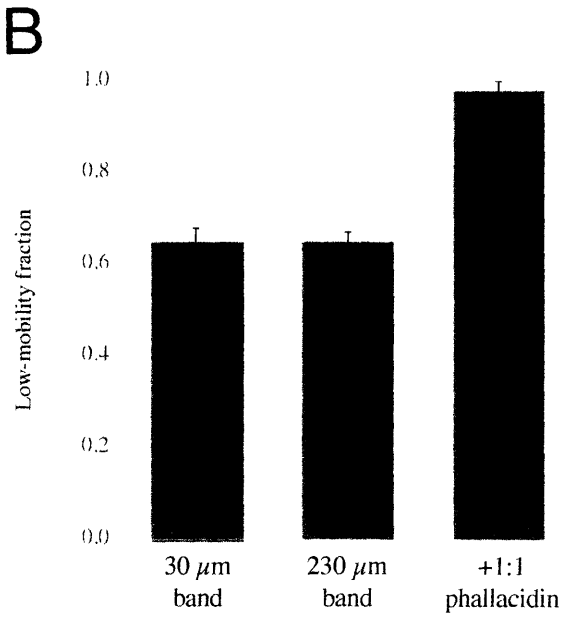

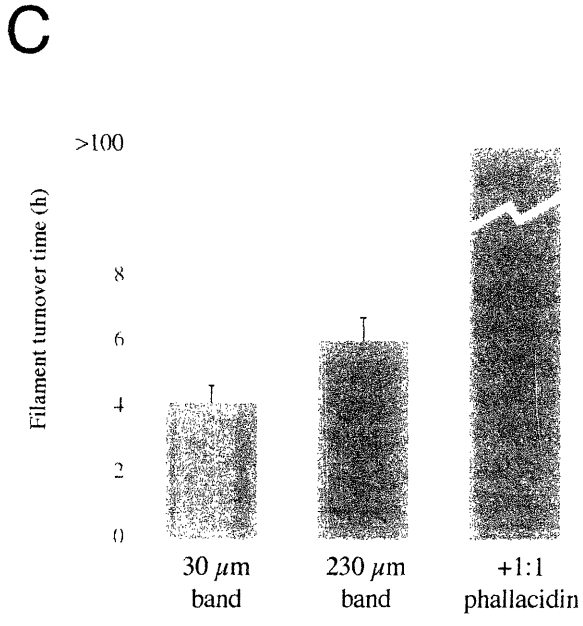

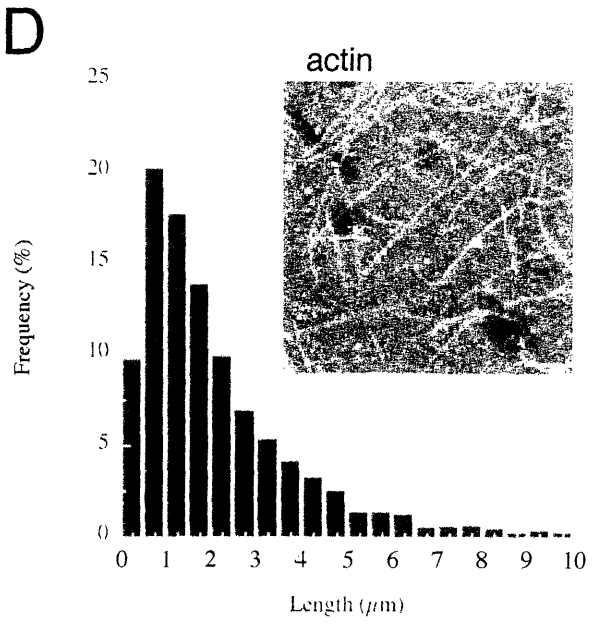

Figure III-4, Osborn et al.

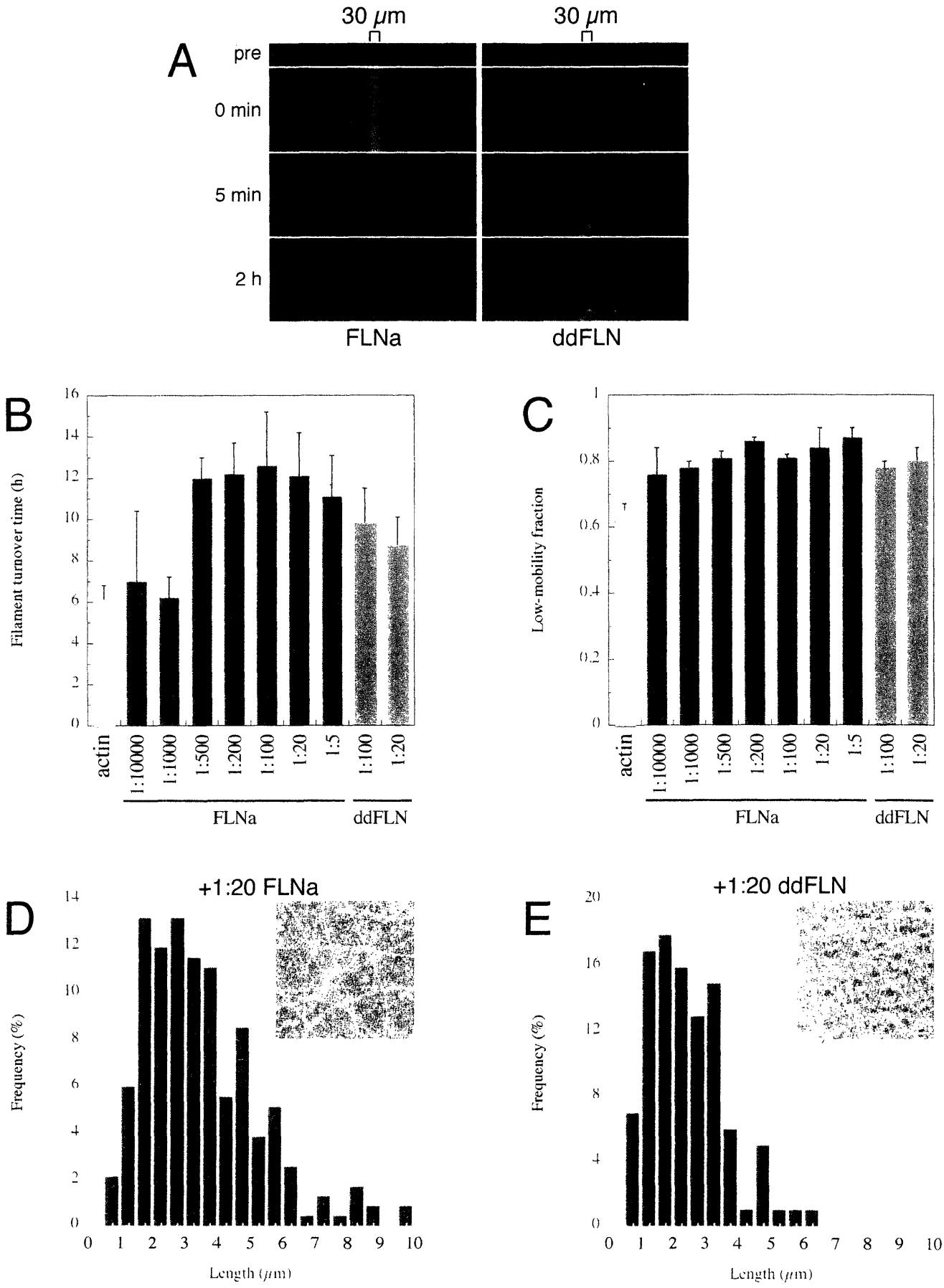

Figure III-5, Osborn et al.

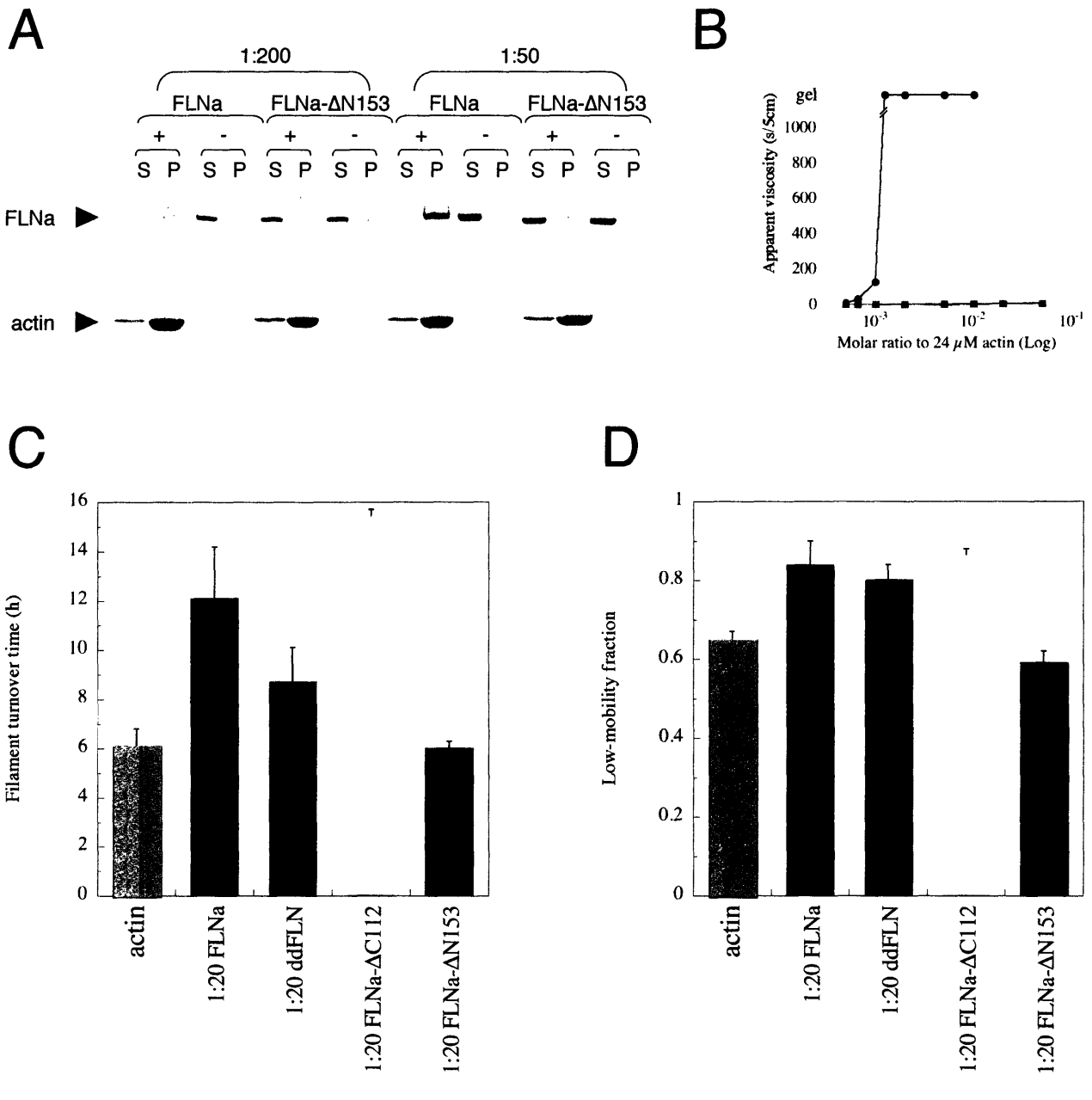

Figure III-6, Osborn et al.

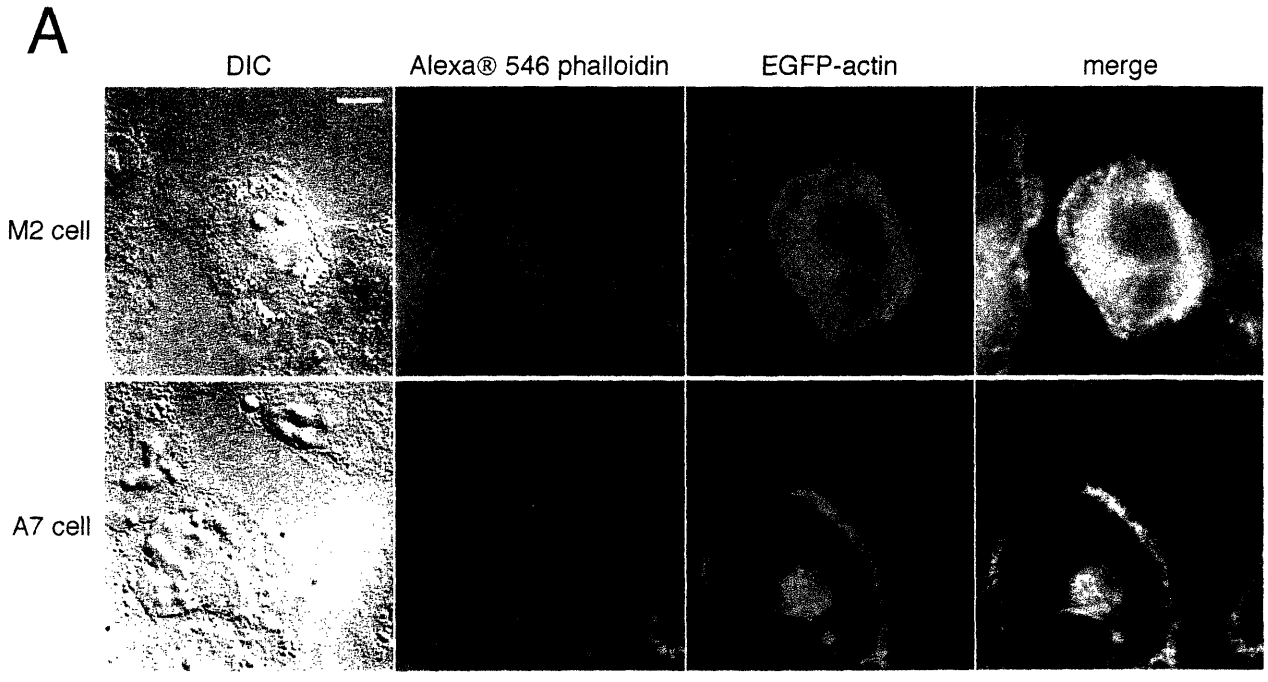

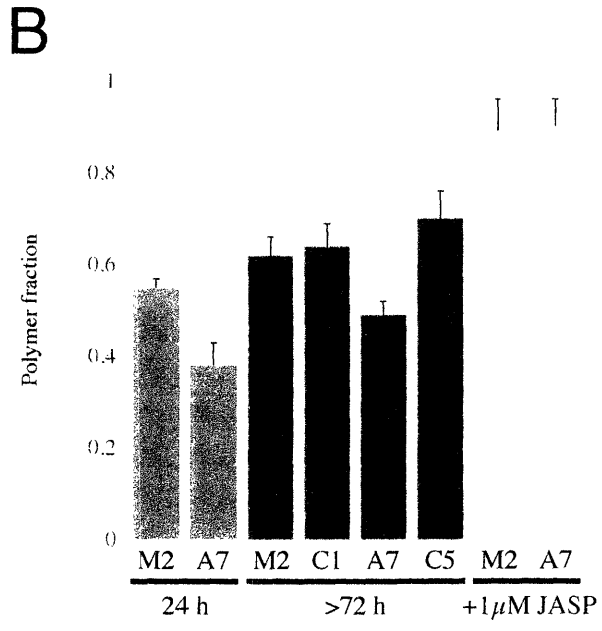

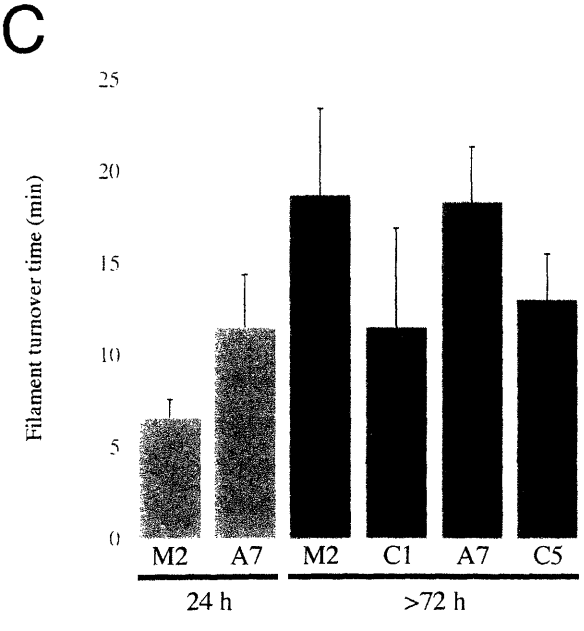

Figure III-7, Osborn et al.

Chapter IV

Discussion and Future Directions

This Thesis addresses important aspects of actin-based processes, focusing on the dynamics and control mechanisms that are at the core of the morphological changes and directed migration of non-muscle cells. Specifically, this work defines actin remodeling events in endothelial cells stimulated with fluid shear stress at their apical surfaces and in reconstituted actin networks with purified actin binding proteins. Together, these complementary approaches are used to further understand endothelial cell actin dynamics, shape change, and motility. A summary of the main conclusions presented in this Thesis is as follows.

In response to fluid shear stress, endothelial cells change their shape, driven by dynamic remodeling of the actin cytoskeleton, to assume an elongated morphology with their long axes aligned parallel to the direction of applied fluid flow [1-3]. From this work, three temporal phases of shear stress-induced endothelial actin dynamics have been identified based on the response of individual cells: (1) turnover-mediated cytoskeletal depolymerization, 0 – 30 min; (2) maintenance of enhanced actin remodeling in the setting of decreased cell movement, 1 – 6 h; (3) partial cytoskeletal recovery in shear

stress-accommodated endothelial cells with recovered motility, ~24 h. These findings indicate that the morphological accommodation process begins early in the endothelial shear stress response, and that enhanced cytoskeletal remodeling occurs continually throughout the shape change response, remaining activated in some cells even after morphological accommodation.

To decipher the role of actin binding proteins outside of the complex cellular environment, a novel photoactivation of fluorescence (PAF) system was employed to analyze the dynamics of reconstituted actin networks. This system is an improvement over existing *in vitro* measurement techniques since it does not require mechanical sample perturbation and the kinetic measurements can be performed on actin networks under true steady state conditions. Increasing the width of the photoactivated region isolates filament turnover from diffusion, which, based on first-order kinetic models for purified actin filaments, allows calculation of the pointed end actin filament subunit dissociation rate.

Measurements on purified actin reveal that filaments turnover slowly and that reconstituted actin networks contain a significant fraction of oligomers at steady state. Introducing filamin causes previously entangled actin networks to become cross-linked, stabilizing filament turnover and immobilizing much of the oligomer by a mechanism involving decreased fragmentation and/or enhanced oligomer annealing to longer filaments. This activity only requires ~1 filamin molecule bound per actin filament and is localized to the actin binding domain of the filamin molecule, independent of its cross-linking activity. Correlations between filamin expression and actin remodeling in

melanoma cells support the *in vitro* findings. These results suggest that FLNa stabilizes actin networks in three distinct ways: (1) cross-linking actin filaments to form a gel, (2) promoting filament annealing and/or inhibiting fragmentation, and (3) decreasing filament subunit cycling.

Dissecting the endothelial mechanotransduction cascade

By defining testable endpoints during the shear stress-induced endothelial shape change process, it is now possible to intelligently identify and dissect the molecular mechanisms responsible for control of actin remodeling during each phase of the endothelial response. Since sparse data is available in the literature to support actin-dependent mechanisms beyond the first minutes following shear stress exposure, the first task will be to identify candidate actin binding proteins that change their association with the cytoskeleton during these times. Once these have been established, each candidate protein can be manipulated using knockdown and knockout technologies and its effect on endothelial actin dynamics, motility, and morphological accommodation examined.

In addition, with the advent of a comprehensive mathematical description of the steady state actin cycle [4], available on the Internet at http://mcgrathlab.urmc.rochester.edu/actincycle/, it is now possible to theoretically test predicted effects of actin binding proteins on the actin cycle. The model allows the user discrete control over actin binding protein mechanisms of action – capping, severing, nucleotide exchange, accelerated disassembly, sequestration, profilin – and solves the

entire nucleotide profile of subunits within the actin filament. This extensive effort provides a significant new tool to advance the understanding of actin dynamics and its control.

Based on theoretical considerations and previous work on endothelial cells in our laboratory [5], gelsolin and ADF/cofilin may be important players in the endothelial shear stress mechanoresponse, particularly in the initial filament turnover-mediated depolymerization phase. With the barbed end capped, ADF/cofilin-mediated acceleration of pointed filament end subunit disassembly results in F-actin depolymerization [6]. This process is amplified by gelsolin, which increases the number of free pointed ends available for depolymerization by severing filaments and then capping the newly formed barbed ends [5, 7]. Evidence from endothelial cells in static culture suggests that gelsolin is required to facilitate ADF/cofilin activity as endothelial cells crawl faster [5]. In addition, since oscillatory Ca^{2+} transients represent one of the earliest responses of endothelial cells to fluid shear stress [8, 9], gelsolin, whose severing activity is Ca^{2+}-dependent [10], may play an important role in disassembling the cytoskeleton during this initial phase. The control mechanisms governing the later stages of the endothelial shear stress response are less clear at this time.

Once candidate shear stress-responsive proteins have been isolated, their individual and combined effects on steady state actin dynamics can be tested using the PAF-based reconstituted actin network system with purified proteins, allowing direct examination of the functions of these proteins *in vitro*. The reconstituted system is the perfect companion to the steady state actin cycle model, which together can be utilized to validate and target

additional experiments. In this way, proteins important to shear stress sensation by endothelium can be tested directly on purified actin networks, and mechanisms observed in this system can then be used to probe cells.

Endothelial shear stress-sensing mechanisms

Endothelial cells sense fluid shear stress by unknown mechanisms. The diversity, complexity, and molecular robustness of the endothelial response to fluid shear stress have made elucidation of a single mechanism difficult [1, 11]. Despite this, numerous mechanisms have been postulated, which can be categorized according to centralized (single receptors) and decentralized (interconnected matrices) responses [1, 12]. However, most likely, the convergence of multiple shear stress-responsive mechanisms initiates a more integrated endothelial response when challenged with fluid flow.

Centralized responses are perhaps the most obvious, involving direct mechanical displacement of surface receptors by the shear force. Candidates include integrins [13], mechanosensistive ion channels [14], G protein-coupled receptors [15], mitogen-activated receptors [11], and others [16]. These may be grouped into functional units at specialized locations on the cell surface, such as caveolae [14]. One interesting new theory implicates PECAM-1, an endothelium specific intercellular adhesion molecule, which is rapidly phosphorylated in response to mechanical stimulation, including fluid shear stress [17].

Recently, however, the focus has shifted more to decentralized signaling mechanisms involving distributed systems that transmit force to attached/associated molecules that initiate signaling [12]. Proposed decentralized sensors include cytoplasmic cytoskeletal polymers (actin filaments, intermediate filaments, and microtubules) connected to integrins and cadherins [18], the apical fibrous glycocalyx meshwork [19], and microvilli that are present on the surface of unstressed endothelial cells in static culture but are lost after morphological accommodation [20]. Direct cytoskeletal force transmission has been implied by recent reports that show rapid intracellular cytoskeletal structural movement in response to shear stress [18]. These studies have allowed creation of strain maps that reveal the presence of cytoskeletal strain gradients throughout the cytosol [21].

Filamin-A, a shear stress mechanosensor?

One candidate protein that may play a role in shear stress mechanotransduction and actin remodeling is the dimeric actin filament cross-linking protein filamin-A (FLNa), which forms stiff actin gels *in vitro* at low stoichiometry [22, 23]. Similar to PECAM-1, FLNa is a mechanosensitive molecule that is phosphorylated in response to mechanical force and becomes recruited to sites of applied tension [24-26]. In addition, FLNa protects cells against apoptotic death after mechanical perturbation [24-26]. However, unlike PECAM-1, the primary functions of FLNa are to bind F-actin, organize structural features of the cytoskeleton [27, 28], and stabilize the dynamics of actin filaments as described in this Thesis. As well, while PECAM-1 is a transmembrane protein localized to intercellular junctions [29], FLNa is cytoplasmic and found throughout the actin cortex of non-muscle

cells in intimate contact with the apical plasma membrane [27], the site of maximal shear stress stimulation [12].

In addition to its proximity to the membrane and potent F-actin binding capacity, FLNa has other properties that may be advantageous for a shear stress mechanosensor, such as a large size (560 kDa), an elongated shape (~160 nm), and significant flexibility (persistence length ~15 nm [30]). Structurally it has been described as resembling a 'molecular leaf spring' [30, 31], implying its mechanical properties. As well, a growing number of binding partners interact with FLNa, predominately near the C-terminus opposite the actin binding domains, such that FLNa has been postulated as a signaling scaffold and organizing center for binding partners to mediate local actin rearrangements [27]. Of particular importance for shear stress transduction are FLNa's association with β-integrins for force transmission [32] and Rac1, RhoA, Cdc42, and RalA for actin rearrangements [33, 34].

FLNa dynamics in endothelium

To determine if FLNa responds to fluid shear stress, fluorescence recovery after photobleaching (FRAP) studies were performed in single endothelial cells expressing a fusion protein between FLNa and enhanced green fluorescent protein (EGFP-FLNa). This technique determines the amount of immobile (e.g. cytoskeletal) FLNa before and after stimulation with fluid shear stress.

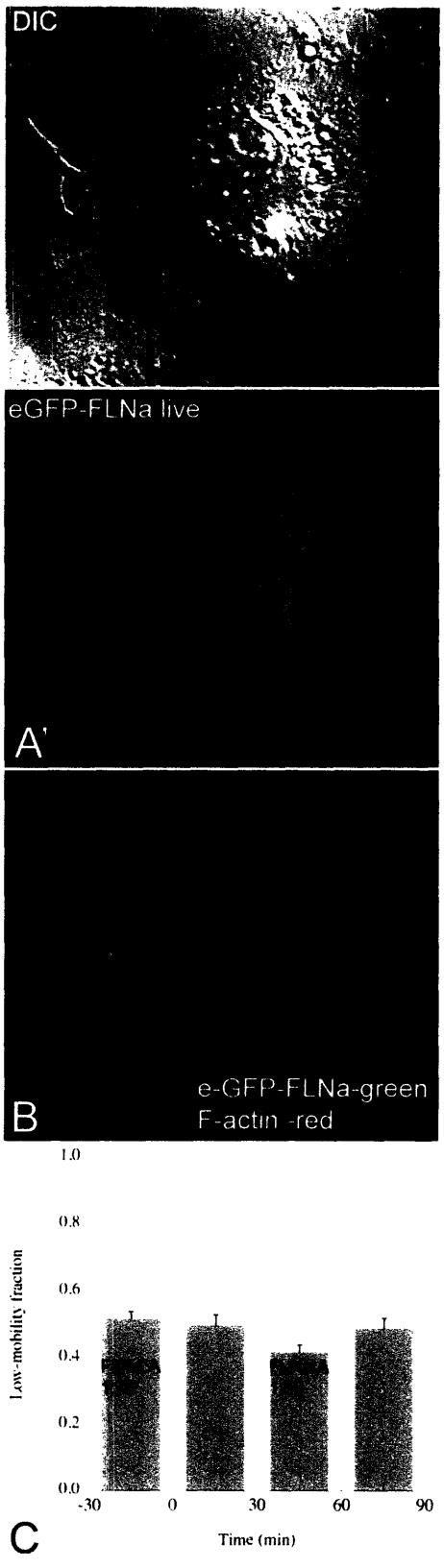

Prior to experiments, the distribution of EGFP-FLNa was determined by fluorescence microscopy in living and fixed cells (Fig. 4-1). EGFP-FLNa incorporates into the actin cytoskeleton of living endothelial cells and has both a cortical and stress fiber-related distribution (Fig. IV-1, A and A'). In fixed cells, EGFP-FLNa co-localizes with F-actin (Fig. IV-1, B), staining small ruffles at the cell edge.

Preliminary evidence suggests that FLNa is responsive to fluid shear stress on the same time scale as actin dynamics are enhanced (Fig. IV-1, C). Under static conditions, ~50% of the total FLNa is immobile in a molar ratio of ~1:75 with F-actin subunits, based on the total amount of F-actin. Approximately 30 min after fluid shear stress stimulation, despite a ~30% decrease in F-actin content, only ~10 % of FLNa dissociates from the

Fig. IV-1. *EGFP-FLNa localization and dynamics in endothelial cells.* (A and A') Live endothelial cell transfected with EGFP-FLNa imaged by DIC and fluorescence, respectively. (B) Fixed endothelial cell expressing EGFP-FLNa stained with Alexa-546 phalloidin to label actin filaments. (C) Low-mobility EGFP-FLNa fraction as measured with FRAP. The ratio of FLNa to F-actin subunits is marked on the bars at selected time ponts. A = actin.

cytoskeleton. Thus, the FLNa to actin ratio increases to 1:50 in response to fluid shear stress. After 1 h of fluid flow, the amount of immobilized FLNa increases to pre-shear stress levels even though the polymer content remains depleted, indicating that the ratio of FLNa to F-actin subunits increases even further.

Therefore, FLNa appears to be involved in mechanical sensing, increasing its cytoskeletal association when stimulated with fluid shear stress, in a similar manner to the FLNa recruitment observed in integrin-ligated magnetic bead pulling experiments [24, 25]. While further targeted studies are required, these results reveal that FLNa may indeed play a role in shear stress mechanosensation and, possibly, signal transduction.

A molecular 'Clutch' or an adhesive 'Trap'?

During the maintenance phase of the shear stress response, enhanced actin filament turnover is not converted into increased cell motility, as measured in single endothelial cells in static culture [5]. Instead, beginning ~1 h after shear stress stimulation, endothelial cells slow their movements in the face of accelerated actin dynamics. There are two alternative hypotheses for this behavior. The first is a 'Trap' mechanism in which increased substrate and/or intercellular adhesion counteracts the accelerated pace of the actin motor. The second is a 'Clutch' mechanism in which the cytoskeletal motor is decoupled from adhesion and movement.

FLNa may participate in cells either by a 'Trap' mechanism or as a molecular 'Clutch'. Evidence supporting a FLNa-mediated 'Trap' comes from reports that increased binding

of FLNa to β integrin tails negatively regulates cell motility [35]. Evidence supporting a FLNa-mediated 'Clutch' mechanism is observed in melanoma cells studies where loss of FLNa inhibits cell movement despite enhanced actin cycling [36-38].

Due to the observed compensatory increase in cytoskeletal FLNa shortly after shear stress stimulation, a 'Trap' mechanism may be favored over a 'Clutch' in the endothelial shear stress-response. However, if FLNa association with the cytoskeleton after shear stress exposure is compartmentalized away from integrin binding sites at the plasma membrane, a 'Clutch' mechanism may be possible. Studies on FLNa- melanoma cells transfected with FLNa engineered to lack β integrin binding activity may provide interesting insights into the coupling between actin dynamics, cell motility, and FLNa function.

Building an actin motor

The necessary components required to reconstitute the 'rocketing' motility of the intracellular pathogens *Listeria* and *Shigella* have been identified, requiring precious few molecules – actin, the activated Arp2/3 complex, ADF/cofilin, and capping protein [39]. To achieve maximal propulsion, α-actinin, profilin, and VASP (for *Listeria*) are also required.

Recently, an extensive effort using RNAi to knockdown ~90 different proteins in *Drosophila* S2 cells has determined the molecular components required for lamella formation [40]. Similar to *Listeria* and *Shigella* movement, S2 cell actin-based lamellae formation requires the activated Arp2/3 complex (with SCAR), capping protein, cofilin,

and profilin, but, in addition, two other proteins are necessary, Aip1 and cyclase-associated protein.

These studies illustrate a simple toolbox of important components to test in reconstituted actin networks and demonstrate the feasibility of such an approach. However, other molecular players are with no doubt required to coordinate actin dynamics and maintain coherence of the leading edge in mammalian cells.

As described in this Thesis, the mechanisms of individual actin binding proteins can be addressed directly by reconstituting actin networks *in vitro* with purified regulatory proteins. The ultimate goal of building the purified protein system is to recapitulate the reactions that mediate filament turnover in cells and build a high-performance actin motor. The work presented here has laid a foundation for understanding actin dynamics in purified actin networks and made progress towards reconstituting an actin filament recycling system that mimics cellular dynamics.

References

1. Davies, P.F., *Flow-mediated endothelial mechanotransduction.* Physiol Rev, 1995. **75**(3): p. 519-60.
2. Dewey, C.F., Jr., et al., *The dynamic response of vascular endothelial cells to fluid shear stress.* J Biomech Eng, 1981. **103**(3): p. 177-85.
3. Davies, P.F., *Mechanisms involved in endothelial responses to hemodynamic forces.* Atherosclerosis, 1997. **131 Suppl**: p. S15-7.
4. Bindschadler, M., et al., *A mechanistic model of the actin cycle.* Biophys J, 2004. **86**(5): p. 2720-39.
5. McGrath, J.L., et al., *Regulation of the actin cycle in vivo by actin filament severing.* Proc Natl Acad Sci U S A, 2000. **97**(12): p. 6532-6537.
6. Carlier, M.F., et al., *Actin depolymerizing factor (ADF/cofilin) enhances the rate of filament turnover: implication in actin-based motility.* J Cell Biol, 1997. **136**(6): p. 1307-22.
7. Sun, H.Q., et al., *Gelsolin, a multifunctional actin regulatory protein.* J Biol Chem, 1999. **274**(47): p. 33179-82.
8. Blackman, B.R., L.E. Thibault, and K.A. Barbee, *Selective modulation of endothelial cell /Ca2+ /i response to flow by the onset rate of shear stress /In Process Citation /.* J Biomech Eng, 2000. **122**(3): p. 274-82.
9. Shen, J., et al., *Fluid shear stress modulates cytosolic free calcium in vascular endothelial cells.* Am J Physiol, 1992. **262**(2 Pt 1): p. C384-90.
10. Yin, H.L. and T.P. Stossel, *Control of cytoplasmic actin gel-sol transformation by gelsolin, a calcium-dependent regulatory protein.* Nature, 1979. **281**(5732): p. 583-6.
11. Barakat, A.I. and P.F. Davies, *Mechanisms of shear stress transmission and transduction in endothelial cells.* Chest, 1998. **114**(1 Suppl): p. 58S-63S.
12. Davies, P.F., J. Zilberberg, and B.P. Helmke, *Spatial microstimuli in endothelial mechanosignaling.* Circ Res, 2003. **92**(4): p. 359-70.
13. Shyy, J.Y. and S. Chien, *Role of integrins in endothelial mechanosensing of shear stress.* Circ Res, 2002. **91**(9): p. 769-75.
14. Traub, O. and B.C. Berk, *Laminar shear stress: mechanisms by which endothelial cells transduce an atheroprotective force.* Arterioscler Thromb Vasc Biol, 1998. **18**(5): p. 677-85.
15. Gudi, S., J.P. Nolan, and J.A. Frangos, *Modulation of GTPase activity of G proteins by fluid shear stress and phospholipid composition.* Proc Natl Acad Sci U S A, 1998. **95**(5): p. 2515-9.

16. Barakat, A.I., *A model for shear stress-induced deformation of a flow sensor on the surface of vascular endothelial cells*. J Theor Biol, 2001. **210**(2): p. 221-36.

17. Osawa, M., et al., *Evidence for a role of platelet endothelial cell adhesion molecule-1 in endothelial cell mechanosignal transduction: is it a mechanoresponsive molecule?* J Cell Biol, 2002. **158**(4): p. 773-85.

18. Helmke, B.P., et al., *Spatiotemporal analysis of flow-induced intermediate filament displacement in living endothelial cells*. Biophys J, 2001. **80**(1): p. 184-94.

19. Weinbaum, S., et al., *Mechanotransduction and flow across the endothelial glycocalyx*. Proc Natl Acad Sci U S A, 2003. **100**(13): p. 7988-95.

20. Satcher, R., C.F. Dewey, Jr., and J.H. Hartwig, *Mechanical remodeling of the endothelial surface and actin cytoskeleton induced by fluid flow*. Microcirculation, 1997. **4**(4): p. 439-53.

21. Helmke, B.P., A.B. Rosen, and P.F. Davies, *Mapping mechanical strain of an endogenous cytoskeletal network in living endothelial cells*. Biophys J, 2003. **84**(4): p. 2691-9.

22. Ito, T., A. Suzuki, and T.P. Stossel, *Regulation of water flow by actin-binding protein-induced actin gelatin*. Biophys J, 1992. **61**(5): p. 1301-5.

23. Nakamura, F., et al., *Comparison of filamin A-induced cross-linking and Arp2/3 complex- mediated branching on the mechanics of actin filaments*. J Biol Chem, 2002. **277**(11): p. 9148-54.

24. Kainulainen, T., et al., *Cell death and mechanoprotection by filamin a in connective tissues after challenge by applied tensile forces*. J Biol Chem, 2002. **277**(24): p. 21998-2009.

25. Glogauer, M., et al., *The role of actin-binding protein 280 in integrin-dependent mechanoprotection*. J Biol Chem, 1998. **273**(3): p. 1689-98.

26. D'Addario, M., et al., *Cytoprotection against mechanical forces delivered through beta 1 integrins requires induction of filamin A*. J Biol Chem, 2001. **276**(34): p. 31969-77.

27. Stossel, T.P., et al., *Filamins as integrators of cell mechanics and signalling*. Nat Rev Mol Cell Biol, 2001. **2**(2): p. 138-45.

28. Hartwig, J.H. and P. Shevlin, *The architecture of actin filaments and the ultrastructural location of actin-binding protein in the periphery of lung macrophages*. J Cell Biol, 1986. **103**(3): p. 1007-20.

29. Albelda, S.M. and C.A. Buck, *Integrins and other cell adhesion molecules*. Faseb J, 1990. **4**(11): p. 2868-80.

30. Hartwig, J.H. and T.P. Stossel, *Structure of macrophage actin-binding protein molecules in solution and interacting with actin filaments.* J Mol Biol, 1981. **145**(3): p. 563-81.

31. Gorlin, J.B., et al., *Human endothelial actin-binding protein (ABP-280, nonmuscle filamin): a molecular leaf spring.* J Cell Biol, 1990. **111**(3): p. 1089-105.

32. Calderwood, D.A., S.J. Shattil, and M.H. Ginsberg, *Integrins and actin filaments: reciprocal regulation of cell adhesion and signaling.* J Biol Chem, 2000. **275**(30): p. 22607-10.

33. Marti, A., et al., *Actin-binding protein-280 binds the stress-activated protein kinase (SAPK) activator SEK-1 and is required for tumor necrosis factor-alpha activation of SAPK in melanoma cells.* J Biol Chem, 1997. **272**(5): p. 2620-8.

34. Ohta, Y., et al., *The small GTPase RalA targets filamin to induce filopodia.* Proc Natl Acad Sci U S A, 1999. **96**(5): p. 2122-8.

35. Calderwood, D.A., et al., *Increased filamin binding to beta-integrin cytoplasmic domains inhibits cell migration.* Nat Cell Biol, 2001. **3**(12): p. 1060-8.

36. Cunningham, C.C., *Actin polymerization and intracellular solvent flow in cell surface blebbing.* J Cell Biol, 1995. **129**(6): p. 1589-99.

37. Cunningham, C.C., et al., *Actin-binding protein requirement for cortical stability and efficient locomotion.* Science, 1992. **255**(5042): p. 325-7.

38. Flanagan, L.A., et al., *Filamin A, the Arp2/3 complex, and the morphology and function of cortical actin filaments in human melanoma cells.* J Cell Biol, 2001. **155**(5).

39. Loisel, T.P., et al., *Reconstitution of actin-based motility of Listeria and Shigella using pure proteins.* Nature, 1999. **401**(6753): p. 613-6.

40. Rogers, S.L., et al., *Molecular requirements for actin-based lamella formation in Drosophila S2 cells.* J Cell Biol, 2003. **162**(6): p. 1079-88.